NASA-UVA LIGHT AEROSPACE ALLOY AND STRUCTURES TECHNOLOGY PROGRAM (LA^2ST)

Program Directors:

Edgar A. Starke, Jr.
Richard P. Gangloff

Co-Principal Investigators:

John R. Scully
Gary J. Shiflet
Glenn E. Stoner
John A. Wert

NASA-Larc Contract Monitor:

Dennis L. Dicus

Department of Materials Science and Engineering
School of Engineering and Applied Science
Thornton Hall
Charlottesville, VA 22903-2442

SEAS Report No. UVA/528266/MSE96/119
January 1996

Copy No._____

TABLE OF CONTENTS

TABLE OF CONTENTS (continued)

NASA-UVa LIGHT AEROSPACE ALLOY AND STRUCTURES TECHNOLOGY PROGRAM *(LA²ST)*

Executive Summary

The NASA-UVa Light Aerospace Alloy and Structures Technology (LA²ST) Program was initiated in 1986 and continues with a high level of activity. Projects are being conducted by graduate students and faculty advisors in the Department of Materials Science and Engineering at the University of Virginia. This work is funded by the NASA-Langley Research Center under Grant NAG-1-745. Here, we report on progress achieved between July 1 and December 31, 1995.

The objective of the LA²ST Program is to conduct interdisciplinary graduate student research on the performance of next generation, light-weight aerospace alloys, composites and thermal gradient structures in collaboration with NASA-Langley researchers. Specific technical objectives are presented for each research project. We generally aim to produce relevant data and basic understanding of material mechanical response, environmental/corrosion behavior, and microstructure; new monolithic and composite alloys; advanced processing methods; new solid and fluid mechanics analyses; measurement and modeling advances; and a pool of educated graduate students for aerospace technologies.

The accomplishments presented in this report are summarized as follows.

- Three research areas are being actively investigated, including: (1) Mechanical and Environmental Degradation Mechanisms in Advanced Light Metals, (2) Aerospace Materials Science, and (3) Mechanics of Materials for Light Aerospace Structures.
- Ten research projects are being conducted by 10 PhD and 1 MS level graduate students, 2 post doctoral fellows and 6 faculty members. Each project is planned and executed in conjunction with a specific branch and technical monitor at NASA-LaRC.
- Two undergraduates conducted research in the Metallic Materials Branch at NASA-LaRC during the Summer of 1995. No undergraduates are currently participating in LA²ST research at UVa.
- Collective accomplishments between July and December of 1995 include: 11 journal or proceedings publications, 1 NASA progress report, 3 presentations at national technical meetings, and 2 PhD dissertations published. Two students graduated during this reporting period; 1 with the Masters of Science Degree in

Materials Science and Engineering, and 1 with the Doctor of Philosophy Degree in Materials Science and Engineering at UVa. The LA²ST totals since 1986 are 113 publications (71 archival journal or book publications), 22 PhD dissertations or MS theses, 112 external technical presentations, 18 NASA progress reports, and 4 NASA Contractor Reports. Since 1986, 34 graduate students, including 31 citizens of the United States, have been involved with LA²ST research; 22 have received the MS or PhD degree. Six post-doctoral research associates have participated in LA²ST research. A total of 13 different faculty have worked on the LA²ST program.

Summary of Recent Results

Research on the elevated temperature fracture toughness of advanced aluminum alloys demonstrates that fracture initiation toughness in thin sheet aluminum alloys is characterized accurately and precisely by a standardized measurement based on direct current potential difference detection of microvoid damage. The critical distance parameter l^* from a micromechanical model of initiation toughness, calculated based on measured toughness and tensile properties, correlates with the three-dimensional nearest neighbor spacing of constituent particles for several aluminum alloys and steels. The multiple of particle spacings that constitutes the critical distance increases with the extent of primary void growth from constituents. (*Project #1*)

Evaluation of alternative inhibited NaCl solutions necessary for the proposed fracture mechanics based SCC testing of AA2096 and C155 alloys in controlled electrochemical environments has begun. Solutions of 1 M Na_2SO_4 + 0.1 M $CH_3COONa \cdot 3H_2O$ acidified to pH=3.8 and with varying levels of NaCl (0, 0.01, 0.1, and 0.5 M) have shown some interesting promise as a possible alternative to chromate-inhibited solutions. The results are somewhat preliminary, with further optimization of solution chemistry underway. (*Project #5*)

Research on the deformation and fracture of high strength titanium alloys demonstrates that the direct current potential difference technique effectively monitors crack initiation and growth in fatigue precracked specimens of TIMET LCB sheet and plate. The initiation fracture toughness of LCB sheet is significantly greater than the corresponding properties of plate. The fracture resistance of TIMET LCB sheet is comparable to that of Beta C and the lower bound on strength dependent toughness for Beta-21S. The fracture toughness of LCB sheet is sufficient to characterize the effects of elevated temperature and

predissolved hydrogen. This work will be augmented by experiments with either Ti-15-3 or Beta-21S sheet. (*Project #6a*)

Unexpectedly low strength and high microstructural segregation of LCB plate and sheet received from TIMET prompted the addition of the more promising Ti 15-3 alloy to this program. Identification of deformation modes in Ti 15-3 will begin first on beta solutionized material. The effects of alpha-beta heat treatment and various ageing processes will then be studied. (*Project #6b*)

The yield strength anisotropy for a series of four microstructurally distinct regions in the 2090 extrusion has been accurately predicted using the plastic inclusion model. A strong understanding of the role that matrix and precipitate effects play in the total plastic anisotropy of aluminum alloys has been achieved. (*Project #7*)

The experimental observation that the tensile ductility in a recently developed Al-0.55Si-2.02Ge (wt.%) alloy decreases with increasing precipitate size while the critical strain for cavity nucleation increases has been explained using finite element calculations and experimental void growth measurements. (*Project #8*)

The precipitate microstructure of the Al-Cu-Mg-Ag alloys C415-T8 and C416-T8 was found to be very stable against coarsening under creep loads of 30 ksi at 275°F and 40 ksi at 225°F. (*Project #9*)

Research on time-cycle-dependent environmental fatigue in 7000-series aluminum alloys characterized the loading frequency dependence of crack growth rate for AA7075 in aqueous NaCl. A complex behavior was observed for T6 and T7 tempers; crack growth rate is reduced ($da/dN \propto f^{-0.1}$) at high frequencies due to reduced time for crack tip embrittlement, and at low frequencies due to increased crack closure in uninhibited solution. Neither crack orientation (S-L vs L-T) nor temper (T651 vs T7351) affected the environmental enhancement of da/dN in the Paris regime. (*Project #10a*)

Research on modeling environmental effects on fatigue crack propagation was completed. Results include a FORTRAN program, UVAFAS, to model da/dN vs ΔK with three approaches; linear superposition, empirical-interpolation, and multiple-power law fitting. This code was tested with literature data for a range of alloys, as well as with new stress corrosion cracking and corrosion fatigue data for AA7075-T651 and Ti-6Al-4V (ELI) in chloride solutions. Linear superposition was inadequate because these two alloys resist SCC. While the interpolative model describes time-cycle-dependent environmental fatigue within the defining data base, a fundamental mechanistic approach is required to broadly predict crack growth kinetics. (*Project #10b*)

INTRODUCTION

Background

In 1986 the Metallic Materials Branch in the Materials Division of the NASA-Langley Research Center initiated sponsorship of graduate student engineering and scientific research in the Department of Materials Science and Engineering at the University of Virginia[1]. This work emphasized the mechanical and corrosion behavior of light aerospace alloys, particularly Al-Li-Cu based compositions, in aggressive aerospace environments[2-4].

In the Fall of 1988, the scope of this program increased to incorporate research on the development and processing of advanced aerospace materials[5]. Additional funding was provided by the Metallic Materials and Mechanics of Materials Branches at NASA-LaRC. In early 1989 the program was further enhanced to include interdisciplinary work on solid mechanics and thermal structures, with funding from several Divisions within the Structures Directorate at NASA-LaRC[6]. The Departments of Civil Engineering (Applied Mechanics Program) and Mechanical and Aerospace Engineering participated in this expanded program. With this growth, the NASA-UVa Light Aerospace Alloy and Structures Technology Program (or LA^{2}ST Program) was formed within the School of Engineering and Applied Science at UVa.

Since 1989, the LA^{2}ST program has operated with full participation from 6 to 13 faculty and 10 to 15 graduate students, yearly, as outlined in the last 11 progress reports[7-19] and six grant renewal proposals[20-26]. Five 2-day Grant Review Meetings have been held in July at the Langley Research Center, with over 25 faculty and graduate students from UVa participating at each meeting[9,11,13,15,17,19]. Since 1990, undergraduate engineering students have been involved in research projects at both NASA-LaRC and UVa.

In October of 1991, E.A. Starke proposed a substantial enhancement to the base LA^{2}ST Program[27,28]. The objective of this supplement was to involve UVa faculty with engineering scientists from aluminum alloy producers and airframe manufacturers in a broad research program to develop aluminum alloys and composites for elevated temperature High Speed Civil Transport applications. This research began in January of 1992 and the results are separately reported. The LA^{2}ST and HSCT activities were merged in 1995[24].

Problem and Needs

Future aerospace structures require high performance light alloys and metal matrix composites with associated processing and fabrication techniques; new structural design methods and concepts with experimental evaluations; component reliability/ durability/damage tolerance prediction procedures; and a pool of masters and doctoral level engineers and scientists. Work on advanced materials and structures must be interdisciplinary and integrated. The thermal and chemical effects of aerospace environments on light metals and composites are particularly important to material performance. Nationally, academic efforts in these areas are limited. The NASA-UVa LA^{2}ST Program addresses these needs.

LA^{2}ST Program

As detailed in the original proposal[6] and affirmed in the most recent renewal[26], faculty from the Departments of Materials Science and Engineering, Mechanical and Aerospace Engineering, and Civil Engineering and Applied Mechanics at UVa have participated in the LA^{2}ST research and education program focused on high performance, light weight, aerospace alloys and structures. We aim to develop long term and interdisciplinary collaborations between graduate students, UVa faculty, and NASA-Langley researchers.

Our research efforts are producing basic understanding of materials performance, new monolithic and composite alloys, advanced processing methods, solid and fluid mechanics analyses, measurement advances, and new methods for modeling material microstructure and properties. A major product of the LA^{2}ST program is graduate students with interdisciplinary education and research experience in materials science, mechanics and mathematics. These advances should enable various NASA technologies.

The scope of the LA^{2}ST Program is broad. Three research areas are being investigated, including:

- Mechanical and Environmental Degradation Mechanisms in Advanced Light Metals and Composites,
- Aerospace Materials Science,
- Mechanics of Materials for Light Aerospace Structures.

Ten research projects are currently ongoing within these areas, and are reported here. These projects involve six faculty, and eleven graduate students. Ninety-one pct of

the graduate students are currently at the doctoral level (10 of 11), all are citizens of the United States, two are cosponsored by private industry, and two are conducting all research at the Langley Research Center. In each case the research provides the basis for the thesis or dissertation requirement of graduate studies at the University of Virginia. Each project is developed in conjunction with a specific LaRC researcher. Research is conducted at either UVa or LaRC, and under the guidance of UVa faculty and NASA staff. Participating students and faculty are closely identified with a NASA-LaRC branch.

Organization of Progress Report

This progress report first provides LA2ST Program administrative information including statistics on the productivity of faculty and graduate student participants, a history of current and graduated students, refereed or archival publications, and a list of ongoing projects with NASA and UVa advisors.

Ten sections summarize the technical accomplishments of each research project, emphasizing the period from July 1 to December 31, 1995. Each section contains a brief narrative of objective, recent progress, conclusions and immediate milestones. Appendices I through III document grant-sponsored publications, conference participation and citations of all LA2ST Progress Reports produced since 1986.

References

1. R.P. Gangloff, G.E. Stoner and M.R. Louthan, Jr., "Environment Assisted Degradation Mechanisms in Al-Li Alloys", University of Virginia, Proposal No. MS-NASA/LaRC-3545-87, October, 1986.

2. R.P. Gangloff, G.E. Stoner and R.E. Swanson, "Environment Assisted Degradation Mechanisms in Al-Li Alloys", University of Virginia, Report No. UVA/528266/MS88/101, January, 1988.

3. R.P. Gangloff, G.E. Stoner and R.E. Swanson, "Environment Assisted Degradation Mechanisms in Advanced Light Metals", University of Virginia, Report No. UVA/528266/MS88/102, June, 1988.

4. R.P. Gangloff, G.E. Stoner and R.E. Swanson, "Environment Assisted Degradation Mechanisms in Advanced Light Metals", University of Virginia, Report No. UVA/528266/MS89/103, January, 1989.

5. T.H. Courtney, R.P. Gangloff, G.E. Stoner and H.G.F. Wilsdorf, "The NASA-UVa Light Alloy Technology Program", University of Virginia, Proposal No. MS NASA/LaRC-3937-88, March, 1988.

6. R.P. Gangloff, "NASA-UVa Light Aerospace Alloy and Structures Technology Program", University of Virginia, Proposal No. MS NASA/LaRC-4278-89, January, 1989.

7. R.P. Gangloff, "NASA-UVa Light Aerospace Alloy and Structures Technology Program", University of Virginia, Report No. UVA/528266/MS90/104, August, 1989.

8. R.P. Gangloff, "NASA-UVa Light Aerospace Alloy and Structures Technology Program", University of Virginia, Report No. UVA/528266/MS90/105, December, 1989.

9. R.P. Gangloff, "NASA-UVa Light Aerospace Alloy and Structures Technology Program", UVa Report No. UVA/528266/MS90/106, June, 1990.

10. R.P. Gangloff, "NASA-UVa Light Aerospace Alloy and Structures Technology Program", UVa Report No. UVA/528266/MS91/107, January, 1991.

11. R.P. Gangloff, "NASA-UVa Light Aerospace Alloy and Structures Technology Program", UVa Report No. UVA/528266/MS91/108, July, 1991.

12. R.P. Gangloff, "NASA-UVa Light Aerospace Alloy and Structures Technology Program", UVa Report No. UVA/528266/MS92/109, January, 1992.

13. R.P. Gangloff, "NASA-UVa Light Aerospace Alloy and Structures Technology Program", UVa Report No. UVA/528266/MS93/111, July, 1992.

14. R.P. Gangloff, "NASA-UVa Light Aerospace Alloy and Structures Technology Program", UVa Report No. UVA/528266/MSE93/112, March, 1993.

15. R.P. Gangloff, "NASA-UVa Light Aerospace Alloy and Structures Technology Program", UVa Report No. UVA/528266/MSE93/113, July, 1993.

16. R.P. Gangloff, "NASA-UVa Light Aerospace Alloy and Structures Technology Program", UVa Report No. UVA/528266/MSE93/114, March, 1994.

17. R. P. Gangloff, "NASA-UVa Light Aerospace Alloy and Structures Technology Program," UVA Report No. UVA/528266/MSE94/116, July, 1994.

18. E.A. Starke, Jr. and R.P. Gangloff, "NASA-UVa Light Aerospace Alloy and Structures Technology Program", UVa Report No. UVA/528266/MSE94/117, March, 1995.

19. R.P. Gangloff, and E.A. Starke, Jr., "NASA-UVa Light Aerospace Alloy and Structures Technology Program", UVa Report No. UVA/528266/MS95/118, July, 1995.

20. R.P. Gangloff, "NASA-UVa Light Aerospace Alloy and Structures Technology Program", University of Virginia, Proposal No. MS- NASA/LaRC-4512-90, November, 1989.

21. R.P. Gangloff, "NASA-UVa Light Aerospace Alloy and Structures Technology Program", University of Virginia, Proposal No. MS- NASA/LaRC-4841-91, September, 1990.

22. R.P. Gangloff, "NASA-UVa Light Aerospace Alloy and Structures Technology Program", University of Virginia, Proposal No. MS- NASA/LaRC-5219-92, October, 1991.

23. R.P. Gangloff, "NASA-UVa Light Aerospace Alloy and Structures Technology Program", University of Virginia, Proposal No. MSE- NASA/LaRC-5691-93, November, 1992.

24. R.P. Gangloff, "NASA-UVa Light Aerospace Alloy and Structures Technology Program", Proposal No. MSE-NASA/LaRC-6074-94, University of Virginia, Charlottesville, VA, November, 1993.

25. R. P. Gangloff and E. A. Starke, Jr., "NASA-UVa Light Aerospace Alloy and Structures Technology Program," Proposal No. MSE-NASA/LaRC-6478-95, University of Virginia, Charlottesville, VA, November, 1994.

26. R.P. Gangloff and E.A. Starke, Jr., "NASA-UVA Light Aerospace Alloy and Structures Technology Program," Proposal No. MSE-NASA/LaRC-6855-96, University of Virginia, Charlottesville, VA, October, 1995.

27. R.P. Gangloff, E.A. Starke, Jr., J.M. Howe and F.E. Wawner, "NASA-UVa Light Aerospace Alloy and Structures Technology Program: Supplement on Aluminum Based Materials for High Speed Aircraft", University of Virginia, Proposal No. MS NASA/LaRC-5215-92, October, 1991.

28. R.P. Gangloff, E.A. Starke, Jr., J.M. Howe and F.E. Wawner, "NASA-UVa Light Aerospace Alloy and Structures Technology Program: Supplement on Aluminum Based Materials for High Speed Aircraft", University of Virginia, Proposal No. MSE NASA/LaRC-5691-93, November, 1992.

SUMMARY STATISTICS

Table I documents the numbers of students and faculty who have participated in the LA2ST Program, both during this reporting period and since program inception in 1986. Academic and research accomplishments are indicated by the degrees awarded, publications and presentations. Graduate students and research associates who participated in the LA2ST Program are named in Tables II and III, respectively.

TABLE I: LA2ST Program Statistics

	Current 7/1/95 to 12/31/95	Cumulative 1986 to 12/31/95
PhD Students--UVa:	9	22
--NASA-LaRC:	1	1
MS Students--UVa:	0	9
--NASA:	1	1
--VPI:	0	1
Undergraduates--UVa:	0	9
--NASA-LaRC:	2	15
Faculty--UVa:	6	12
--VPI:	0	1
Research Associates--UVa:	2	5
PhD Awarded:	2	15
MS Awarded:	0	7
Employers--NASA:	1	4
--Federal:	0	4
--University:	0	1
--Industry:	1	7
--Next degree:	0	5
Publications:	11	113
Presentations:	3	112
Dissertations/Theses:	2	22
NASA Reports:	1	22

TABLE II

GRADUATE STUDENT PARTICIPATION IN THE NASA-UVa LA²ST PROGRAM
December, 1995

POS #	GRADUATE STUDENT EMPLOYER	ENTERED PROGRAM	DEGREE COMPLETED	LANGLEY RESIDENCY	RESEARCH TOPIC	UVa/NASA-LaRC ADVISORS
1.	R. S. Piascik NASA-Langley	6/86	Ph.D. 10/89		Damage Localization Mechanisms in Corrosion Fatigue of Aluminum-Lithium Alloys	R. P. Gangloff D. L. Dicus
2.	J. P. Moran NIST	9/88	Ph.D. 12/89		An Investigation of the Localized Corrosion and Stress Corrosion Cracking Behavior of Alloy 2090	G. E. Stoner W. B. Lisagor
3.	R. G. Buchheit Sandia National Laboratories	6/87	Ph.D. 12/90		Measurements and Mechanisms of Localized Aqueous Corrosion in Aluminum-Lithium Alloys	G. E. Stoner D. L. Dicus
4.	D. B. Gundel Ph.D.-UVa	9/88	M.S. 12/90		Investigation of the Reaction Kinetics Between SiC Fibers and Titanium Matrix Composites	F. E. Wawner W. B. Brewer
5.	F. Rivet (VPI)	9/88	M.S. 12/90		Deformation and Fracture of Aluminum-Lithium Alloys: The Effect of Dissolved Hydrogen	R. E. Swanson (VPI) D. L. Dicus
6.	C. Copper Ph.D.-UVa	4/89	M.S. 12/90		Design of Cryogenic Tanks for Space Vehicles	W. D. Pilkey J. K. Haviland D. R. Rummler M.J. Shuart
7.	J. A. Wagner NASA-Langley	6/87	Ph.D.	PhD Research @ LaRC	Temperature Effects on the Deformation and Fracture of Al-Li-Cu-In Alloys	R. P. Gangloff W. B. Lisagor J. C. Newman
8.	W. C. Porr, Jr. David Taylor Naval Ship R&DC	1/88	Ph.D. 6/92		Elevated Temperature Facture of an Advanced Powder Metallurgy Aluminum Alloy	R. P. Gangloff C. E. Harris
9.	J. B. Parse Consultant	9/88	Ph.D. 6/92		Quantitative Characterization of the Spatial Distribution of Particles in Materials	J. A. Wert D. R. Tenney
10.	D. C. Slavik Knolls Atomic Power Laboratory	9/89	Ph.D. 6/93		Environment Enhanced Fatigue of Advanced Aluminum Alloys and Composites	R. P. Gangloff D. L. Dicus
11.	C. L. Lach NASA-Langley	9/89	M.S.	MS Research @LaRC	Effect of Temperature on the Fracture Toughness of Weldalite™ 049	R. P. Gangloff W. B. Lisagor

TABLE II (continued)

GRADUATE STUDENT PARTICIPATION IN THE NASA-UVa LA²ST PROGRAM
(continued)

POS #	GRADUATE STUDENT EMPLOYER	ENTERED PROGRAM	DEGREE COMPLETED	LANGLEY RESIDENCY	RESEARCH TOPIC	UVa/NASA-LaRC ADVISORS
12.	R. J. Kilmer General Motors	11/89	Ph.D. 9/93		Effect of Zn Additions on the Environmental Stability of Alloy 8090	G. E. Stoner W. B. Lisagor
13.	M. F. Coyle	12/89	Ph.D.		Visoplastic Response of High Temperature Structures	E. A. Thornton J. H. Starnes, Jr.
14.	C. J. Lissenden University of Kentucky; Engineering Mechanics	9/90	Ph.D. 6/93		Inelastic Response of Metal Matrix Composites Under Biaxial Loading	C. T. Herakovich M. J. Pindera W. S. Johnson
15.	C. Cooper AMP Incorporated	1/91	Ph.D. 6/93		Shell Structures Analytical Modeling	W. D. Pilkey J. K. Haviland M. Shuart J. Stroud
16.	Douglas Wall Babcock & Wilcox	4/91	Ph.D. 1/96		Measurements and Mechanisms of Localized Corrosion in Al-Li-Cu Alloys	G. E. Stoner D. L. Dicus
17.	S. W. Smith NASA-LaRC	4/91	Ph.D. 5/95		Hydrogen Interactions with Al-Li Alloys	J. R. Scully W. B. Lisagor
18.	D. B. Gundel Wright Laboratories US Air Force	4/91	Ph.D. 9/94		Effect of Thermal Exposure on the Mechanical Properties of Titanium/SiC Composites	F. E. Wawner W. B. Brewer
19.	K. McCarthy	5/91	M.S. 6/93 (Nonthesis)		Shell Structures Analytical Modeling	W. D. Pilkey M. J. Shuart J. Stroud
20.	M. Lyttle	12/91	M.S. 12/93		Superplasticity in Al-Li-Cu Alloys	J. A. Wert T. T. Bales
21.	T. Johnson NASA-LaRC	12/91	Ph.D. 6/93	(NASA Minority Grantee)	Shell Structures Analytical Modeling	W. D. Pilkey M. J. Shuart J. Stroud
22.	S. T. Pride Rohm and Haas	12/91	Ph.D. 6/94	(NASA Minority Grantee)	Metastable Pitting of Al Alloys	J. R. Scully D. L. Dicus
23.	M. A. Rowley	1/92	M.S. 12/93	(UVa AEP Sponsored)	Viscoplasticity of Metals	E. A. Thornton J. H. Starnes, Jr.
24.	M. J. Haynes	9/92	M.S./Ph.D. 5/94		Elevated Temperature Fracture of Advanced	R. P. Gangloff TBD
25.	M. Mason Allied Signal	9/92	M.S. 11/94		Environmental Effects in Fatigue Life Prediction	R. P. Gangloff R. S. Piascik

TABLE II (continued)

GRADUATE STUDENT PARTICIPATION IN THE NASA-UVa LA²ST PROGRAM
(continued)

POS #	GRADUATE STUDENT EMPLOYER	ENTERED PROGRAM	DEGREE COMPLETED	LANGLEY RESIDENCY	RESEARCH TOPIC	UVa/NASA-LaRC ADVISORS
26.	H. J. Koenigsmann	6/93	Ph.D.		Precipitation Hardening and Microstructural Stability in Al-Si-Ge-Cu	E.A. Starke, Jr. W.B. Lisagor
27.	E. Richey	9/93	M.S. 5/95		Computer Modeling of Environmental Fatigue Crack Propagation	R.P. Gangloff R.S. Piascik
28.	M. Lyttle	1/94	Ph.D.		Wide-Panel Aluminum Alloy Extrusions	J.A. Wert W.B. Lisagor
29.	Z. Gasem	1/94	Ph.D.		Time-Dependent Environmental Fatigue in 7000-Series Al Alloys	R.P. Gangloff R.S. Piascik
30.	S. P. Hayes	9/94	Ph.D.		Temperature and Hydrogen-Effects on Fracture in Ti Alloys	R.P. Gangloff D.L. Dicus
31.	S. M. Kazanjian	12/94	Ph.D.		Temperature and Microstructure Effects on Fracture in Ti Alloys	E.A. Starke, Jr. D.L. Dicus
32.	R. D. Schroedter, III	6/93	Ph.D.		Damage Evolution in Polymeric Composites	C.T. Herakovich C.E. Harris

TABLE III

Post-Doctoral Research Associate Participation
in NASA-UVA LA2ST Program
December, 1995

Pos #	Research Assoc.	Tenure	Research	Supervisor
1.	Yang Leng	3/89 to 12/91	Elevated Temperature Deformation and Fracture of PM AL Alloys and Composites	R. P. Gangloff
2.	Farshad Mizadeh	7/89 to 12/91	Deformation of Metal Matrix Composites	C. T. Herakovich Marek-Jerzy Pindera
3.	A. K. Mukhopadhyay	6/91 to 6/92	Aluminum Alloy Development	E. A. Starke, Jr.
4.	Sang-Shik Kim	12/91 to 2/94	Environmental Fatigue Life Prediction	R. P. Gangloff
5.	B. Skrotzki	1/95 to 9/95	Mechanical Property Anisotropy	E. A. Starke, Jr. G. J. Shiflet
6.	H. Hargarter	8/95	Mechanical Property Anisotropy	E. A. Starke, Jr. G. J. Shiflet
			Temperature and Microstructure Effects on Facture in Ti Alloys	E. A. Starke, Jr. D. L. Dicus

GRANT PUBLICATIONS: (REFEREED JOURNALS, ARCHIVAL VOLUMES AND NASA CONTRACTOR REPORTS)

The following papers are based on research conducted under LA2ST Program support, and are published in the referred or archival literature.

71. J.A. Wert and M.T. Lyttle, "Microstructure Evolution Dduring High-Temperature Deformation of Aluminum Alloys", 16th Riso International Symposium on Microstructural and Crystallographic Aspects of Recrystallization, N. Hansen, D. Juul Jensen, Y.L. Liu and B. Ralph (eds), Riso National Laboratory, Roskilde, Denmark, 1995, pp.589-594.

70. B. Skrotzki, G.J. Shiflet, and E.A. Starke, Jr. On the Effect of Sstress on Nucleation and Growth of Parecipitates in an Al-Cu-Mg-Ag Alloy. Submitted to Metallurgical Transactions A.

69. B. Skrotzki, H. Hargarter and E.A. Starke, Jr. Microstructural stability under creep conditions of two Al-Cu-Mg-Ag Alloys. Submitted to The 5th International Conference on Aluminum Alloys, ICAA-5, Grenoble, France.

68. B. Skrotzki, E.A. Starke, and G.J. Shiflet, "Alterung einer Al-Cu-Mg-Ag-Legierung unter äußerer Spannung," Hauptversammlung 1995 der Deutschen Gesellschaft für Materialkunde e.V., Bochum, Germany, June 6-9, 1995.

67. H. J. Koenigsmann and E. A. Starke, Jr., "Cavity Nucleation and Fracture in an Al-Si-Ge Alloy", submitted to Proceedings of the 5th International Conference on Aluminum Alloys - Their Physical and Mechanical Properties (Grenoble, France, July 1-5, 1996).

66. H. J. Koenigsmann, E. A. Starke, Jr., and P. E. Allaire, "Finite Element / Experimental Analysis of Cavity Nucleation in an Al-Si-Ge Alloy", Acta Metallurgica et Materialia, in press (1996).

65. J.R. Scully, Co-editor *"Electrochemical Noise-Application to Analysis and Interpretation of Corrosion Data,"* American Society for Testing of Materials Special Technical Publication, Philadelphia, PA, in press, 1995.

64. J.R. Scully, S.T. Pride, H.S. Scully, J.L.Hudson, "Some Correlations Between Metastable Pitting and Pit Stabilization in Metals" Electrochemical Society Localized Corrosion II Symposia Proceedings, P. Natishan, R. Newman, G. Frankel, R. Kelly, eds. Electrochemical Soc., in press, 1995. (invited)

63. S.T. Pride, S.T. Pride, J.L.Hudson, "Analysis of Electrochemical Noise from Metastable Pitting in Al, Aged Al-2%Cu and AA 2024-T3," in *"Electrochemical Noise - Application to Analysis and Interpretation of Corrosion Data,"* American Society for Testing of Materials Special Technical Publication, Philadelphia, PA, in press, 1995.

62. Michael J. Haynes and Richard P. Gangloff, "High Resolution R-Curve Characterization of the Fracture Toughness of Thin Sheet Aluminum Alloys", Journal of Testing and Evaluation, in review (1996).

61. Michael J. Haynes, Brian P. Somerday, Cynthia L. Lach and Richard P. Gangloff, "Micromechanical Modeling of Temperature-Dependent Initiation Fracture Toughness in Advanced Aluminum Alloys", in 27th National Symposium on Fatigue and Fracture Mechanics, ASTM STP, R.S. Piascik, R.P. Gangloff, N.E. Dowling and J.C. Newman, eds., ASTM, Philadelphia, PA, in press (1996).

60. B. Skrotzki, E. A. Starke and G. J. Shiflet, "The Effect of Stress on Nucleation and Growth of Precipitates in Al-Cu-Mg-X Alloys", Proc. of the 2nd International Conference on Microstructure and Mechanical Properties of Aging Materials, TMS-AIME, Warrendale, PA, in press (1995).

59. P.N. Kalu and J.A. Wagner, " A Microtexture Investigation of the Fracture Behavior of Al- Li Alloy 2090", Lightweight Alloys for Aerospace Applications III, TMS-AIME, Warrendale, PA, in press (1995).

58. Donald C. Slavik and Richard P. Gangloff, "Environment and Microstructure Effects on Fatigue Crack Facet Orientation in an Al-Li-Cu-Zr Alloy", Acta Metallurgica et Materialia, in press (1996).

57. S.T. Pride, J.R. Scully and J.L. Hudson, "Analysis of Electrochemical Noise from Metastable Pitting in Al, Aged Al-2%Cu and AA 2024-T3," in Electrochemical Noise Methods in Corrosion ASTM STP, ASTM, Philadelphia, PA, in review (1994).

56 R.G. Buchheit, G.E. Stoner and G.J. Shiflet, "Corrosion Properties of a Rapidly Solidified Al90Fe5Gd5 Alloy", J. Electrochem. Soc., in revision (1994).

55. C. J. Lissenden, B. A. Lerch, and C. T. Herakovich, "Response of SiC/Ti Tubes Under Combined Loading - Part III: Microstructural Evaluation", J. Composite Materials, in review (1994).

54. H.J. Koenigsmann and E.A. Starke, Jr., "Fracture Behavior in Al-Si-Ge Alloys", in Proceedings of the 2nd International Conference on Microstructures and Mechanical Properties of Aging Materials, TMS-AIME, Warrendale, PA, in press (1995).

53. S.S. Kim, M. J. Haynes and R.P. Gangloff, "Localized Deformation Control of Elevated Temperature Fracture in Submicron Grain Aluminum with Dispersoids", Materials Science and Engineering A, in press (1995).

52. R. S. Piascik and R. P. Gangloff, "Modeling Environment-Enhanced Fatigue Crack Growth in Al-Li-Cu-Zr," in Hydrogen Effects on Material Behavior, N. R. Moody and A. W. Thompson, eds., TMS-AIME, Warrendale, PA, in press (1995).

51. E.A. Thornton and J.D. Kolenski, "Viscoplastic Response of Structures with Intense Local Heating", Journal of Aerospace Engineering, in press (1995).

50. S. W. Smith and J. R. Scully, "Hydrogen Trapping and Its Correlation to the Hydrogen Embrittlement Susceptibility of Al-Li-Cu-Zr Alloys," in TMS Hydrogen Effects on Materials Behavior, N. R. Moody and A. W. Thompson, eds., TMS-AIME, Warrendale, PA, in press (1995).

49. C. J. Lissenden, C. T. Herakovich, and M-J. Pindera, "Response of SiC/Ti Tubes Under Combined Loading - Part II: Room Temperature Creep Effects", J. Composite Materials, in press (1995).

48. C. J. Lissenden, C. T. Herakovich, and M-J. Pindera, "Response of SiC/Ti Tubes Under Combined Loading - Part I: Theory and Experiment for Imperfect Bonding", J. Composite Materials, in press (1995).

47. E.A. Thornton, M.F. Coyle, and R.N. McLeod, "Experimental Study of Plate Buckling Induced by Spatial Temperature Gradients," Journal of Thermal Stresses, in press (1995).

46. C. J. Lissenden, C. T. Herakovich, and M-J. Pindera, "Inelastic Deformation of TMC Under Multiaxial Loading" in Life Prediction Methodology for Titanium Matrix Composites, ASTM STP, W.S. Johnson, ed., ASTM, Philadelphia, PA, in press (1995).

45. B. Skrotzki, E. A. Starke and G. J. Shiflet, "Effect of Texture and Precipitates on Mechanical Property Anisotropy of Al-Cu-Mg-X Alloys", Proc. of the 4th International Conference on Aluminum Alloys, Vol. II, EMAS, Warley Heath, UK p. 40 (1994).

44. R.G. Buchheit, F.D. Wall, G.E. Stoner and J.P. Moran, "Anodic Dissolution-Based Mechanism for the Rapid Cracking, Preexposure Phenomenon Demonstrated by Aluminum-Lithium-Copper Alloys", Corrosion, Vol. 51, pp. 417-428 (1995).

43. J. R. Scully, "Electrochemical Tests," in Manual on Corrosion Tests: Application and Interpretation, R. Baboian, ed., ASTM, Philadelphia, PA, pp. 75-90 (1995).

42. R.P. Gangloff, "Corrosion Fatigue Cracking", in Manual on Corrosion Tests: Application and Interpretation, R. Baboian, ed., ASTM, Philadelphia, PA, pp. 253-271 (1995).

41. M.E. Mason and R. P. Gangloff, "Modeling Time-Dependent Corrosion Fatigue Crack Propagation in 7000 Series Aluminum Alloys," in FAA/NASA International Symposium on Advanced Structural Integrity Methods for Airframe Durability and Damage Tolerance, C. E. Harris, ed., NASA Conference Publication 3274, Part 1, NASA-Langley Research Center, Hampton, VA, pp. 441-462 (1994).

40. J. M. Duva, J. Aboudi, and C. T. Herakovich, "A Probabilistic Micromechanics Model for Damaged Composites", Damage Mechanics in Composites, D. H. Allen and J. W. Ju, eds., ASME, AMD-Vol. 185, pp. 1-20 (1994).

39. S.T. Pride, J.R. Scully and J.L. Hudson, "Metastable Pitting of Aluminum and Criteria for the Transition to Stable Pit Growth," Journal of the Electrochemical Society, Vol. 141, No. 11, p. 3028 (1994).

38. C. J. Lissenden, C. T. Herakovich, and M-J. Pindera, "Damage Induced Room Temperature Creep of Titanium Matrix Composites", Durability of Composite Materials, R. C. Wetherhold, ed., ASME MD-Vol. 51, pp. 39-50 (1994).

37. H.J. Koenigsmann and E.A. Starke, Jr.,"Microstructural Stability and Fracture Behavior in Al-Si-Ge Alloys", Proceedings of the 4th International Conference on Aluminum Alloys - Their Physical and Mechanical Properties, T.H. Sanders, Jr. and E.A. Starke, Jr., eds., Atlanta, GA, Vol. II, pp. 24-31 (1994).

36. M.T. Lyttle and J.A. Wert, "Modeling of Continuous Recrystallization in Aluminum Alloys," Journal of Materials Science, Vol. 29, pp. 3342-3350 (1994).

35. Edward Richey, III, A.W. Wilson, J.M. Pope, and R.P. Gangloff, "Computer Modeling the Fatigue Crack Growth Rate Behavior of Metals in Corrosive Environments", NASA CR194982, NASA-Langley Research Center, Hampton, VA (1994).

34. R.G. Buchheit, J.P. Moran and G.E. Stoner, "The Electrochemical Behavior of the T1 (Al2CuLi) Intermetallic Compound and Its Role in Localized Corrosion of Al-3Cu-2Li Alloys", Corrosion, Vol. 50, pp. 120-130 (1994).

33. D. Gundel, P. Taylor and F. Wawner, "The Fabrication of Thin Oxide Coatings on Ceramic Fibers by a Sol-Gel Technique", Journal of Materials Science, Vol. 29, pp. 1795-1800 (1994).

32. M.T. Lyttle and J.A. Wert, "Simulative Modeling of Continuous Recrystallization of Aluminum Alloys", in Advances in Hot Deformation Textures and Microstructures, J.J. Jonas, T.R. Bieler and K.J. Bowman, eds., TMS-AIME, Warrendale, PA, pp. 373-383 (1994).

31. R.P. Gangloff, R.S. Piascik, D.L. Dicus and J.C. Newman, "Fatigue Crack Propagation in Aerospace Aluminum Alloys", Journal of Aircraft, Vol. 31, pp. 720-729 (1994).

30. W.C. Porr, Jr. and R.P. Gangloff, "Elevated Temperature Fracture of RS/PM Alloy 8009: Part I-Fracture Mechanics Behavior", Metall. Trans. A, Vol. 25A, pp. 365-379 (1994).

29. J. R. Scully, T. O. Knight, R. G. Buchheit, and D. E. Peebles, "Electrochemical Characteristics of the Al_2Cu, Al_3Ta and Al_3Zr Intermetallic Phases and Their Relevancy to the Localized Corrosion of Al Alloys," Corrosion Science, Vol. 35, pp. 185-195 (1993).

28. E.A. Thornton, "Thermal Buckling of Plates and Shells," Applied Mechanics Reviews, Vol. 46, No. 10, pp. 485-506 (1993).

27. R.P. Gangloff and Sang Shik Kim, "Environment Enhanced Fatigue Crack Propagation in Metals: Inputs to Fracture Mechanics Life Prediction", NASA CR-191538, NASA-Langley Research Center, Hampton, VA (1993).

26. R.S. Piascik and R.P. Gangloff, "Environmental Fatigue of an Al-Li-Cu Alloy: Part II - Microscopic Hydrogen Cracking Processes", Metall. Trans. A, Vol. 24A, pp. 2751-2762 (1993).

25. D.C. Slavik, J.A. Wert and R.P. Gangloff, "Determining Fracture Facet Crystallography Using Electron Back Scatter Patterns and Quantitative Tilt Fractography", Journal of Materials Research, Vol. 8, pp. 2482-2491 (1993).

24. D.C. Slavik, C.P. Blankenship, Jr., E.A. Starke, Jr. and R.P. Gangloff, "Intrinsic Fatigue Crack Growth Rates for Al-Li-Cu-Mg Alloys in Vacuum", Metall. Trans. A, Vol. 24A, pp. 1807-1817 (1993).

23. D. Gundel and F. Wawner, "The Influence of Defects on the Response of Titanium/SiC Fiber Composites to Thermal Exposure", Composites Engineering, Vol. 4, No. 1, pp. 47-65 (1993).

22. J.B. Parse and J.A. Wert, "A Geometrical Description of Particle Distributions in Materials", Modeling and Simulation in Materials Science and Engineering, Vol. 1, pp. 275-296 (1993).

21. D.C. Slavik and R.P. Gangloff, "Microscopic Processes of Environmental Fatigue Crack Propagation in Al-Li-Cu Alloy 2090", in Fatigue '93, Vol. II, J.-P. Bailon and J.I. Dickson, eds., EMAS, West Midlands, UK, pp. 757-765 (1993).

20. C.J. Lissenden, M-J. Pindera and C.T. Herakovich, "Response of SiC/Ti Tubes Under Biaxial Loading in the Presence of Damage," Damage Mechanics in Composites, D.H. Allen and D.C. Lagoudas, Eds., ASME- AMD-Vol. 150, pp. 73-90 (1992).

19. J.A. Wagner and R.P. Gangloff, "Fracture Toughness of Al-Li-Cu-In Alloys", Scripta Metallurgica et Materialia, Vol. 26, pp. 1779-1784 (1992).

18. R.G. Buchheit, Jr., J.P. Moran, F.D. Wall, and G.E. Stoner, "Rapid Anodic Dissolution Based SCC of 2090 (Al-Li-Cu) by Isolated Pit Solutions," Parkins Symposium on Fundamental Aspects of Stress Corrosion Cracking, S.M. Bruemmer, E.I. Meletis, R.H. Jones, W.W. Gerberich, F.P. Ford and R.W. Staehle, eds., TMS-AIME, Warrendale, PA, p. 141 (1992).

17. J.P. Moran, R.G. Buchheit, Jr., and G.E. Stoner, "Mechanisms of SCC of Alloy 2090 (Al-Li- Cu) - A Comparison of Interpretations from Static and Slow Strain Rate Techniques", Parkins Symposium on Fundamental Aspects of Stress Corrosion Cracking, S.M. Bruemmer, E.I. Meletis, R.H. Jones, W.W. Gerberich, F.P. Ford and R.W. Staehle, eds., TMS-AIME, Warrendale, PA, p. 159 (1992).

16. R.J. Kilmer, T.J. Witters and G.E. Stoner, "Effect of Zn Additions on the Precipitation Events and Implications to Stress Corrosion Cracking Behavior in Al-Li-Cu-Mg-Zn Alloys", Proceedings of the Sixth International Al-Li Conference, M. Peters and P.J. Winkler, eds., DGM Informationsgesellschaft, Verlag, pp. 755-760 (1992).

15. C.T. Herakovich and J.S. Hidde, "Response of Metal Matrix Composites with Imperfect Bonding", Ultramicroscopy, Vol. 40, pp. 215-228 (1992).

14. R.G. Buchheit, Jr., F.D. Wall, G.E. Stoner and J.P. Moran, "Stress Corrosion Cracking of Al- Li-Cu-Zr Alloy 2090 in Aqueous Cl- and Mixed Cl-/CO3-2 Environments", CORROSION/91, Paper No. 99, NACE, Houston, TX (1991).

13. R.P. Gangloff, D.C. Slavik, R.S. Piascik and R.H. Van Stone, "Direct Current Electrical Potential Measurement of the Growth of Small Fatigue Cracks", in Small Crack Test Methods, ASTM STP 1149, J.M. Larsen and J.E. Allison, eds., ASTM, Philadelphia, PA, pp. 116-168 (1992).

12. R.J. Kilmer and G.E. Stoner, "The Effect of Trace Additions of Zn on the Precipitation Behavior of Alloy 8090 During Artificial Aging", Proceedings, Light Weight Alloys for Aerospace Applications II, E.W. Lee, ed., TMS-AIME, Warrendale, PA, pp. 3-15, 1991.

11. W.C. Porr, Jr., Anthony Reynolds, Yang Leng and R.P. Gangloff, "Elevated Temperature Cracking of RSP Aluminum Alloy 8009: Characterization of the Environmental Effect", Scripta Metallurgica et Materialia, Vol. 25, pp. 2627-2632 (1991).

10. J. Aboudi, J.S. Hidde and C.T. Herakovich, "Thermo-mechanical Response Predictions for Metal Matrix Composites", in Mechanics of Composites at Elevated and Cryogenic Temperatures, S.N. Singhal, W.F. Jones and C.T. Herakovich, eds., ASME AMD, Vol. 118, pp. 1-18 (1991).

9. R.S. Piascik and R.P. Gangloff, "Environmental Fatigue of an Al-Li-Cu Alloy: Part I - Intrinsic Crack Propagation Kinetics in Hydrogenous Environments", Metallurgical Transactions A, Vol. 22A, pp. 2415-2428 (1991).

8. W.C. Porr, Jr., Y. Leng, and R.P. Gangloff, "Elevated Temperature Fracture Toughness of P/M Al-Fe-V-Si", in Low Density, High Temperature Powder Metallurgy Alloys, W.E. Frazier, M.J. Koczak, and P.W. Lee, eds., TMS- AIME, Warrendale, PA, pp. 129-155 (1991).

7. Yang Leng, William C. Porr, Jr. and Richard P. Gangloff, "Time Dependent Crack Growth in P/M Al-Fe-V-Si at Elevated Temperatures", Scripta Metallurgica et Materialia, Vol. 25, pp. 895-900 (1991).

6. R.J. Kilmer and G.E. Stoner, "Effect of Zn Additions on Precipitation During Aging of Alloy 8090", Scripta Metallurgica et Materialia, Vol. 25, pp. 243-248 (1991).

5. D.B. Gundel and F.E. Wawner, "Interfacial Reaction Kinetics of Coated SiC Fibers", Scripta Metallurgica et Materialia, Vol. 25, pp. 437-441 (1991).

4. R.G. Buchheit, Jr., J.P. Moran and G.E. Stoner, "Localized Corrosion Behavior of Alloy 2090-The Role of Microstructural Heterogeneity", Corrosion, Vol. 46, pp. 610-617 (1990).

3. Y. Leng, W.C. Porr, Jr. and R.P. Gangloff, "Tensile Deformation of 2618 and Al-Fe-Si-V Aluminum Alloys at Elevated Temperatures", Scripta Metallurgica et Materialia, Vol. 24, pp. 2163-2168 (1990).

2. R.P. Gangloff, "Corrosion Fatigue Crack Propagation in Metals", in Environment Induced Cracking of Metals, R.P. Gangloff and M.B. Ives, eds., NACE, Houston, TX, pp. 55-109 (1990).

1. R.S. Piascik and R.P. Gangloff, "Aqueous Environment Effects on Intrinsic Corrosion Fatigue Crack Propagation in an Al-Li-Cu Alloy", in Environment Induced Cracking of Metals, R.P. Gangloff and M.B. Ives, eds., NACE, Houston, TX, pp. 233-239 (1990).

COMPLETED PROJECTS: (1986 to present reporting period)

1. DAMAGE LOCALIZATION MECHANISMS IN CORROSION FATIGUE OF ALUMINUM-LITHIUM ALLOYS
   Faculty Investigator: R.P. Gangloff
   Graduate Student: Robert S. Piascik
   Degree: PhD
   UVa Department: Materials Science and Engineering (MS&E)
   NASA-LaRC Contact: D. L. Dicus (Metallic Materials)
   Start Date: June, 1986
   Completion Date: November, 1989
   Employment: NASA-Langley Research Center

2. AN INVESTIGATION OF THE LOCALIZED CORROSION AND STRESS CORROSION CRACKING BEHAVIOR OF ALLOY 2090 (Al-Li-Cu)
   Faculty Investigator: Glenn E. Stoner
   Graduate Student: James P. Moran
   Degree: PhD
   UVa Department: MS&E
   NASA-LaRC Contact: W.B. Lisagor (Metallic Materials)
   Start Date: September, 1988
   Completion Date: December, 1989
   Co-Sponsor: ALCOA
   Employment: ALCOA Laboratories

3. MECHANISMS OF LOCALIZED CORROSION IN AL-LI-CU ALLOY 2090
   Faculty Investigator: G.E. Stoner
   Graduate Student: R.G. Buchheit
   Degree: PhD
   UVa Department: MS&E
   NASA-LaRC Contact: D.L. Dicus (Metallic Materials)
   Start Date: June, 1987
   Completion Date: December, 1990
   Cosponsor: Alcoa
   Employment: Sandia National Laboratories

4. DEFORMATION AND FRACTURE OF ALUMINUM-LITHIUM ALLOYS: THE EFFECT OF DISSOLVED HYDROGEN
   Faculty Investigator: R.E. Swanson (VPI)
   Graduate Student: Frederic C. Rivet
   Degree: MS
   VPI Department: Materials Engineering
   NASA-LaRC Contact: D.L. Dicus (Metallic Materials)
   Start Date: September, 1988
   Completion Date: December, 1990
   Employment: Not determined

5. INVESTIGATION OF THE REACTION KINETICS BETWEEN SiC FIBERS AND SELECTIVELY ALLOYED TITANIUM MATRIX COMPOSITES AND DETERMINATION OF THEIR MECHANICAL PROPERTIES

Faculty Investigator: F.E. Wawner
Graduate Student: Douglas B. Gundel
Degree: MS
UVa Department: MS&E
NASA-LaRC Contact: D.L. Dicus and W.B. Brewer (Metallic Materials)
Start Date: January, 1989
Completion Date: December, 1990
Employment: Graduate School, University of Virginia; PhD candidate on LA^{2}ST Program; Department of Materials Science

6. DESIGN OF CRYOGENIC TANKS FOR SPACE VEHICLES

Faculty Investigators: W.D. Pilkey and J.K. Haviland
Graduate Student: Charles Copper
Degree: MS
UVa Department: Mechanical and Aerospace Engineering (MAE)
NASA-LaRC Contact: D.R. Rummler (Structural Mechanics Division), R.C. Davis and M.J. Shuart (Aircraft Structures)
Start Date: April, 1989
Completion Date: December, 1990
Employment: Graduate School, University of Virginia; PhD candidate on NASA- Headquarters sponsored program; Department of Mechanical and Aerospace Engineering

7. ELEVATED TEMPERATURE FRACTURE OF AN ADVANCED RAPIDLY SOLIDIFIED, POWDER METALLURGY ALUMINUM ALLOY

Faculty Investigator: R.P. Gangloff
Graduate Student: William C. Porr, Jr.
Degree: PhD
UVa Department: MS&E
NASA-LaRC Contact: C.E. Harris (Mechanics of Materials)
Start Date: January, 1988
Completion Date: June, 1992
Employment: David Taylor Naval Ship R&D Center

8. QUANTITATIVE CHARACTERIZATION OF THE SPATIAL DISTRIBUTION OF PARTICLES IN MATERIALS: APPLICATION TO MATERIALS PROCESSING

Faculty Investigator: John A. Wert
Graduate Student: Joseph Parse
Degree: PhD
UVa Department: MS&E
NASA-LaRC Contact: D.R. Tenney (Materials Division)
Start Date: September, 1988
Completion Date: June, 1992
Employment: Private Consultant

9. ENVIRONMENTAL FATIGUE CRACK GROWTH AND CRACKING MECHANISMS IN Al-Li-Cu Alloy 2090
   Faculty Investigator: R.P. Gangloff
   Graduate Student: Donald C. Slavik
   Degree: PhD
   UVa Department: MS&E
   NASA-LaRC Contact: D.L. Dicus (Metallic Materials)
   Start Date: September, 1989
   Completion Date: June, 1993
   Employment: Knolls Atomic Power Laboratory

10. INELASTIC DEFORMATION OF METAL MATRIX COMPOSITES UNDER BIAXIAL LOADING
   Faculty Investigators: Carl T. Herakovich and Marek-Jerzy Pindera
   Graduate Student: Mr. Clifford J. Lissenden
   Degree: PhD
   UVa Department: Civil Engineering and the Applied Mechanics Program
   NASA-LaRC Contact: W.S. Johnson (Mechanics of Materials)
   Start Date: September, 1990
   Completion Date: June, 1993
   Employment: University of Kentucky, Department of Engineering Mechanics

11. EFFECT OF TEMPERATURE ON THE RESPONSE OF METALLIC SHELL STRUCTURES
   Faculty Investigators: W.D. Pilkey and J.K. Haviland
   Graduate Student: Karen McCarthy
   Degree: MS (non-thesis)
   Graduate Student: Theodore Johnson (NASA Minority Grantee)
   Degree: PhD
   Employment: NASA-LaRC
   Graduate Student: Charles Copper
   Degree: PhD
   Employment: AMP Incorporated
   UVa Department: MAE
   NASA-LaRC Contact: M.J. Shuart and Jeffrey Stroud (Aircraft Structures)
   Start Date: April, 1991
   Completion Date: May, 1993

12. EFFECTS OF Zn ADDITIONS ON THE PRECIPITATION AND STRESS CORROSION CRACKING BEHAVIOR OF ALLOY 8090

Faculty Investigator: Glenn E. Stoner
Graduate Student: Raymond J. Kilmer
Degree: PhD
Department: MS&E
NASA-LaRC Contact: W.B. Lisagor (Metallic Materials)
Start Date: September, 1989
Completion Date: September, 1993
Cosponsor: Alcoa
Employment: General Motors

13. PROCESSING AND SUPERPLASTIC PROPERTIES OF WELDALITETM SHEET

Faculty Investigator: John A. Wert
Graduate Student: Mark Lyttle
Degree: MS
Department: MS&E
NASA-LaRC Contact: T.T. Bales (Metallic Materials)
Start Date: September, 1991
Completion Date: December, 1993
Employment: Graduate School, University of Virginia; PhD Candidate in Materials Science and Engineering

14. METASTABLE PITTING OF Al ALLOYS AND CRITERIA FOR THE TRANSITION TO STABLE PITTING

Faculty Investigators: John R. Scully and J.L. Hudson
Graduate Student: Sheldon T. Pride
Degree: PhD
Department: Chemical Engineering
NASA-LaRC Contact: D.L. Dicus (Metallic Materials)
Start Date: September, 1991
Completion Date: May, 1994
Cosponsor: NASA Graduate Student Researchers Program,Under Represented Minority Emphasis
Employment: Rohm and Haas Chemical Company

15. THE EFFECT OF THERMAL EXPOSURE ON THE MECHANICAL PROPERTIES OF Ti-1100/SCS-6 COMPOSITES

Faculty Investigator: F.E. Wawner
Graduate Student: Douglas B. Gundel
Degree: PhD
UVa Department: MS&E
NASA-LaRC Contact: D.L. Dicus and W.B. Brewer (Metallic Materials)
Start Date: April, 1991
Completion Date: June, 1994
Employment: Wright Laboratories (WL/MLLM), US Air Force Materials Laboratory

16. ENVIRONMENTAL EFFECTS IN FATIGUE LIFE PREDICTION: MODELING ENVIRONMENTAL CRACK PROPAGATION IN LIGHT AEROSPACE ALLOYS

Faculty Investigator: R. P. Gangloff
Graduate Student: Mark E. Mason
Degree: MS
UVa Department: MS&E
NASA-LaRC Contact: R. S. Piascik (Mechanics of Materials)
Start Date: January, 1992
Completion Date: November, 1994
Employment: Allied-Signal; Hopewell, VA

17. ENVIRONMENTAL EFFECTS IN FATIGUE LIFE PREDICTION: MODELING ENVIRONMENTAL CRACK PROPAGATION IN LIGHT AEROSPACE ALLOYS

Faculty Investigator: R. P. Gangloff
Graduate Student: Edward Richey, III
Degree: MS
UVa Department: MANE
NASA-LaRC Contact: R. S. Piascik (Mechanics of Materials)
Start Date: September, 1993
Completion Date: May, 1995
Employment: Graduate School, University of Virginia; PhD Candidate in Materials Science and Engineering

18. HYDROGEN INTERACTIONS IN ALUMINUM-LITHIUM 2090 AND SELECTED MODEL ALLOYS

Faculty Investigator: John R. Scully
Graduate Student: Stephen W. Smith; PhD Candidate
UVa Department: MS&E
NASA-LaRC Contact: W.B. Lisagor and D.L. Dicus (Metallic Materials)
Start Date: April, 1991
Anticipated Completion Date: May, 1995
Cosponsor: Virginia CIT
Employment: NASA-LaRC

19. MECHANISMS OF LOCALIZED CORROSION IN ALLOYS 2090 AND 2095

Faculty Investigator: G.E. Stoner
Graduate Student: F.D. Wall
UVa Department: MS&E
NASA-LaRC Contact: M.S. Domack (Metallic Materials)
Start Date: April, 1991
Completion Date: January, 1996
Employment: Babcock & Wilcox

ADMINISTRATIVE PROGRESS

Post Doctoral Participation

Dr. Hinrich Hargarter replaces Dr. Birgit Skrotzki as a Post Doctoral Fellow on the LA²ST Program. Dr. Skrotzki returned to Germany and has joined the faculty at the University of Bochum.

Graduate Student Recruitment

The LA²ST Program has encountered no problems in recruiting the best graduate students entering the participating Departments at UVa, and in sufficient numbers to achieve our education and research objectives. Ms. Susan M. Kazanjian joins the program after spending nine years in industry as a materials engineer. She received her B.S. in Materials Science and Engineering from Rensselaer Polytechnic Institute in May, 1986. Her LA²ST research focuses on microstructure/property relationships in Ti alloys.

Undergraduate Research Participation

In April of 1990, the LA²ST Program was increased in scope to include undergraduate engineering students. Four students worked at NASA-LaRC during the Summer of 1990, none were recruited for the 1991 program, and seven were successfully recruited to work at NASA-LaRC during the Summer of 1992. Each student was a rising senior in an engineering or science major closely related to aerospace materials and mechanics. Represented universities have included Harvard, Georgia Institute of Technology, Virginia Polytechnic Institute, Duke, the University of Missouri, California Polytechnical Institute, and North Carolina State University. Professor Glenn E. Stoner assumed responsibility for the 1993 Summer Undergraduate Program. In the summer of 1995, two students from the Pennsylvania State University and Duke University worked in the Metallic Materials Branch at NASA-LaRC. Two rising seniors from Duke and Pennsylvania State University will be participating in the program during the summer of 1996.

CURRENT PROJECTS

MECHANICAL AND ENVIRONMENTAL DEGRADATION MECHANISMS IN ADVANCED LIGHT METALS AND COMPOSITES

1. TIME-TEMPERATURE DEPENDENT FRACTURE IN ADVANCED WROUGHT INGOT METALLURGY, AND SPRAY DEPOSITED ALUMINUM ALLOYS
   Faculty Investigator: R.P. Gangloff
   Graduate Student: Michael J. Haynes; PhD (direct) candidate
   UVa Department: MS&E
   NASA-LaRC Contact: A. P. Reynolds (Metallic Materials)
   Start Date: September, 1992
   Completion Date: September, 1996
   Project #1

2. CRYOGENIC TEMPERATURE EFFECTS ON THE DEFORMATION AND FRACTURE OF Al-Li-Cu-In ALLOYS
   Faculty Investigator: R.P. Gangloff
   Graduate Student: John A. Wagner; PhD candidate and NASA-LaRC employee
   UVa Department: MS&E
   NASA-LaRC Contacts: W.B. Lisagor (Metallic Materials) and J.C. Newman (Mechanics of Materials)
   Start Date: June, 1987
   Anticipated Completion Date: December, 1995
   Project #2

3. EFFECTS OF AGING AND TEMPERATURE ON THE DUCTILE FRACTURE OF AA2095 AND AA2195
   Faculty Investigator: R.P. Gangloff
   Graduate Student: Cynthia L. Lach; MS candidate and NASA- LaRC employee
   UVa Department: MS&E
   NASA-LaRC Contacts: W.B. Lisagor (Metallic Materials)
   Start Date: August, 1990
   Anticipated Completion Date: December, 1995
   Project #3

4. MECHANISMS OF LOCALIZED CORROSION IN 2090 AND X2095
   Faculty Investigator: G.E. Stoner
   Graduate Student: Douglas Wall; PhD candidate
   UVa Department: MS&E
   NASA-LaRC Contact: M.S. Domack (Metallic Materials)
   Start Date: April, 1991
   Completion Date: December, 1995
   Cosponsor: Reynolds Metals Company (A. Cho)
   Project #4

5. HYDROGEN INTERACTIONS IN ALUMINUM-LITHIUM 2090 AND SELECTED MODEL ALLOYS

Faculty Investigator: John R. Scully
Graduate Student: Keith Eklund; PhD Candidate
UVa Department: MS&E
NASA-LaRC Contact: W.B. Lisagor and D.L. Dicus (Metallic Materials)
Start Date: April, 1991
Anticipated Completion Date: May, 1995
Cosponsor: Virginia CIT
Project #5

6a. MECHANISMS OF DEFORMATION AND FRACTURE IN HIGH STRENGTH TITANIUM ALLOYS: EFFECTS OF TEMPERATURE AND DISSOLVED HYDROGEN

Faculty Investigators: R. P. Gangloff
Graduate Student: Sean P. Hayes; PhD Candidate
UVa Department: MS&E
NASA-LaRC Contact: To be determined (Metallic Materials)
Start Date: September, 1994
Completion Date: September, 1997
Project #6a

6b. MECHANISMS OF DEFORMATION AND FRACTURE IN HIGH STRENGTH TITANIUM ALLOYS: EFFECTS OF TEMPERATURE AND MICROSTRUCTURE

Faculty Investigators: E. A. Starke, Jr.
Graduate Student: Susan M. Kazanjian, PhD Candidate
UVa Department: MS&E
NASA-LaRC Contact: To be determined (Metallic Materials)
Start Date: December, 1994
Completion Date: To be determined
Project #6b

AEROSPACE MATERIALS SCIENCE

7. EVALUATION OF WIDE-PANEL ALUMINUM ALLOY EXTRUSIONS

Faculty Investigator: John A. Wert
Graduate Student: Mark T. Lyttle, Ph.D. Candidate
UVa Department: Materials Science and Engineering
NASA-LaRC Contact: T. T. Bales (Metallic Materials)
Start Date: January, 1994
Completion Date: September, 1996
Project #7

8. Al-Si-Ge-Cu ALLOY DEVELOPMENT
Faculty Investigator: E.A. Starke, Jr.
Graduate Student: H.J. Koenigsmann, Ph.D. Candidate
UVa Department: Materials Science and Engineering
NASA-LaRC Contact: W.B. Lisagor
Start Date: September, 1993
Completion Date: To be determined
Project #8.

9. EFFECTS OF TEXTURE AND PRECIPITATES ON MECHANICAL PROPERTY ANISOTROPY OF Al-Cu-Mg-X ALLOYS
Faculty Investigators: E.A. Starke, Jr. and G.J. Shiflet
Graduate Student: None
Post Doctoral Research Associate: B. Skrotzki, H. Hargarter
UVa Department: Materials Science and Engineering
NASA-LaRC Contact: W.B. Lisagor
Start Date: January, 1995
Completion Date: To be determined
Project #9.

MECHANICS OF MATERIALS FOR LIGHT AEROSPACE STRUCTURES

10a: FREQUENCY-DEPENDENT FATIGUE CRACK PROPAGATION IN 7000 SERIES ALUMINUM ALLOYS IN AN AGGRESSIVE ENVIRONMENT
Faculty Investigator: R.P. Gangloff
Graduate Student: Z. Gasem, Ph.D. Candidate
UVa Department: MS&E
NASA-LaRC Contact: R.S. Piascik (Mechanics of Materials)
Start Date: January, 1992
Anticipated Completion Date: December, 1996
Project #10a

10b: COMPUTER MODELING ENVIRONMENTAL EFFECTS ON FATIGUE CRACK PROPAGATION IN LIGHT AEROSPACE ALLOYS
Faculty Investigator: R.P. Gangloff
Graduate Student: Edward Richey III; Ph.D. Candidate
UVa Department: MS&E
NASA-LaRC Contact: R.S. Piascik (Mechanics of Materials)
Start Date: January, 1992
Anticipated Completion Date: June, 1995 (Richey)
Project #10b

RESEARCH PROGRESS AND PLANS (July 1 to December 31, 1995)

Research progress, recorded during the period from July 1, 1995 to December 31, 1995, is summarized for each project in the following sections. The standard format includes the program objective, recent progress, conclusions, and immediate milestones:

Project #1: TIME-TEMPERATURE DEPENDENT FRACTURE IN ADVANCED WROUGHT INGOT METALLURGY AND SPRAY DEPOSITED ALUMINUM ALLOYS

Faculty Investigator: R.P. Gangloff
Graduate Assistant: Michael J. Haynes

Objectives

The first objective of this Ph.D. research is to characterize the initiation and growth fracture toughness of AA2519-type alloys as a function of temperature. A second goal is to establish the evolution and microscopic fracture mechanisms at ambient and elevated temperatures by studying microvoid nucleation, void growth, and shear instability controlled coalescence. A third goal is to evaluate a critical strain-critical distance micromechanical model of microvoid-based fracture. As a supplement to research on the AA2519-type alloys, we will study novel plastic instability fracture mechanisms in an ultra-fine grain sized aluminum alloy (cryogenically milled Al+2.5vol% Al_2O_3).

Background and Problem Statement

A significant effort is currently aimed at developing advanced aluminum alloys for elevated temperature aerospace applications, particularly for airframes such as the high speed civil transport[1,2]. Since existing precipitation hardened aluminum alloys (e.g., 2024, 7075/7475 and 2090/8090) may not be sufficient to meet microstructural stability combined with strength/ toughness requirements, new compositions of wrought ingot metallurgy, spray deposited, and rapidly solidified powder metallurgy (RS/PM) alloys are under development. As promising compositions are determined, it is necessary to characterize the critical effects of loading rate and temperature on fracture toughness and creep-fatigue damage tolerance, and to establish metallurgical fracture mechanisms and predictive micromechanical models for such properties.

Technical Approach

Research is currently focused on two alloy shets from the advanced ingot metallurgy class ([1] I/M 2519-T87 (+Mg+Ag): Al-5.75Cu-0.52Mg-0.30Mn-0.49Ag-0.16Zr-0.09V by wt% and [2] Peak Aged C416: Al-5.4Cu-0.5Mg-0.5Ag-0.3Mn-0.13Zr-0.09 by wt%), a spray formed and

extruded alloy (N203: Al-4.9Cu-0.5Mg-0.5Mn-0.4Ag-0.5Zr-0.2Ti-0.2V by wt%), and a cryogenically milled aluminum alloy in the ultra fine grain size class (CM Al: Al-3.0Al_2O_3 by wt%). The general approach was outlined in past renewal proposals[3-5]. In summary, our approach focuses on:

(1) Characterizing microstructures of as-received alloys through optical, scanning electron, and transmission electron microscopy.

(2) Implementing J-Integral fracture mechanics methods and direct current potential drop (DCPD) crack length measurements to determine crack initiation and propagation resistance at ambient and elevated temperatures.

(3) Establishing microstructural fracture paths and mechanisms through SEM fractography, crack tip profiles, and transmission electron microscopy.

(4) Performing uniaxial compression tests to determine yield strength, strain hardening exponent and strain rate sensitivity.

(5) Employing smooth and notched tensile tests to estimate intrinsic fracture strain as a function of stress state triaxiality.

(6) Evaluating the predictive capabilities of micromechanical models in explaining the temperature dependence of ductile fracture initiation toughness, K_{JICi}.

(7) Interrupting smooth and notched tensile tests at various strain levels before failure to determine the onset (using DCPD monitoring) and three dimensional distribution of microvoid damage in the notch root at ambient and elevated temperatures.

Progress During the Reporting Period

The results for this period are divided into three sections. Section I presents conclusions from a Journal of Testing and Evaluation (JTEVA) paper on our experimental method of determining initiation toughness and R-curve behavior for thin sheet aluminum alloys. The reproducibility of R-curve measurements on AA2024-T3 sheet are discussed. Section II discusses conclusions from a paper written on the micromechanical modeling of temperature-dependent initiation fracture toughness in advanced aluminum alloys. The paper has been peer reviewed and revised for publication in Elevated Temperature Effects on Fatigue and Fracture, ASTM STP 1296. Section III presents tensile results for spray formed and extruded N203.

Section I: High Resolution R-Curve Characterization

Initiation fracture toughness (K_{JICi}) and R-curve behavior (K_J-Δ a curves) have been determined under NASA-LaRC sponsored research for a variety of aluminum alloy sheets; including AA2519-T87 (+Mg), AA2519-T87 (+Mg+Ag), AA2024-T3, AA2650-T6, and C416

[6-8]. A manuscript detailing our experimental technique was submitted to the Journal of Testing and Evaluation[9]. Three testing issues were of great concern. First, what resolution of fracture initiation is necessary to obtain a lower bound initiation toughness, K_{JICi}, when plane strain constraint is rapidly lost with crack extension? Second, How do room temperature R-curves for AA2024-T3 (determined from our technique) compare to those of other laboratories participating in the NASA sponsored round-robin testing? Third, how reproducible are K_{JICi} and K_J- Δa measurements? The conclusions of the manuscript answer these questions and are listed below:

1. Direct current potential difference (DCPD) monitoring is an effective technique for detecting microvoid fracture initiation in precracked CT specimens of aluminum alloy sheet, with a resolution of 20 μm of crack tip damage. Crack initiation develops under plane strain constraint at the midplane of the thin CT specimen, and is thus representative of plane strain initiation toughness.

2. For 3.2 mm sheet of precipitation hardened 2xxx Al alloys, the plane strain initiation toughness measured according to ASTM E813 is thickness-dependent and 50% higher than the plane strain initiation toughness based on DCPD monitoring (K_{JICi}), due to a rapid loss of plane strain constraint with crack extension. The thickness criterion for geometry-independent initiation toughness is non-conservative for thin sheet aluminum alloys.

3. The plane strain initiation toughnesses of AA2024-T3 and AA2650-T6 are independent of specimen thickness, when K_{JICi} is defined based on high resolution detection of an early stage of crack tip process-zone damage.

4. Ambient temperature J- Δa resistance curves of 3.2 mm thick AA2024-T3 sheet, measured from CT specimens by the J-integral/DCPD method, are reproducible and compare closely with data from larger middle tension (MT) and smaller CT geometries.

5. Results from the small specimen J-integral/DCPD method are relevant to prediction of large specimen R-curve behavior, alloy development, and mechanistic studies.

Detection of Microvoid Fracture Initiation: A standard method was developed to define crack initiation for each fracture toughness experiment, using the electrical potential difference (V) versus load-line displacement (δ) curve. A characteristic V- δ curve for AA2519-T87 (+Mg+Ag) is shown in Figure 1(a). An estimated load-line displacement (δ') where the V-δ curve changes slope is used as a reference point for linear regressions to the V-δ data. Baseline V-δ data (i.e.- not associated with crack growth) are fit by linear regression from $0.5\delta'$ to $0.95\delta'$, while crack growth V-δ data are fit from $1.05\delta'$ to $1.30\delta'$. From $0.0\delta'$ to $0.5\delta'$, V-δ data were excluded from the baseline regression because of artifacts such as closure contact of the fatigue crack surface. These

linear fits are indicated in the figure. The change in slope of the V-δ curve is dramatic from the baseline fit (-0.06 μV/mm) to the crack growth fit (3.85 μV/mm). The intersection of the two linear fits indicates the transition from baseline response to crack growth, and the potential difference at this point (V_{ai}) is the potential difference associated with the fatigue precrack length (a_i). For V below V_{ai}, the crack length is assumed to equal a_i.

In practice, the DCPD technique resolves 0.1 μV to 0.2 μV changes, or 0.025% to 0.05% of the potential difference associated with a_i. A fracture initiation toughness, representative of 20 μm of process-zone crack growth, is defined by a positive 0.2 μV vertical offset of the baseline V-δ regression. The intersection of the 0.2 μV offset fit and crack growth fit defines fracture initiation; the associated V_i and δ_i are shown in Figure 1(a). J-integral expressions from ASTM E1152 are used with a potential difference-crack length calibration to calculate J and Δa from measured load (P), V, and δ. The J value at the data point (P_i, V_i, δ_i) is J_{ICi}, the DCPD-detected fracture initiation toughness, which is readily converted to K_{JICi} [9].

Crack initiation in AA2519+Mg+Ag developed by void nucleation at large constituent particles, followed by limited void growth and coalescence to the precrack tip (pt) by void-sheeting coalescence (Figure 1(b)). The large constituents are primarily undissolved Al_2Cu, and void sheeting coalescence involves void nucleation, growth, and coalescence at submicron dispersoids located between constituent-nucleated voids. Optically measured crack growth of 86 μm is in excellent agreement with 88 μm of crack growth calculated from the increase in measured V (Figure 1(a)) using a potential difference-crack length calibration relationship [9].

Reproducibility of K_J- a Measurements for AA2024-T3: The K_J-Δa curve for 3.2 mm sheet of AA2024-T3 is reproducible, as shown by the four replicate experiments in Figure 2. R-curves for each CT specimen correspond closely, even with the introduction of sidegrooves (2024#1)[1]. Table 1 list parameters from K_J-Δa, including K_{JICi}, K_{JIC}, and K_J^{3mm}. Average values, standard deviations, and a 95% confidence interval, also listed in Table 1, quantify the precision of each measurement. Based on the statistics, we are "95% confident" that the true mean of K_{JICi} is between 29.6 MPa$\sqrt{m}$ and 37.0 MPa$\sqrt{m}$, that the true mean of K_{JIC} is between 42.9 MPa$\sqrt{m}$ and 54.1 MPa$\sqrt{m}$, and that the true mean of K_J is between 83.0 MPa m and 88.4 MPa$\sqrt{m}$. K_{JIC} for

---

1 The agreement between R-curves for CT specimens that are sidegrooved and not sidegrooved is unexpected. Sidegrooves are thought to promote plane strain constraint ahead of the crack tip, and the R-curve should be less steep.

AA2024-T3 is about 50% higher than K_{JICi} for 3.2 mm thick CT specimens, and is an overestimate of the true initiation toughness. The "average" K_J-Δa curve for 3.2 mm sheet of AA2024-T3 compares well to R-Curves determined by NASA-LaRC and Fracture Technology Associates with the same alloy sheet [9,10].

Section II: Micromechanical Modeling of Initiation Fracture Toughness

The temperature dependence of K_{JICi} was modeled for a variety of the advanced aluminum alloys characterized under separate NASA-LaRC sponsored research [6,11-18]. The model predicted temperature dependencies for precipitation-hardened ingot metallurgy alloys (AA2519, AA2095, AA2195, and AA2618), a spray formed alloy (N203), ultra-fine grain size alloys (AA8009 and cryogenically milled aluminum), and a metal matrix composite (AA2009/SiC/20p). The critical plastic strain-controlled model discussed in previous reports[6,12] was revised by incorporating a locus of failure strain *vs* stress state triaxiality and new crack-tip stress and strain fields. The failure locus replaces the somewhat ambiguous constraint ratio that we employed previously to account for the triaxial stress state ahead of the crack tip.

A manuscript, which discusses the model and its applicability to predicting the temperature dependencies of the eight alloys mentioned above, was peer reviewed and revised for publication in Elevated Temperature Effects on Fatigue and Fracture, ASTM STP 1296[19]. The conclusions of the manuscript are listed below:

1. The critical plastic strain-controlled model successfully predicts the temperature dependence of initiation fracture toughness (K_{JICi}) for a variety of advanced aluminum alloys that crack by microvoid processes. Predictions are based on smooth bar tensile deformation properties, an estimate of the exponential decay of the fracture strain (ε_f^p) with stress-state triaxiality (σ_m/σ_{fl}), and a single adjustable parameter (the critical microstructural distance, l*).

2. Approximately temperature insensitive K_{JICi} is predicted and observed for 2000 series precipitation-hardened alloys from cryogenic to elevated temperatures, while a degradation of K_{JICi} with increasing temperature is correctly modeled for submicron grain size alloys.

3. The temperature dependencies of K_{JICi} are traceable to the interplay between thermally-sensitive intrinsic fracture resistance and the crack tip strain field that is temperature dependent through σ_{ys}, E, and n. Both components are necessary to predict temperature insensitive initiation toughness in precipitation hardened aluminum alloys, where the fracture strain (ε_f^p) generally rises with temperature and σ_{ys}, E, and n decline.

4. The model correctly accounts for the effect of manganese on the toughness of AA2134, including changes in the nearest neighbor particle spacing as Mn-rich constituents form, varying ε_f^* due to slip mode changes, and a varying dependence of ε_f^p on σ_m/σ_{fl}.

5. Uncertainties in the critical distance l* and the failure loci $\bar{\varepsilon}_f^p(\sigma_m/\sigma_{fl})$ preclude predictions of absolute values of K_{JICi}. Accurate determination of $\bar{\varepsilon}_f^p(\sigma_m/\sigma_{fl})$ is complicated by the need to correlate damage at the initiation event, within tensile specimens and the process zone ahead of a crack tip. The Bridgman approximation of ε_f^p, uncertainty in the deformation history, and uncertainty in the alloy-dependent effect of σ_m/σ_{fl} on $\bar{\varepsilon}_f^p$ also hinder accurate measurements.

6. Model calculated critical distance, l*, correlates with the nearest neighbor spacing of second phase particles in a volume (Δ_3) for several aluminum alloys and steels, and $l^*/_3$ correlates with the extent of primary void growth (R_V/R_I). Both correlations suggest an approach to predict absolute toughness values from tensile properties coupled with microstructural and fractographic observations.

Interpretation of Calculated l:* The critical distance, the sole adjustable parameter in the strain-controlled model, is calculated by equating the measured and predicted K_{JICi} at a single temperature, and hence depends on accurate determination of this measured initiation toughness and each model input. Calculated l* is not affected significantly by measurements or estimates of σ_{ys} and E. Values of d_n vary modestly depending on whether analytical[20] or FEM[21] solutions are employed, affecting calculated l* by about 20%. The strongest effect on calculated l* is uncertainties in measuring the failure locus $\bar{\varepsilon}_f^p(\sigma_m/\sigma_{fl})$; generally $\bar{\varepsilon}_f^p(\sigma_m/\sigma_{fl})$ is overestimated, causing l* to be underestimated.

Ultimately, l* must be determined by an independent means for absolute toughness predictions. This distance should relate to the primary void-nucleating particle spacing for alloys that fail by microvoid fracture, and may represent the distance required for void coalescence at $K=K_{JICi}$. The nearest-neighbor spacing of primary void-nucleating particles, randomly distributed in a plane (Δ_2) or in a volume (Δ_3), should relate to l*, because the nearest neighbor particles govern the direction and size scale of void coalescence.

Tensile and K_{IC} data were available for steels, such that l* could be calculated with the model and compared to Δ_3[22,23]. Figure 3 shows correlations between l* and Δ_3 for steels (solid symbols) and six of the advanced Al alloys (open symbols) studied under NASA-LaRC sponsored research. The distance, l*, was calculated using the model and measured σ_{ys}, E, n, (%RA), and

K_{JICi}. The standard deviation of l^* is given for the aluminum alloys, where the error bars include the effect of temperature, if any, on l^*.

The data in Figure 3 are analyzed further based on the extent of primary void growth prior to coalescence. Data legends with an asterisk represent alloys where the primary void growth ratio was quantified by the measured ratio of the final void radius (R_V) to the nucleating-particle radius (R_I). Values of R_V and R_I were measured from fracture-surface dimples in high constraint regions, directly ahead of the specimen fatigue precrack[22,23]. Figure 4 displays a unique relationship between R_V/R_I and l^*/Δ_3. The function $l^*/\Delta_3 = 1.24 + 0.038(R_V/R_I)^2$ was obtained by least squares curve fitting, with a coefficient of determination (r^2) equal to 0.71. For no primary void growth ($R_V/R_I=1$), voids coalesce spontaneously upon nucleation, and l^*/Δ_3 might be expected to equal one. The quadratic fit yields an l^*/Δ_3 value of 1.28 at R_V/R_I equal to one. Because this value is reasonably close to one, it provides a physical basis for the correlation.

The effect of primary void growth on l^*/Δ_3 in Figure 4 is interpreted as follows. The critical distance for each alloy is a fixed multiple of Δ_3, with the multiple dependent on R_V/R_I. The parameter R_V/R_I is a direct measure of an alloy's resistance to void coalescence. The steels in Figure 4 posses higher R_V/R_I ratios relative to AA2519+Mg+Ag due to higher n (which retards coalescence) and/or a unimodal particle distribution (which precludes strain softening between primary voids). For the high R_V/R_I case, primary void growth allows particles further from the crack tip to nucleate voids as K increases and the plastic strain distribution spreads. Since more particles are involved in the critical coalescence event that constitutes K_{JICi}, l^* is a larger multiple of Δ_3. For the low R_V/R_I case (such as in AA2519+Mg+Ag), the void-coalescence conditions are satisfied before void damage accumulates over more than one or two particle spacings. The bimodal particle distribution favors this behavior because secondary void damage from smaller second-phase particles promotes void sheeting between primary voids [12,24]. The ratio, l^*/Δ_3, is relatively low due to this strain-localized coalescence.

Section III - Spray Formed N203 Extrusion: Flow Curves

Figure 5 shows true stress-true strain curves for Spray Formed N203 as a function of temperature, as well as curve fits to the Ramberg-Osgood constitutive relationship[6,25]. The yield strength, elastic modulus, and strain hardening exponent (n) decrease with increasing temperature and %RA increases, as shown in Table 2. N203 displays higher work hardening relative to I/M AA2519+Mg+Ag[8].

Proposed Research for Next Reporting Period

For the remainder of this Ph.D. research, we plan to complete fracture toughness characterization of spray formed N203 extrusion and I/M C416 sheet, as well as investigate the relationship between fracture toughness and continuum and microstructural mechanisms of microvoid fracture. For the latter study, the alloys AA1100, AA2519+Mg+Ag, and CM Al are chosen since they exhibit markedly different fracture evolutions. Microvoid fracture in AA1100 should be characterized by void nucleation and growth from iron- and silicon-based constituents, with void coalescence by void impingement. In AA2519+Mg+Ag, the growth of voids nucleated at undissolved Al_2Cu particles is truncated by void sheeting associated with submicron dispersoids. Fracture of CM Al at elevated temperature is characterized by void nucleation at clusters of Al_2O_3 dispersoids, followed by irregular void growth and strain localized void coalescence. These three alloys cover a wide range of the primary void growth ratio R_V/R_I, which should be high for AA1100, intermediate for AA2519+Mg+Ag, and low for CM Al.

In each of the three alloys, smooth and notched tensile experiments will be interrupted at various strains prior to coalescence. The goal of these fracture evolution study is to determine local conditions for microvoid coalescence, and to relate the extent of primary void growth to the critical distance l^*. Local conditions for void coalescence will depend on strain hardening, strain rate hardening, and the distribution of second phase particles. All three alloys will be characterized at 25°C. To study the influence of temperature on microvoid fracture in an alloy where ductility rises with temperature and in an alloy where ductility decreases, AA2519+Mg+Ag and CM Al will be characterized at 150°C and 175°C, respectively.

December of 1996 is scheduled tentatively as a completion date for the Ph.D. dissertation. To complete the dissertation research, we propose to:

1) Complete measurements of J-Δa resistance curves for N203 extrusion and C416 sheet (from 25°C to 200°C) and determine the plane strain initiation toughness (K_{JICi}) and plane stress tearing modulus (T_R^{ps}) from each curve.
2) Measure the J-Δa resistance curve for AA1100 at ambient temperature and determine K_{JICi} and T_R^{ps}.
3) Employ SEM methods, including high-magnification tilt fractography and stereo-pair viewing, to explore the role of microstructure and temperature on void nucleation as well as on localized shear instabilities affecting void growth to coalescence.

4) Measure the primary void growth ratio (R_V/R_I) from the CT fracture surfaces of AA1100 tested at 25°C.

5) Determine the strain rate sensitivity of flow stress (m) at 25°C and 150°C for AA2519+Mg+Ag and at 25°C and 175°C for CM Al with compression strain-rate change tests.

6) Deform uniaxial and notched tensile bars of AA1100, AA2519+Mg+Ag, and CM Al to various levels of strain before the onset of void coalescence, and interrupted prior to fracture.

7) Monitor damage in these tensile bars by the in-situ DCPD technique and by precise density measurements.

8) Section interrupted tensile bars to the midplane and observe microstructural aspects and micromechanisms of dimpled rupture.

9) Using transmission electron microscopy, observe void nucleation at dispersoids in AA2519+Mg+Ag with thin foils taken from interrupted tensile experiments.

10) If time permits, construct a FEM mesh to simulate the influences of strain and strain rate hardening on intravoid strain localization.

Throughout this work, we strive to understand the factors that affect intravoid plastic instability, and how such processes affect microvoid coalescence and fracture toughness in advanced aluminum alloys.

References

1. W.B. Lisagor, in Thermal Structures and Materials for High-Speed Flight, E.A. Thornton, Ed., Volume 140, *Progress in Astronautics and Aeronautics*, A.R. Seebass, Editor-in-Chief, AIAA, Washington, DC, pp. 161-179, (1992).

2. R.P. Gangloff, E.A. Starke, Jr., J.M. Howe and F.E. Wawner,Jr., "Aluminum Based Materials for High Speed Aircraft", University of Virginia, Proposal No. MS-NASA/LaRC-5691-93, November (1992).

3. R.P. Gangloff, "NASA-UVa Light Aerospace Alloy and Structures Technology Program", Proposal No. MSE-NASA/LaRC-6074-94, November (1993).

4. R.P. Gangloff, "NASA-UVa Light Aerospace Alloy and Structures Technology Program", Proposal No. MSE-NASA/LaRC-6478-95, November (1994).

5. R.P. Gangloff, "NASA-UVa Light Aerospace Alloy and Structures Technology Program", Proposal No. MSE-NASA/LaRC-6855-96, November (1995).

6. R.P. Gangloff, "NASA-UVa Light Aerospace Alloy and Structures Technology Program", University of Virginia Report No. UVA/528266/MSE94/114, March (1994).

7. R.P. Gangloff, "NASA-UVa Light Aerospace Alloy and Structures Technology Program", University of Virginia Report No. UVA/528266/MSE94/116, July (1994).

8. R.P. Gangloff, "NASA-UVa Light Aerospace Alloy and Structures Technology Program", University of Virginia Report No. UVA/528266/MS95/118, July (1995).

9. M.J. Haynes and R.P. Gangloff, "High Resolution R-Curve Characterization of the Fracture Toughness of Thin Sheet Aluminum Alloys", Journal of Testing and Evaluation, in review, (1996).

10. A.P. Reynolds, "Multilab Comparison of R-Curve Methodologies: Alloy 2024-T3," *NASA CR 195004*, NASA-Langley Research Center, Hampton, VA, 1994.

11. R.P. Gangloff, "NASA-UVa Light Aerospace Alloy and Structures Technology Program", University of Virginia Report No. UVA/528266/MS93/112, March (1993).

12. R.P. Gangloff, "NASA-UVa Light Aerospace Alloy and Structures Technology Program", University of Virginia Report No. UVA/528266/MS94/117, March (1995).

13. B.P. Somerday, "Elevated Temperature Fracture Toughness of a SiC Particulate-Reinforced 2009 Aluminum Composite", Masters Thesis, University of Virginia, (1993).

14. B.P. Somerday, Yang Leng, and R.P. Gangloff, Fatigue and Fracture of Engineering Materials and Structures, vol. 18, pp. 565-582, (1995).

15. B.P. Somerday, Yang Leng, and R.P. Gangloff, Fatigue and Fracture of Engineering Materials and Structures, vol. 18, pp. 1031-1050, (1995).

16. W.C. Porr, Jr., "Elevated Temperature Fracture of Advanced Powder Metallurgy Aluminum Alloy 8009", PhD Dissertation, University of Virginia, (1992).

17. W.C. Porr, Jr., and R.P. Gangloff, Metall. Trans. A, vol. 25A, pp. 365-379, (1994).

18. S.S Kim, M.J. Haynes, and R.P. Gangloff, Materials Science and Engineering A, Vol. 203, pp. 256-271, (1995).

19. M.J. Haynes, B.P. Somerday, C.L. Lach, and R.P. Gangloff, "Micromechanical Modeling of Temperature-Dependent Initiation Fracture Toughness in Advanced Aluminum Alloys", in Elevated Temperature Effects of Fatigue and Fracture, ASTM STP 1296, R.S. Piascik, R.P. Gangloff, N.E. Dowling, and A. Saxena, eds., ASTM, Philadelphia, PA, in press, (1996).

20. C.F. Shih, Journal of Mechanics and Physics of Solids, Vol. 29, pp. 305-326, (1981).

21. R.M. McMeeking, Journal of Mechanics and Physics of Solids, Vol. 25, pp. 357-381, (1977).

22. J.W. Bray, K.J. Handerhan, W.M. Garrison, Jr., and A.W. Thompson, Metallurgical Transactions A, Vol. 23A, pp. 485-496, (1992).

23. J.A. Psioda, "The Effect of Microstructure and Strength on the Fracture Toughness of an 18 Nickel 300 Grade Maraging Steel", Ph. D. Thesis, Carnegie Mellon University, Pittsburgh, PA, (1977).

24. M.J. Haynes and R.P. Gangloff, "Elevated Temperature Fracture Toughness of an Al-Cu-Mg-Ag Alloy", Metall. Trans. A, in review, (1996).

25. Y. Leng, W.C. Porr, Jr., and R.P. Gangloff, Scripta Metallurgica et. Materials, Vol. 24 (11), pp. 2163-2168, (1990).

Table 1 - Elastic-Plastic and Equivalent Linear-Elastic Initiation and Growth Fracture Toughnesses for 3.2 mm Thick Sheet of AA2024-T3.

Sample Id.	Test Temperature (°C)	K_{JICi} (MPa√m)	K_{JIC} (MPa√m)	K_{JIC}/K_{JICi}	K_J3mm (MPa√m)
2024-#1	25	32.6	45.8	1.40	85.5
2024-#2		36.7	52.4	1.43	86.9
2024-#3		32.0	45.2	1.41	86.9
2024-#4		31.9	50.5	1.58	83.4
Average		33.3	48.5	1.46	85.7
St. Dev.		±2.3	±3.5	±0.08	±1.7
95% C.I.		±3.7	±5.6	±0.13	±2.7

Table 2 - Tensile Results for Spray Formed N203 Extrusion

Test Temperature (°C)	σ_{ys} (MPa)	E (GPa)	n	%RA
25	447	72.1	.085	26.4
100	432	70.7	.063	42.5
150	392	68.9	.045	46.3
190	342	66.0	.016	61.2

a)

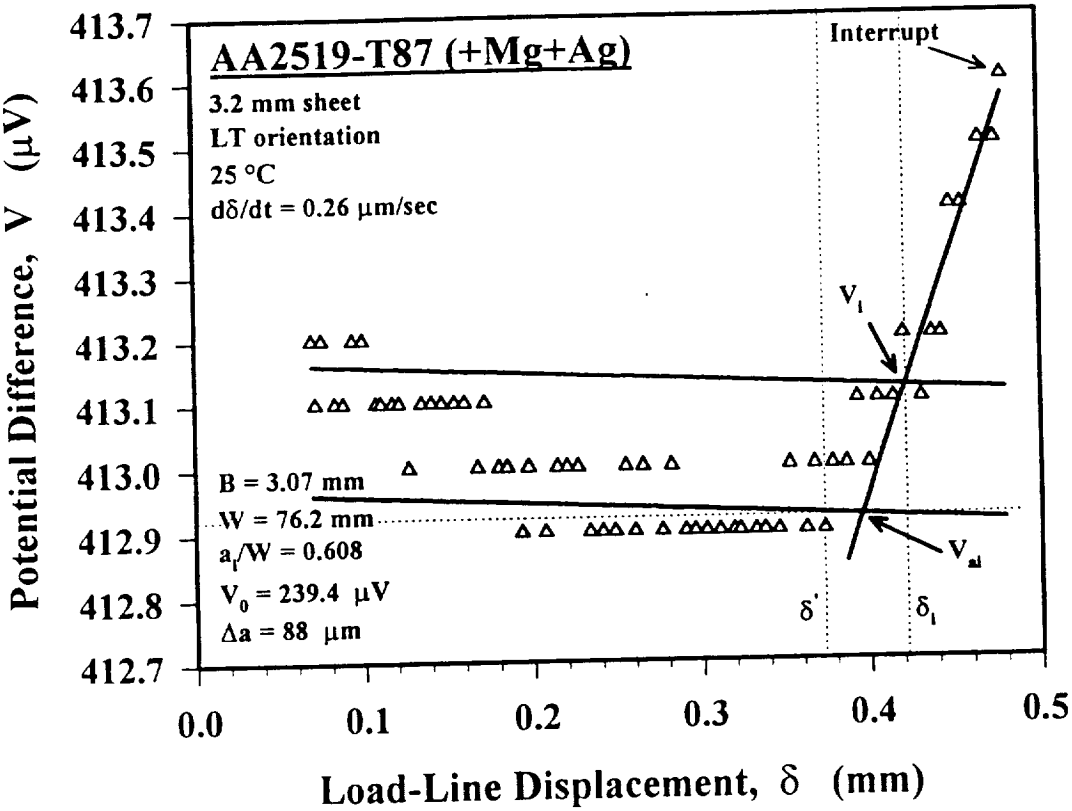

b)

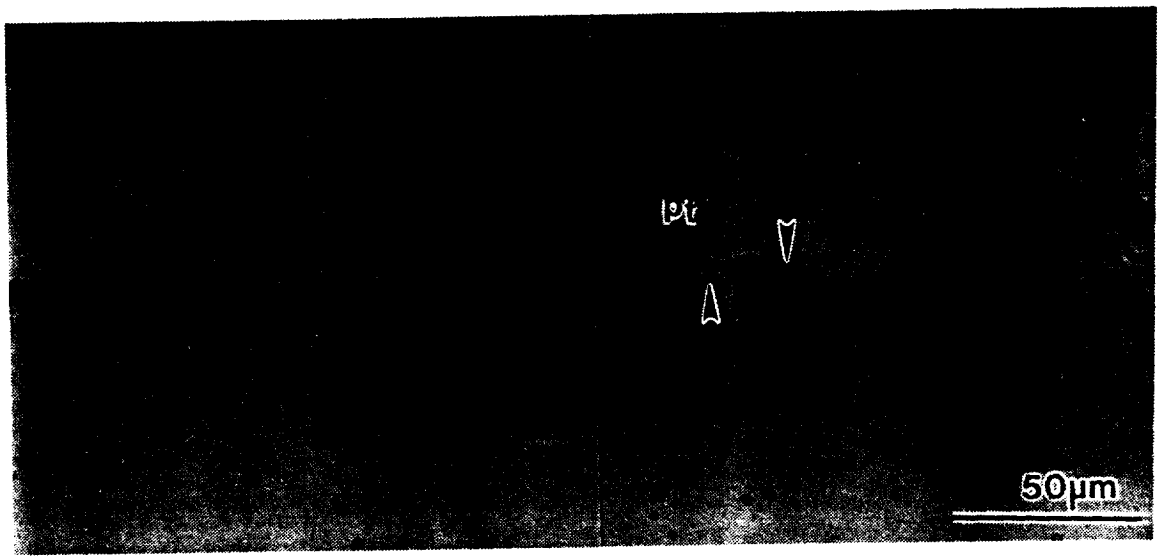

Figure 1: (a) Electrical potential difference versus load-line displacement trace from an interrupted rising-test. (b) The corresponding polished crack tip profile of AA2519-T87 (+Mg+Ag) illustrating the process-zone damage associated with ductile fracture initiation near K_{JICi}. Voids nucleate at large second phase particles and coalesce with the precrack tip (pt) by void sheet coalescence (arrows).

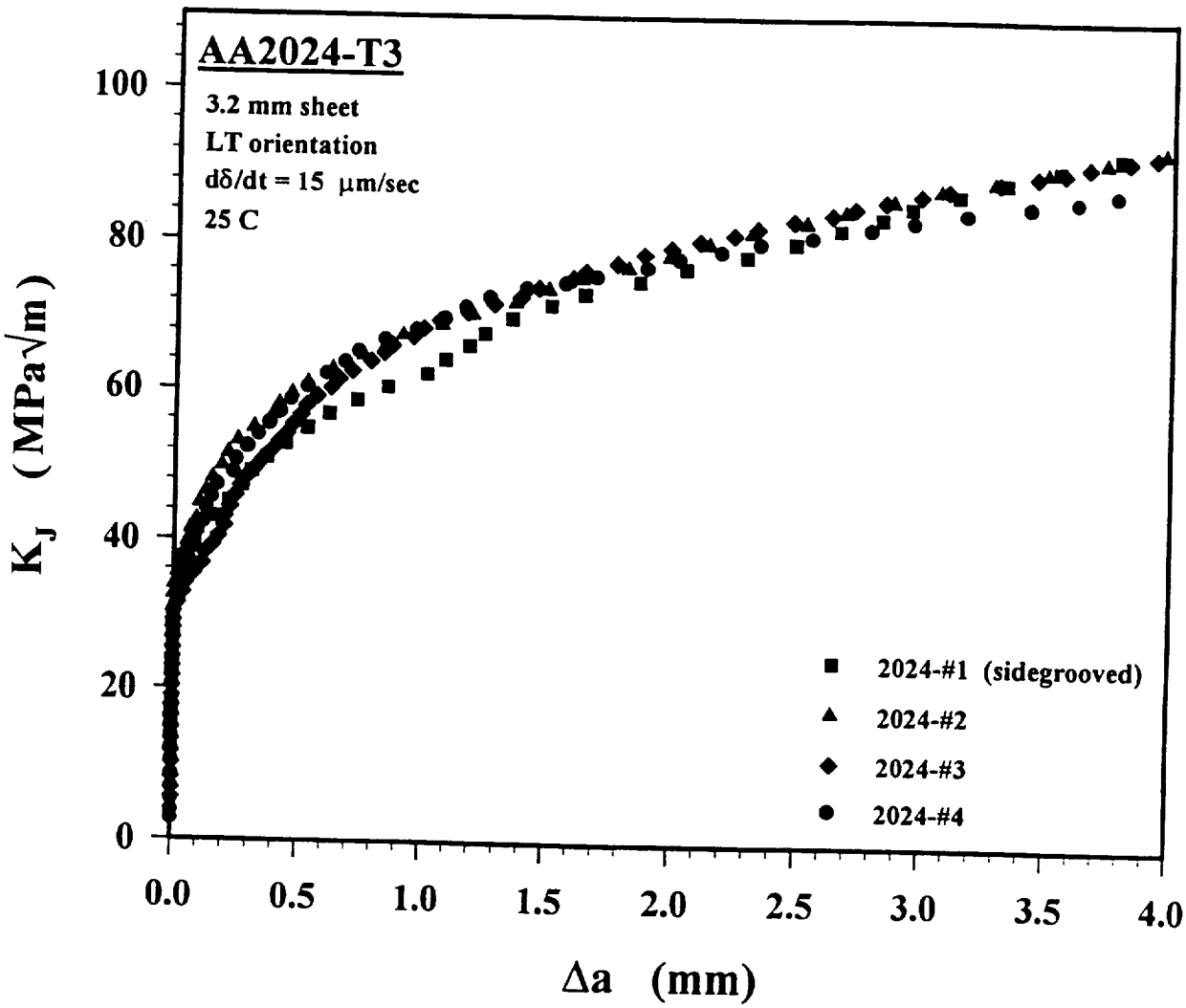

Figure 2: Replicate R-curve experiments for 3.2 mm sheet of AA2024-T3.

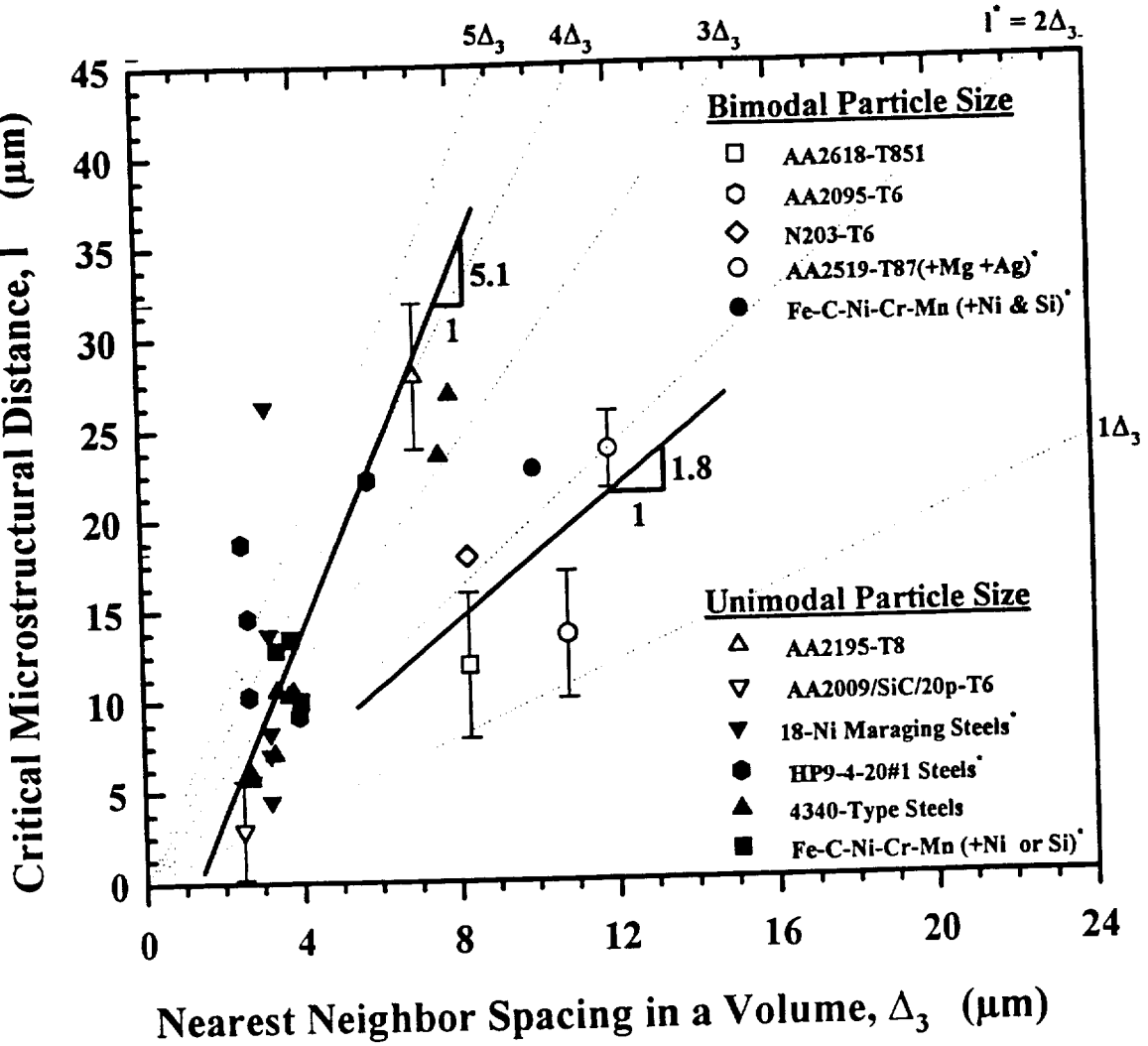

Figure 3: Correlations between nearest neighbor particle spacing in a volume (Δ_3) and the calculated critical distance (l^*) in steels[22,23] and aluminum alloys[24], for a single population of void-nucleating particles and a bimodal distribution of void-nucleating particles.

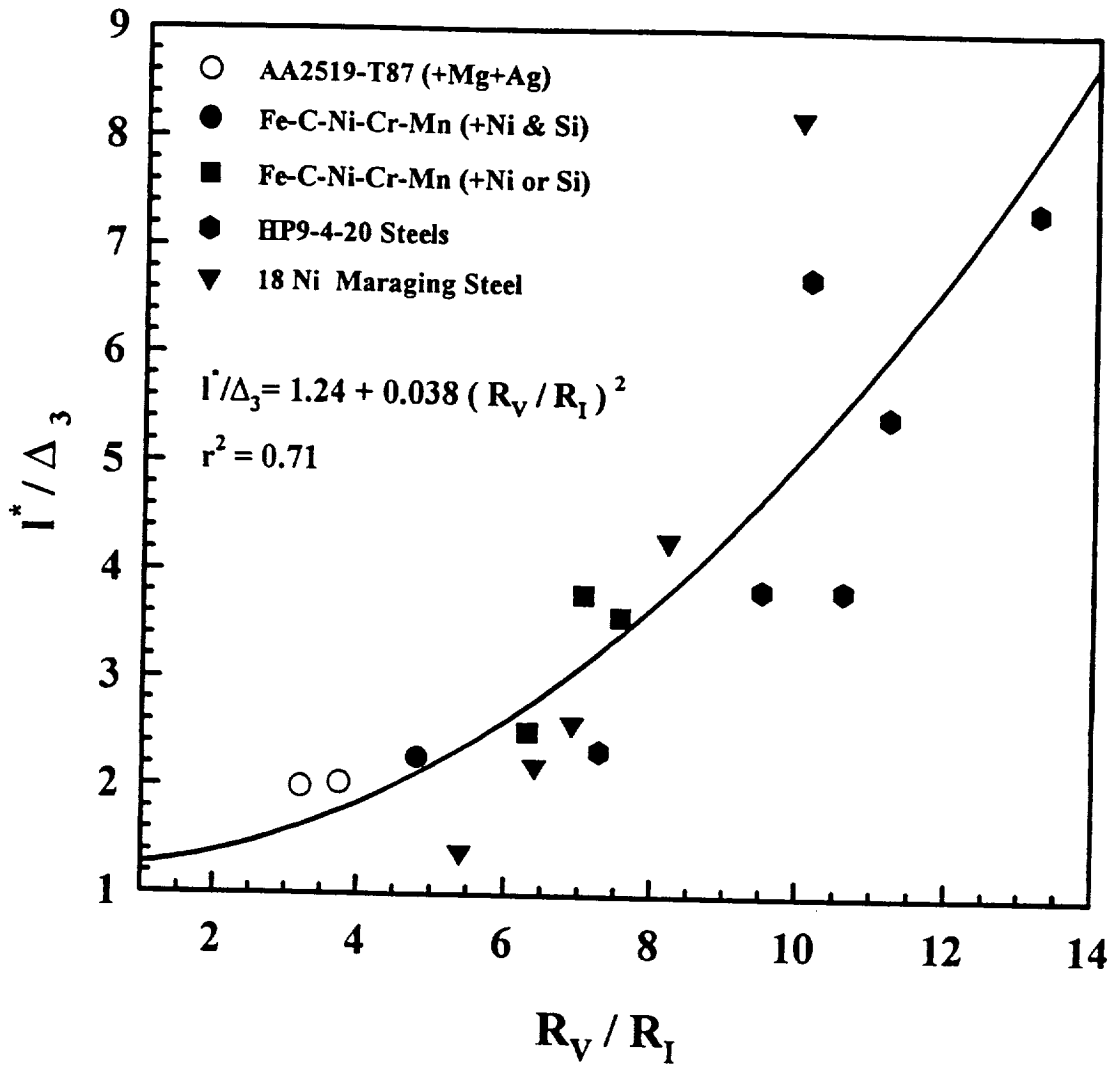

Figure 4: Quadratic relationship between the extent of stable void growth (quantified by the ratio of final void radius to initial void-nucleating particle radius) and l^* normalized by the inclusion or constituent particle spacing in a volume. Data are for steels[22,23] (solid symbols) and a single aluminum alloy (open symbol)[24].

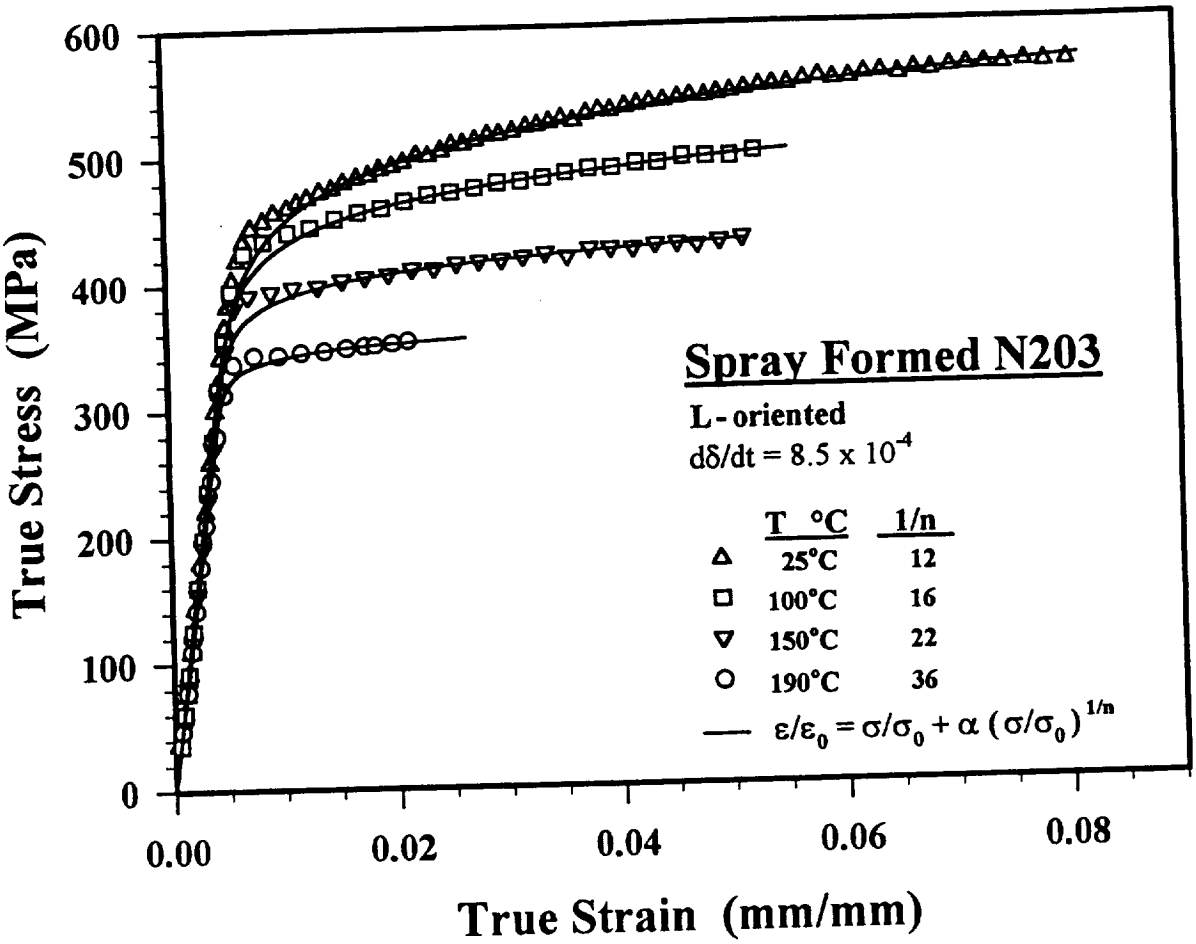

Figure 5: True stress-true strain curves plotted as a function of testing temperature for spray formed N203 extrusion.

Project #2: CRYOGENIC TEMPERATURE EFFECTS ON DEFORMATION AND FRACTURE OF Al-Li-Cu-In ALLOYS

Faculty Investigator: R.P. Gangloff
Graduate Student: J.A. Wagner

Objective

The objective of this PhD research is to characterize and optimize the crack initiation and growth resistance of Al-Li-Cu-Zr and Al-Li-Cu-Zr-In alloys for possible cryogenic propellant tank applications. The aim of the program is to understand microscopic fracture mechanisms as influenced by temperature, stress state and microstructure.

Approach

The approach to this objective was outlined in the proposal for the 1994 LA^{2}ST Program and is focusing on several areas including: (1) produce experimental direct chill cast Al-Li-Cu-Zr alloys with and without indium additions, (2) characterize both experimental Al-Li-Cu-Zr alloys and commercially available 2090-T81 plate, (3) implement J-integral fracture mechanics methods to measure crack initiation and fracture resistance for primarily plane stress and plane strain conditions at ambient and cryogenic temperatures, (4) establish the effect of stress state, temperature and microstructure on fracture toughness, (5) analyze fracture surfaces and correlate fracture features with grain structure, and (6) develop and apply advanced mechanical test and metallographic techniques to investigate the deformation and fracture processes that are relevant to crack initiation and growth toughnesses.

Progress During the Reporting Period

Progress to date on this program is summarized in the report from the June, 1995 LA^{2}ST Grant Review.

Project #3: THE EFFECT OF CRYOGENIC TEMPERATURE ON THE FRACTURE TOUGHNESS OF WELDALITE™ X2095

Faculty Investigator: R.P. Gangloff
Graduate Assistant: C.L. Lach

Objective

The objective of this research is to characterize the effect of cryogenic to mildly elevated temperature on the tensile deformation and fracture toughness of an emerging composition of Weldalite™-type alloys. We will determine quantitative stress versus strain data, and initiation and growth fracture toughnesses, as well as the associated microscopic fracture mechanisms, and conduct micromechanical modeling to understand temperature-dependent fracture.

Background

Aluminum-lithium-copper alloys are being developed to replace conventional 2XXX and 7XXX aluminum alloys for aerospace structural applications. Al-Li-Cu alloys such as 2090 offer increased stiffness and decreased density due to lithium, and exhibit increased strength and potentially increased fracture toughness with decreasing temperature from room to cryogenic levels. Increasing toughness at cryogenic temperature facilitates fracture mechanics damage tolerant designs because cold proof-testing is not required; a room temperature evaluation suffices. With the addition of Ag, Al-Li-Cu alloys exhibit exceptionally high yield strength, that further increases with decreasing temperature, without the necessity for post-solution treatment stretch deformation. The fracture toughness of such alloy compositions must be understood as a function of temperature.

Approach

The approach to this research was outlined in past renewal proposals.

Material

Two Weldalite™ compositions were selected for study to examine the limits of the Cu and Li levels for the alloy registered as AA2095. Specifically, a high Cu-Li alloy (Al-4.64Cu-1.53Li-0.34Ag-0.37Mg-0.17Zr; wt%) at the upper extreme of the AA2095 specification, and a low copper alloy (Al-4.04Cu-1.00Li-0.37Ag-0.36Mg-0.15Zr; wt%) at the low end of the AA2095 composition specification and in the middle of the AA2195 specification were chosen for evaluation.

The selected alloys should contain substantially different amounts of primary phase to enable examination of the effect of this feature on fracture toughness. Several artificial aging

conditions, produced at NASA-LaRC, will be employed to vary yield strength, work hardening rate, and the volume fraction and distribution of the θ' and T_1 strengthening precipitates. Metallurgical and temperature effects on toughness will be assessed for similar flow properties.

Deformation and Fracture

The approach of the proposed research is following that developed by Haynes in Project #1 and Wagner in Project #2. Measurements will produce uniaxial tensile stress-strain relationships and J-Integral based crack initiation and growth fracture toughnesses. This latter method will enable determination of plane strain fracture toughness data from relatively thin specimens (eg., 3.9 mm thick), as well as an estimate of the plane stress crack growth resistance. Microstructural effects on the complete crack initiation and growth resistance relationship will be studied.

Progress During the Reporting Period

Progress to date on this program is summarized in the report from the June, 1995 LA2ST Grant Review.

Project #4: MECHANISMS OF ENVIRONMENTALLY ASSISTED CRACKING IN ALLOYS 2090 AND 2095

Faculty Investigator: G.E. Stoner
Graduate Student: F.D. Wall

Research Objective

The objectives of this research project were to define the conditions sufficient to cause cracking in Al-Li-Cu alloys, to identify microstructural features which may contribute to anodic dissolution based cracking in PA tempers: to describe the critical solution chemistry changes associated with cracking under alternate immersion conditions in chloride solution; to develop an in-situ technique for quantifying EC propagation rates; and to investigate the influence of material temper, sample orientation, stress intensity level, applied external electrochemical potential and bulk aqueous environment on the environmental cracking of Al-Li-Cu alloys.

Progress During the Period

Doug Wall completed his disseration in January of 1996.

Occluded Environments Associated With the Environmentally Assisted Cracking of Al-Li-Cu Alloys in Aqueous Chloride Solutions

Efforts have been made to examine the cation content and pH of occluded environments pertaining to environmental cracking of Al-Li-Cu alloys. The initial focus of this project is to develop techniques which allow (1) the simulation and analysis of the solution chemistry associated with an isolated pit, (2) the extraction and analysis of solution chemistry from an environmental crack. The first of these techniques will be used to test the hypothesis that an inhibiting, alkaline occluded chemistry is necessary for environmental crack initiaition. The second technique will be utilized to measure the critical chemistry associated with a propagating crack.

The chemistry of isolated, occluded fissures has been simulated by exposing small quantities of near neutral NaCl solution to large areas of test material in the absence of a bulk aqueous environment. Real time measurements of pH were made via in-situ pH electrodes and post-test analysis of ion content was carried out using capillary electrophoresis. The pH response of a deep fissure was modeled using a simulated crevice experiment under alternate immersion conditions. In this experiment pH was monitored real-time with a micro-reference electrode and post-test using indicator paper.

Techniques were developed to investigate the occluded chemistry of real environmental cracks based on freezing and fracturing double cantilever beam specimens which had undergone alternate immersion testing. Frozen fracture surfaces were sampled using two techniques intended to provide spatial information on solution concentrations within a propagating environmental crack. Solutions were analyzed using capillary electrophoresis analysis.

It was found that the pH of simulated isolated, occluded fissures obtained an alkaline value for all materials tested; whereas the pH of the modeled deep fissure obtained an acidic pH. It is proposed that the alkaline pH is relevant to initiation of environmental cracking but that the crack tip is acidic in nature.

Cation analysis of simulated chemistries and real environmental crack solutions revealed the presence of significant aluminum and lithium ions in solution. It is likely that these species are critical in defining the conditions necessary for cracking. The techniques used for spatially resolving crack tip chemistries produced promising results. While the data are insufficient to make absolute quantification of species possible at this time, they do indicate the ability to make localized measurements and detect relevant species with the capillary electrophoresis method.

Evaluation Of The Critical Electrochemical Potentials Influencing Environmentally Assisted Cracking Of Al-Li-Cu Alloys In Selected Environments

The objective of this research is to test the hypothesis that a region of Cu-depleted aluminum exhibits the necessary electrochemical behavior to provide a pathway for anodic dissolution based environmental cracking. This is accomplished by documenting the potential dependance of environmental cracking and the potential-current relationship for oxide-free aluminum-copper binary alloys.

The electrochemical behavior of aluminum has been determined as a function of copper content using potentiodynamic polarization and scratching electrode techniques. This information has been correlated to trends in environmental cracking of Al-Li-Cu alloys in inhibited sodium chloride environments. Scratching electrode/ constant extension testing of stressed tensile samples has revealed a change from no failures to rapid failures due to a 10 mV change in applied potential. The potentials where these transitions occur appear to be linked to the electrochemistry of a copper-depleted region along microstructural boundaries.

The Correlation of Critical Electrochemical Potentials Associated with Environmental Cracking of Al-Li-Cu Alloys to Cu Depletion Along Grain Boundaries

The objective of this research is to test the electrochemical predictions of a copper depleted region against measurements of copper concentration as a function of distance from a microstructural boundary in an Al-Li-Cu material. Environmental cracking behaviors of tempered aluminum alloys 2090 and 2095 were assessed as a function of applied electrochemical potential through the use of constant extension / scratching electrode experiments. Correlations were observed with the repassivation potentials of solutionized Al-Cu binary materials tested in the same environment. An electrochemical prediction of Cu depletion along high angle boundaries arises from analysis of these data and is in relatively good agreement with energy dispersive spectroscopy measurements which revealed a Cu depleted region adjacent to high angle boundaries in peak-aged 2095.

A Technique for Evaluating Environmental Crack Growth Kinetics in an Al-Li-Cu Alloy Under Constant Immersion Conditions

The objectives of this paper are to (1) test the ability of the developed software and hardware to provide real-time stress intensity control for environmental cracking of Al-Li-Cu alloys, (2) determine the conditions under which crack growth can be quantified using the developed technique. A technique has been developed which allows the growth and monitoring of environmental cracks in Al-Li-Cu alloys 2090 and 2095 under constant immersion in an inhibited chloride environment. The use of direct current potential drop allows real-time monitoring of crack length with the capability to detect transient crack growth events. Crack measurements in conjunction with computer control of the load frame makes it possible to perform experiments in constant or ramped stress intensity control. By enclosing the specimen in an environmental cell, electrochemical control is established and tests can be performed in fixed potential mode. Overall, the technique allows for reproducible measurement of crack growth kinetics with good control of stress state, bulk aqueous environment and electrochemical potential. The use of controlled K testing represents an improvement over fixed displacement or rising CMOD testing since crack growth rate can be examined without the K level varying with some other experimental parameter (such as experiment duration or crack length).

Evaluation of Environmental Cracking Susceptibility in Terms of Externally Controlled Variables for Al-Li-Cu Alloys in an Inhibited Chloride Environment

The primary objectives of the current work are to (1) document the range of stress intensity overwhich environmental cracking is observed in a PA 2095 alloy, (2) test the proposed temper dependance of environmental cracking susceptability (UA worse than PA), and (3) determine if critical electrochemical potentials associated with crack initiation can be extrapolated to crack propagation. The susceptibility of Al-Li-Cu alloys to environmental cracking has been evaluated using smooth tensile samples in a constant extension experiment and fracture mechanics wedge open loading specimens under stress intensity control and fixed displacement testing. All testing has been performed under constant immersion conditions in a chromate-inhibited chloride environment. Under aged (UA) and peak aged (PA) specimens have been shown to be susceptible to cracking under similar chemical, electrochemical and mechanical conditions although quantification of crack velocities indicates that the UA tempers crack at least 20 to 200 times faster than PA materials. Fractographic inspection suggests a brittle failure mode for the UA specimens which display matching environmental fracture surfaces. The PA specimens generally display a tortuous, corroded surface although decreasing the electrochemical or mechanical driving forces leads to a change in fractography similar to that of the UA specimens. Fractographic and crack velocity data are discussed in terms of anodic dissolution and hydrogen embrittlement crack advance models. The electrochemical criteria for crack propagation is also discussed in terms of critical potentials.

Project #5: METALLURGICAL FACTORS CONTROLLING STRESS CORROSION CRACKING IN AA2096 AND C155

Faculty Investigator: John R. Scully
Graduate Student: Keith Eklund; PhD Candidate

Research Objectives

This study seeks to characterize two selected alloys (AA 2096 with Ag; and C155 or C255 without Ag) in order to clarify the various roles of alloyed Ag and δ' particles on localized corrosion and SCC under controlled electrochemical conditions. The initial goal is to characterize the K_{Iscc}, and stage II crack velocities for the two alloys after recommended pre-stretch and aging treatments, as well as after selected "diagnostic" aging times and temperatures (analogous to the development of the "Speidel" SCC curve). An inhibited chloride-containing solution (other than chromate containing solutions) will be selected to aid in the determination of SCC paths by SEM fractography. A second objective is to determine the influence of Ag on SCC behavior. Moreover, we seek to examine on a fundamental level the differences between the aqueous stress corrosion cracking results for these two alloys, should important differences be confirmed. In this phase of the study, various diagnostic procedures including thermal desorption spectroscopy (TDS) analysis of hydrogen trapping behavior will be utilized to develop a mechanistic understanding of conventional fracture mechanics-based SCC results.

Background

The stress corrosion cracking behavior of emerging advanced Al-Cu-Li-Ag and Al-Cu-Li alloys has not been well defined. The majority of the data in the literature focuses on AA 2090[1]. Fracture mechanics-based stress corrosion cracking data such as K_{Iscc} and stage II crack growth velocities as well as localized corrosion data under well-controlled electrochemical conditions in aqueous Cl- solutions are lacking for emerging alloys such as AA2096 and 2097 (or C155 and C255). Moreover, a strong connection between alloy microstructure and SCC resistance has only been established for AA2090 and 2195[2,3]. In the case of the latter alloy, a strong role for Cu depletion at high angle grain boundaries was hypothesized[4]. However, the role of Ag on slip/film rupture/dissolution and/or the slip/film rupture/hydrogen-absorption/local embrittlement aspects of stress corrosion has not been clarified. In the case of 2195, the high Cu content (3.7-4.3%) of this alloy may dominate over any beneficial or detrimental role of Ag. As an example, is the main influence of Ag upon SCC in an alloy containing less Cu than 2195 related to its role in producing a high density of fine T_1 plates[5,6] that resist formation of an active grain boundary dissolution

path, or does Ag enrichment at α/T_1 and/or α/Ω interfaces[7,8] alter the electrochemical activity of these phases? Alternatively, critical questions can be posed concerning the role of Ag in the context of hydrogen environment-assisted cracking (HEAC). Recall that the previous NASA LA2ST HEAC study has identified T_1 plates as a strong hydrogen trap site and that HEAC growth occurred on boundaries containing T_1, T_2 or T_b plates.[9] The presence of Ag located at α/T_1 or α/Ω interfaces might alter the hydrogen trap binding energy of these interfaces. Alternatively, Ag's role in promoting a high density of fine T_1 particles may disrupt the connectivity of the stress corrosion crack path regardless of the mechanistic details of SCC.

Other important variables in SCC initiation and growth are the Li content and Cu/Li ratio. Formation of δ' can be suppressed at high Cu/Li ratios and low Li contents, especially with higher aging temperatures. Alternatively, δ' formation may be promoted with low temperature aging. Suppression of δ' can alter the deformation mode, reducing the chance for coplanar slip. Coplanar slip can affect the likelihood of film rupture, has been shown to enhance hydrogen uptake, and influences its repartitioning[10]. The effects of these variables on the stress corrosion resistance of emerging Al-Li-Cu-Ag materials remains largely uncharacterized.

Approach

Materials

The alloys AA 2096 (with Ag) and C155 or C255 (without Ag) were specifically chosen for this study in order to clarify the roles of Ag and δ' particles on their SCC resistance. AA2096 (2.6Cu, 1.6Li, 0.8Mg, 0.18Zr, 0.6Ag, 0.25Zn, wt. %) is produced by Reynolds. C155 (similar in composition to AA 2097: 2.8Cu, 1.5Li, 0.35Mg, 0.16Zr, 0.6Mn, 0.35Zn, wt. %) is produced by ALCOA. These two alloys have nearly identical Li contents and Li/Cu ratios (0.61 vs. 0.57, respectively). C155 does not contain Ag but instead contains Mn. Although the Li/Cu ratio of both alloys is greater than 0.25, it may be possible to suppress δ' formation by using a slightly higher aging temperature than usual. Hence, these two alloys offer the unique opportunity to compare Ag vs non-Ag containing Al-Li-Cu-Mg materials with very similar compositions. Moreover, it may be possible to control δ' formation and, consequently, deformation mode.

Determination of Suitable Inhibited NaCl Solutions

The long-term goal is to study the SCC resistance of each alloy in a selected inhibited NaCl solution under full immersion and alternate immersion conditions. K_{ISCC} and da/dt_{II} will be generated using fracture mechanics-based specimens under controlled electrochemical conditions, while the effects of hydrogen embrittlement (HE), if any, will be analyzed with Thermal Desorption Spectroscopy (TDS). Several factors dictate the choice of stress-corrosion test solutions.

The alloys must, of course, be susceptible to SCC in the electrolyte chosen, with Cl- levels between 0.01 M and 1 M being known to increase the stage II crack growth velocities of 7075-T651 relative to those in distilled water.[11] The solution should be sufficiently inhibited to prevent excessive localized corrosion and buildup of corrosion products on the fracture surfaces which would obscure SEM imaging of the fracture path. It is therefore desirable to conduct all electrochemically controlled tests in a region of potential anodic to the open circuit potential (E_{OCP}), yet below the pitting potential (E_{pit}). Also, the potential at which the sample repassivates (E_{repass}) is an important consideration, indicating the potential below which oxide film repair may be achieved. While the success of chromate inhibited solutions is well known,[12] it would be advantageous to find an alternative inhibitor which avoids the toxicity of the chromate solutions. It is known that stage II crack growth rates of 7075-T651 can change by 2 to 3 orders of magnitude with just a few hundred millivolts shifts in applied potential.[11] Since a wide range of potentials should be utilized to observe any noticeable trends in metallurgical factors, one ideally wishes to select a solution for SCC testing in which the material exhibits a large interval between the E_{OCP} and E_{pit} potentials for a range of Cl- concentrations. Alternate immersion testing may be undertaken, which would require that the pitting and repassivation potentials should be more positive than the open circuit potentials in an aerated solution. Otherwise, localized corrosion may dominate corrosion processes under the alternate immersion conditions.

Recent Results

The mechanical properties of AA2096 wide panel extrusions in the T3 temper are under investigation at NASA-Langley for a matrix of aging times and temperatures. Where possible, these properties will be obtained from NASA-Langley.

Potentiodynamic tests have been conducted on AA2096-T3 panel extrusions recently obtained from NASA-Langley to determine a suitable combination of inhibited solution and potential. As a comparative base-line, 99.999% Al was also tested. The solution investigated to

date was 1M Na_2SO_4 + 0.1M $CH_3COONa(3H_2O$ with varying levels of NaCl (0, 0.01, 0.1, and 0.5 M), currently the leading choice in a separate UVa project on the SCC resistance of AA7050.[13] All solutions were brought to a pH of 3.8 with additions of acetic acid.

Figure 1 shows the potentiodynamic scan for AA2096-T3 in deaerated 0.5 M NaCl solution, with the plane orthogonal to the short transverse direction exposed to solution. Each of the critical potentials previously discussed is apparent, with a difference between E_{OCP} and E_{pit} of nearly 280 mV. Figure 2 shows a compilation of all results for pure aluminum in various NaCl concentrations, as does Figure 3 for AA2096-T3. Note that reverse scans are not shown for brevity. All pertinent potentials are listed in Table 1. For both Al and AA2096-T3, no pitting potential is observed in deaerated solutions containing 0.0 M NaCl, and none is seen in the AA2096-T3 for the 0.01 M NaCl solution. Microscopic inspection of the sample surfaces after these tests also showed no signs of pitting. The general trend is that as the Cl- concentration increases, the pitting potentials decreases. This is as expected.[14] Note also that at any given chloride concentration, the critical potentials for the AA2096-T3 material are more positive than those of the high purity Al.

Figure 4 shows the complete scan of the AA2096-T3 in 0.01M NaCl. Note the increase in current within the passive range of the plot at approximately -0.200 V_{SCE}. This could be indicative of oxygen evolution which is suppressed to rates below the passive dissolution rate with insulating oxide film thickening. This phenomenon is observed on many insulating oxides.[15] Upon reversing the scan, the oxide film is sufficiently thick, and the effect is no longer apparent.

Conclusions

1) AA2096-T3 shows no pitting in dearated 1 M Na_2SO_4 + 0.1 M $CH_3COONa{\cdot}3H_2O$ solution acidified to pH=3.8 with acetic acid with 0 M or 0.01 M NaCl up to an applied potential of 0.6 V_{SCE} (1.4V_{OCP}).

2) The open circuit, pitting, and repassivation potentials of AA2096-T3 are consistently higher than those of high purity aluminum in the same solution.

3) A solution with an inhibitor base of 1 M Na_2SO_4 + 0.1 M $CH_3COONa{\cdot}3H_2O$ has shown promise as an alternative to chromate inhibited solutions for the purpose of electrochemically controlled SCC tests.

Tasks for Next Reporting Period

The electrochemical tests outlined herein will be extended to include the T and L orientations of the AA2096 material, and the C155 material will be subjected to the same test matrix once received from ALCOA. Though the search for and evaluation of alternate inhibited NaCl solutions will continue, it will still be necessary to utilize some chromate-based solutions for comparisons. The effects of aging on the SCC resistance must also be studied. The proper T8 aging practice for AA2096 is currently being determined at NASA-Langley. Once completed, the potentiodynamic tests outlined in this report will be applied to the T8 and some underaged conditions. Appropriate combinations of aging/ applied potential/ bulk solution chemistry will then be chosen for the future fracture mechanics-based SCC testing (most likely to begin in the second reporting period of this year).

	99.999 % Al			2096-T3		
$[Cl^-]$, **M**	E_{OCP}	E_{pit}	E_{repass}	E_{OCP}	E_{pit}	E_{repass}
0	-0.945	-----	----	-0.863	----	----
0.01	-1.000	-0.361	-0.685	-0.846	----	----
0.1	-0.973	-0.534	-0.723	-0.861	-0.500	-0.625
0.5	-0.965	-0.650	-0.763	-0.842	-0.561	-0.703

Table 1: E_{OCP} , E_{pit} and E_{repass} for 99.999% Al and AA2096-T3 (surface orthogonal to the short transverse direction) as a function of NaCl additions to a deaerated solution of 1 M Na_2SO_4 + 0.1 M $CH_3COONa \cdot 3H_2O$ + acetic acid to pH=3.8. All potentials are reported as volts versus the Standard Calomel Electrode (V_{SCE}).

References

1. R.G. Buchheit, F.D. Wall, G.E. Stoner, and J.P. Moran, Corrosion, vol. 51, no. 6, pp. 417-428.

2. R.G. Buchheit, "Mechanisms of Localized Aqueous Corrosion in Aluminum-Lithium Copper Alloys", Ph.D. Thesis Dissertation, University of Virginia, January 1991.

3. J.P. Moran, "Mechanisms of Localized Corrosion and Stress Corrosion Cracking of an Al-Li-Cu Alloy 2090", Ph.D. Thesis Dissertation, University of Virginia, January 1990.

4. F.D. Wall, Jr., "Mechanisms of environmetally Assisted Cracking in Al-Li-Cu Alloys 2090 and 2095", Ph.D. Thesis Dissertation, University of Virginia, January 1996.

5. J.R. Pickens, K.S. Kumar, S.A. Brown, and F.W. Gayle, "Evaluation of the Microstructure of Al-Cu-Li-Ag-Mg Weldalite Alloys", NASA Contractor report 4386, 1991.

6. C.P. Blankenship, Jr., and E.A. Starke, Jr., Acta Metall., 42, pp. 845-855, 1994.

7. K. Hono, et al., Acta Metall., 41, pp. 829-838, 1993.

8. J.M. Howe, Private communication, U.Va., September, 1994

9. S.W. Smith, "Hydrogen Interactions and Their Correlation to the Hydrogen Embrittlement Susceptibility of Al-Li-Cu-Zr Alloys," Ph.D. Thesis Dissertation, University of Virginia, May 1995.

10. S.W. Smith, J.R. Scully, "Hydrogen Trapping and Its Correlation to the Hydrogen Embrittlement Susceptibility of Al-Li-Cu-Zr Alloys", TMS Conference on Hydrogen in Metals, Jackson, Wyoming, 1994.

11. N.J.H. Holroyd in Envionment-Induced Cracking of Metals, NACE-10, R.P. Gangloff and M.B. Ives editors, NACE, TX, pp. 311-346, 1988.

12. ASM Metals Handbook, 9th ed. Vol 13, pp. 389-395, Metals Park, OH, 1987.

13. Personal Communication with Robert Kelly of the University of Virginia.

14. S.T. Pride, S.T. Pride, J.L.Hudson, "Analysis of Electrochemical Noise from Metastable Pitting in Al, Aged Al-2%Cu and AA 2024-T3," in *"Electrochemical Noise - Application* to Analysis and Interpretation of Corrosion Data," ASTM Special Technical Publication, Philadelphia, PA, in press, 1995

15. N. Sato, G. Okamoto in Comprehensive Trieatise of Electochemistry, Vol. 4, Bockris, Conway, Yeager and White eds., Plenum Press, NY, 1981.

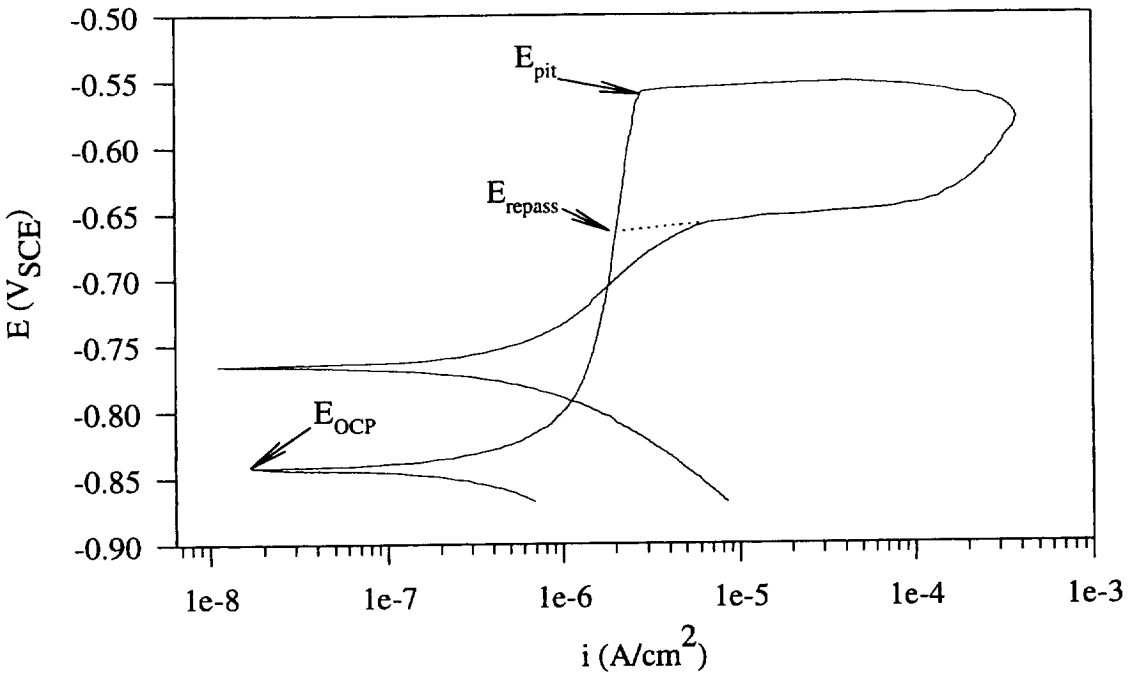

Figure 1: Potentiodynamic scan of AA2096-T3 in a deaerated solution of 0.5 M NaCl + 1 M Na_2SO_4 + 0.1 M $CH_3COONa\text{-}3H_2O$ + acetic acid to pH=3.8. E_{OCP}, E_{pit}, and Erepass are indicated. Only the plane orthogonal to the short transverse direction was exposed to solution.

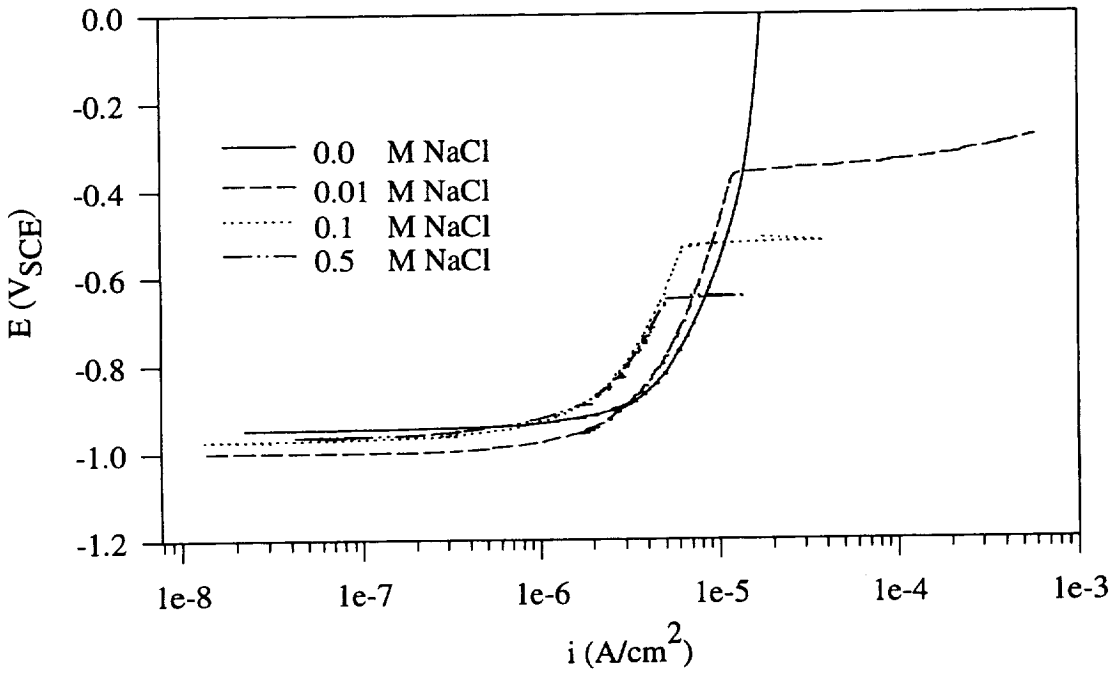

Figure 2: Composite of potentiodynamic scans of 99.999% Al in deaerated solutions of X M NaCl + 1 M Na_2SO_4 + 0.1 M $CH_3COONa\text{-}3H_2O$ + acetic acid to pH=3.8. The plane orthogonal to the short transverse direction was exposed to solution. Only forward scans shown for brevity.

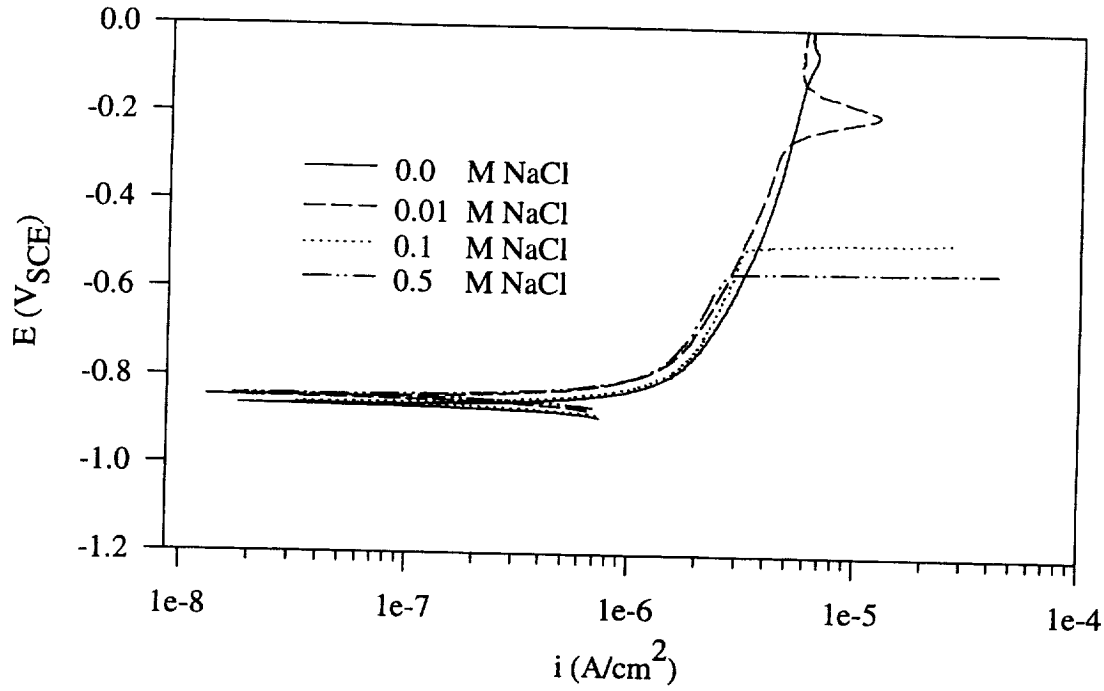

Figure 3: Composite of potentiodynamic scans of AA 2096-T3 in deaerated solutions of X M NaCl + 1 M Na_2SO_4 + 0.1 M $CH_3COONa\text{-}3H_2O$ + acetic acid to pH=3.8. The plane orthogonal to the short transverse direction was exposed to solution. Only forward scans shown for brevity.

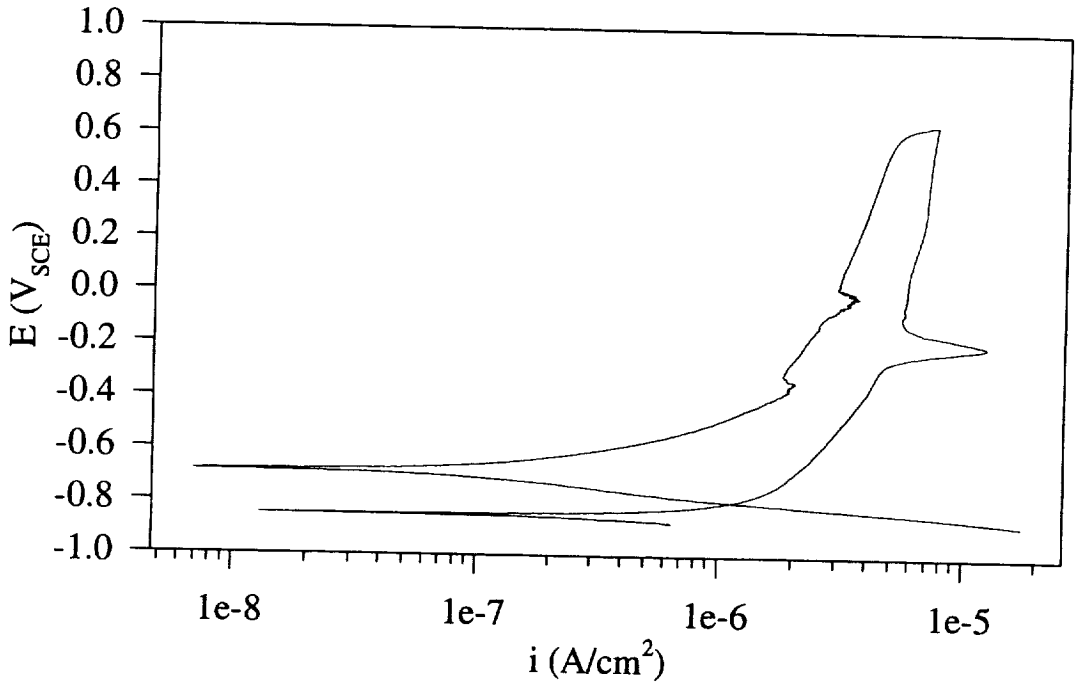

Figure 4: Potentiodynamic scan of AA2096-T3 in a deaerated solution of 0.01 M NaCl + 1 M Na_2SO_4 + 0.1 M $CH_3COONa\text{-}3H_2O$ + acetic acid to pH=3.8. Note the increase in current density within the passive region on the forward scan.

Project #6a: **MECHANISMS OF DEFORMATION AND FRACTURE IN HIGH-STRENGTH TITANIUM ALLOYS: EFFECTS OF TEMPERATURE AND HYDROGEN**

Faculty Investigator: R.P. Gangloff
Graduate Assistant: S.P. Hayes

Research Objectives

The broad objective of this research is to characterize and understand the relationships between microstructure, deformation mode, and fracture resistance of high strength alloys for HSCT applications. This Ph.D. program emphasizes the effects of time, temperature, and dissolved hydrogen on the fracture toughness of an advanced metastable ß-titanium alloy. The objective of this reporting period is to establish the room temperature fracture resistance of an advanced metastable ß-titanium alloy, TIMET LCB, in both plate and sheet forms. These properties are compared with those of other beta alloys to determine if LCB is a reasonable candidate for mechanistic research in support of HSCT applications, before hydrogen charging or elevated temperature experiments are performed. As a basis for this work, it was necessary to improve the R-curve fracture toughness characterization method applied to thin sheet titanium alloy specimens.

Background and Approach

Material

A metastable -titanium alloy, TIMET LCB, was selected for study; its composition was reported previously [1]. The alloy was provided by TIMET in both sheet (4 sheets @ 0.15 cm x 20.32 cm x 40.64 cm) and plate forms (1 plate @ 0.94 cm x 17.78 cm x 40.01 cm). The thermal-mechanical processing of the sheet was as follows:

19.05 cm diameter x 25.4 cm long ingot
Beta forge to 10.16 cm x 15.24 cm from 1093°C
Alpha/Beta forge to 4.45 cm x 16.51 cm from 760°C
Beta roll to 0.51 cm x 16.51 from 849°C
Alpha/Beta roll to 0.31 cm x 16.51 cm from 752°C
Cold roll to 0.18 cm (42% reduction)
Alpha/Beta solution treat at 760°C (20 minutes)
Fan air Cool
Age at 593°C for 20 hours

The plate was processed from the same ingot as the sheet but was extracted from the processing sequence at the 0.95 cm thickness. It was solution treated at 760°C for 20 minutes, air cooled, and aged at 593°C for 20 hours.

Fracture Mechanics Characterization

Fracture mechanics were successfully used to characterize and understand the time-temperature dependent fracture behavior of elevated temperature aluminum alloys [2-5]. These methods will be used for testing titanium alloys, with the most significant difference in the test setup arising from the substantial increase in the electrical resistivity of titanium compared to aluminum. This experimental method measures load, load-line displacement, and crack length (from direct current electrical potential) as a function of time for a fatigue-precracked specimen mounted in a computer-automated closed-loop servoelectric test machine and operated under constant actuator-displacement control. The experiment employs a fixed grip displacement rate rising load R-curve method, measured in terms of the applied J-integral versus crack extension, Δa, curve. This technique yields three measurements of initiation fracture toughness (K_{ICi}, K_{JICi}, and K_{JIC}) and the plane stress tearing resistance with a single fracture mechanics specimen [5]. In addition, when stable cracking occurs, J-Δa can be analyzed to yield K versus crack growth rate, da/dt. Plate compact tension (CT) specimens are 6.35 mm thick and 30.5 mm wide, while sheet CT specimens are 1.7 mm thick and 76.2 mm wide and restrained with face-plates to prevent buckling.

Results During the Reporting Period

The rising load R-curve test method was used to determine the fracture toughness of TIMET LCB plate and sheet at room temperature with constant load-line displacement rates of 0.67 and 5.08 μm/sec, respectively. The results of these experiments are summarized in Table I.

Table I TIMET Low Cost Beta Room Temperature Results

Specimen Id.	Hardness (HRC)	UTS (MPa)	$J_{ICi}^{(1)}$ (kJ/m^2)	$K_{JICi}^{(1)}$ (MPa$\sqrt{m}$)	$J_{ICi}^{(2)}$ (kJ/m^2)	$K_{JIC}^{(2)}$ (MPa$\sqrt{m}$)	$K_{ICi}^{(1)}$ (MPa$\sqrt{m}$)
Plate 1	40.3	1197	8.1	32.5	17.3	47.5	32.5
Plate 2	39.8	1178	7,8	31.9	19.1	50.0	32.0
Sheet 4	40.4	1201	28.1	59.6	34.5	66.0	59.7
Sheet 5	41.6	1247	17.3	47.2	25.1	56.8	47.3
Sheet 6	41.3	1235	18.3	48.4	49.9	79.9	48.5

As Table I indicates, five LCB specimens have been tested using the rising load R-curve method. Hardness was measured and ultimate tensile strength (UTS) was determined from a correlation of hardness with UTS developed for LCB sheet of 1.6 mm thickness [6]. The equation of the line given by this correlation is:

$$\text{U.T.S.} = 5.59 * \text{Hardness} - 47.69 \qquad (1)$$

where UTS is given in ksi and hardness in Rockwell C. These predicted ultimate tensile strengths agree well with those measured at UVa by Kazanjian which averaged 1176 and 1157 MPa for LCB plate and sheet, respectively.

The initiation fracture toughness parameters (J_{ICi}, K_{ICi}, K_{JICi}, and K_{JIC}) were determined from J-Δa data, while K_{ICi} was based on ASTM Standard E 399 with the assumption that plane strain deformation controlled fracture initiation. The three columns with the superscript (1) and subscript (i) denote that fracture initiation was detected by a resolvable increase in the DCPD signal. J_{ICi} was calculated from the load, load-line displacement, and crack length data points at the time when the DCPD signal increased signifying crack initiation. J_{ICi} was converted to a linear elastic initiation toughness (K_{JICi}) by the following relation:

$$K_{JICi} = \left(\frac{J_{ICi}E}{1-\nu^2}\right)^{1/2} \qquad (2)$$

K_{ICi} is the linear elastic fracture toughness based on the K-solution given in ASTM Standard E 399 which is:

$$K_{ICi} = \left(\frac{P_i}{BW^{1/2}}\right) f\left(\frac{a_i}{W}\right) \qquad (3)$$

where P_i and a_i are the load and crack length at initiation, and B and W are specimen thickness and width, respectively. However, unlike ASTM Standard E 399 (K_{IC}) which is based on a secant offset method to determine crack initiation, K_{ICi} is based on a resolvable increase in the DCPD signal to determine crack initiation. The load and crack length recorded at the time of the increase in DCPD are used in equation 3 to determine K_{ICi}. The tabulated values of K_{ICi} and K_{JICi} for all LCB specimens tested are approximately equal (to within $\pm$0.1 MPa). Both values were

determined based on DCPD-detected crack initiation with the only difference arising from the method of calculating K. Recalling that J_{Total} has both plastic and elastic components, as given by:

$$J_{Total} = J_{Plastic} + J_{Elastic} \quad (4)$$

J-integral calculations indicated that the plastic contribution ($J_{Plastic}$) to J_{Total} is insignificant compared to the elastic contribution ($J_{Elastic}$) so that small scale yielding is maintained and linear elastic K analysis is sufficient.

The two columns with the superscript (2) denote that fracture initiation was determined using ASTM Standard E 813 which utilizes a 0.2 mm offset blunting line to calculate J_{IC}. K_{JIC} is then determined using equation 2.

Figures 1 and 2 show the K_J-Δa curves for the sheet and plate CT specimens of STA LCB. As Figure 1 shows, there is variation in the general appearance of the R-curves for the replicate experiments of the sheet specimens, with initiation fracture toughness (both K_{JIC} and K_{JICi}) ranging from 47 to 80 MPa$\sqrt{m}$ (Table I). In addition these curves show that crack bursting occurs rather than continuous growth as would be expected for thin CT specimens of a ductile alloy. Figure 2 shows that the initiation toughness is dramatically reduced for the plate specimens compared to sheet. Crack growth is not continuous but rather occurs by bursting. The stress intensity achieved at 3 mm of crack extension (K_{3mm}) in sheet and plate specimens is less scattered than the initiation values (K_{JIC}) reported (K_{3mm} equals 68 and 80 MPa$\sqrt{m}$ for plate and 72, 92, and 92 MPa m for sheet LCB). As shown in an ensuing section, the toughness differences are generally explained by modest hardness differences and by the precise definition of initiation toughness. The results for sheet in Figure 1c are outside this norm.

Macroscopic observations of the fracture surfaces of the sheet specimens revealed that shear growth occurred after initiation, while the plate specimen fracture surfaces appear to be plane strain type but more complicated. The microstructure of the plate was not fully recrystallized and as a result was heterogeneous with elongated, pancaked beta grains. The boundary between these pancaked grains could provide an easy path for crack propagation which would account for the reduced toughness of the plate relative to the sheet. Increased plane stress shear cracking in sheet specimens may explain the increased K_{3mm} values compared to the plate. The existence of an R-curve for low toughness plate may be related to modest delamination due to the heterogeneous microstructure.

Crack initiation and growth in precracked CT specimens were monitored continuously by DCPD [7]. A constant current of 10 A was supplied to the specimen with a DC power supply, and the direct current electrical potential difference across the notch and growing crack was amplified with a 10^3 gain amplifier and read by a computer. The computer averaged 808 readings per data point which significantly reduced random noise. Figure 3 shows measured potential and load versus CMOD for one of the sheet specimens tested. Noise in the DCPD signal had been one of the major limitations in establishing an R-curve for TIMET LCB, but as this figure demonstrates, the noise is now ±1 μV for a 6500 μV base signal (±0.015%) which is sufficiently low to accurately detect crack initiation. Crack initiation is indicated by an increase in the DCPD signal since the electrical resistance of a cracked body increases as the crack extends.

For this test, crack initiation occurred when the DCPD signal jumped 4 μV at a CMOD of 0.91 mm. This jump in measured DCPD was coincident with the first resolved load drop in the load-CMOD data which further supports crack initiation. The load (P_i), measured potential ($DCPD_i$), and CMOD ($CMOD_i$) at initiation are labeled in Figure 3. This 4 μV jump was the first time that consecutive DCPD data points differed by more than 1 μV, and there is a definite trend in the data immediately following this jump which signifies growth. The DCPD signal for tests on this alloy did not gradually rise after initiation as has been typically seen for aluminum and other titanium alloys. Instead, it jumps and then remains stable much like the preinitiation signal until the next burst occurs.

Figure 4 shows initiation fracture toughness (both K_{JIC} and K_{JICi}) versus ultimate tensile strength for TIMET LCB sheet and plate. The data for the two methods of characterizing fracture toughness are described with lines for both the plate and sheet. Plate toughness is less than that of sheet, independent of the parameter definition. An important point is demonstrated in this figure, consistent with results found by Haynes et al. for 3.2 mm sheet of precipitation hardened 2xxx Al alloys [5]. The initiation fracture toughness (K_{JIC}) as determined by ASTM E-813 is consistently greater than the value determined by DCPD (K_{JICi}). This occurs because ASTM E-813 uses a 0.2 mm offset blunting line to determine initiation and as a result, determines initiation after some finite crack growth has occurred.

In order to evaluate TIMET LCB as a candidate for HSCT applications, it is important to compare its fracture toughness with other high strength ß-titanium alloys. Figure 5 shows fracture toughness versus yield strength of various ß-titanium alloys which have been tested at UVa. The initiation fracture toughness values (K'_{IC}, filled symbols) for Beta-21S and Ti-15-3 were defined by the first resolved nonlinearity in the load vs actuator displacement record, which was generally

coincident with the first change in slope of the DCPD vs displacement record. These initiation fracture toughness values are for plane strain constraint based on ASTM Standard E 813 and are slightly less than or equal to K_{IC} from ASTM Standard E 399 [8]. The initiation fracture toughness values (K_{ICi}) for Beta-C, Beta-21S (open symbols) and TIMET LCB were calculated using equation (3) based on a resolvable increase in the DCPD signal to determine crack initiation, while the values for McDonnell Douglas LCB (K_{IC}, filled symbols) were based on a 95% slope-intercept method. The yield strengths were calculated from a hardness correlation. The data for the various alloys have been described with lines to show the strength dependent toughness trends for the specific alloy systems. TIMET LCB sheet is described by a band rather than a line to account for uncertainty in the yield strength since measured and correlated values differ by about 50 MPa.

This figure shows that the properties of TIMET LCB sheet are similar to Beta C, but appear inferior to both STA Beta-21S and Ti-15-3. However, it must be recognized that Beta-21S and Ti-15-3 were characterized by a less sensitive engineering-toughness parameter. The first resolvable increase in DCPD is more sensitive to crack initiation than either the 95% slope-intercept method that ASTM Standard E 399 specifies or the first change in slope of the load vs actuator displacement record. The data for Beta C, Beta-21S (open symbols), and TIMET LCB sheet are based on DCPD-detected initiation (K_{ICi}) and show that the strength dependent toughnesses are similar and could be described by a singular band. The data (closed symbols) for Beta-21S and Ti-15-3 are elevated due solely to the differences in the initiation fracture toughness characterization methods employed. This is clearly demonstrated by the significant difference in reported toughness of the same heat of Beta-21S (open vs closed symbols) when comparing the two characterization methods (K_{ICi} vs K'_{IC}). (K_{JIC} for this experiment equals 65.9 MPa$\sqrt{m}$ while K_{ICi} equals 50.6 MPa$\sqrt{m}$.) A similar decrease in toughness would be expected for the Ti-15-3 alloy system if DCPD, rather than the actuator displacement record, was used to detect crack initiation. The fracture toughness of TIMET LCB plate and perhaps McDonnell Douglas LCB, are atypically low.

Figure 6 shows initiation fracture toughness (K_{JIC}) versus ultimate tensile strength (UTS) for TIMET LCB sheet and plate as well as Beta-21S sheet processed different ways [6]. The initiation fracture toughnesses for TIMET LCB reported in this figure are based on ASTM Standard E 813 and a 0.2 mm offset blunting line instead of DCPD-detected initiation. This initiation parameter (K_{JIC}) was chosen to be consistent with the values reported for Beta-21S [6]. The TIMET LCB data are described by a band to account for uncertainty in UTS since the

measured and correlated values differ by about 50 MPa. The toughness of LCB sheet is similar to the lower bound for the Beta-21S sheet data, with the exception of the single high toughness LCB result that may be anomalous. The plane strain fracture toughness of LCB plate is clearly less than that reported for the Beta-21S sheet microstructure.

Conclusions

Direct current potential difference is an effective technique for detecting crack-growth initiation in fatigue precracked CT specimens of TIMET LCB sheet and plate.

The initiation fracture toughness and growth fracture resistance of LCB sheet CT specimens were variable and significantly greater than the corresponding properties of the plate. A large part of the variability was traced to alloy strength differences and the precision of crack growth monitoring.

The fracture resistance of TIMET LCB sheet is comparable to Beta C and the lower bound values of toughness for Beta-21S (excluding a single high toughness LCB result) when consistent initiation fracture toughness parameters are used as a basis of comparison. No direct comparison of fracture resistance can be made between TIMET LCB and Ti-15-3, but based on the trends of different initiation fracture toughness parameters, their fracture resistances should be similar. The initiation fracture toughnesses and maximum stress intensities achieved appear to be sufficient to characterize the effects of temperature and dissolved hydrogen on the fracture resistance of TIMET LCB sheet.

K_{3mm} is a useful parameter in comparing experimental results to determine the effects of temperature and dissolved hydrogen on the fracture resistance of TIMET LCB sheet.

Future Work

Future work will focus on: (1) improving the R-curve fracture toughness characterization method applied to thin sheet titanium alloy specimens, specifically for long term exposure at elevated temperature, (2) beginning a systematic study of internal hydrogen embrittlement of STA LCB sheet, (3) investigating the fracture modes in LCB at various test temperatures and predissolved hydrogen concentrations, and (4) beginning characterization of the fracture resistance of solution treated and aged Ti-15-3 or Beta-21S sheet.

References

1. S.P. Hayes and R.P. Gangloff, UVa Progress Report No. 528266/MS94/117, p. 125, March, 1995.
2. W.C. Porr, Jr. and R.P. Gangloff, Metall. And Matls. Trans. A, Vol. 25A, p. 365 (1994).
3. B.P. Somerday, Yang Leng and R.P. Gangloff, Fatigue Fract. Engng Mater. Struct., Vol.18, No. 5, p. 565 (1995).
4. S.S. Kim, M.J. Haynes and R.P. Gangloff, Materials Science and Engineering A, 203 p. 256 (1995).
5. M.J. Haynes and R.P. Gangloff, *Journal of Testing and Evaluation*, JTEVA, in review, 1995.
6. HSR Metallic Materials Task Reviews, NASA Langley Research Center, April 4-7, 1995.
7. J.K. Donald and J. Ruschau, Fatigue Crack Measurement: Techniques and Applications, K.J. Marsh, R.O. Ritchie, and R.A. Smith, eds., EMAS, West Midlands, UK, p.11 (1991).
8. L.M. Young, G.A. Young, J.R. Scully and R.P. Gangloff, Metall. And Matls. Trans. A, Vol. 26A, p. 1257 (1995).

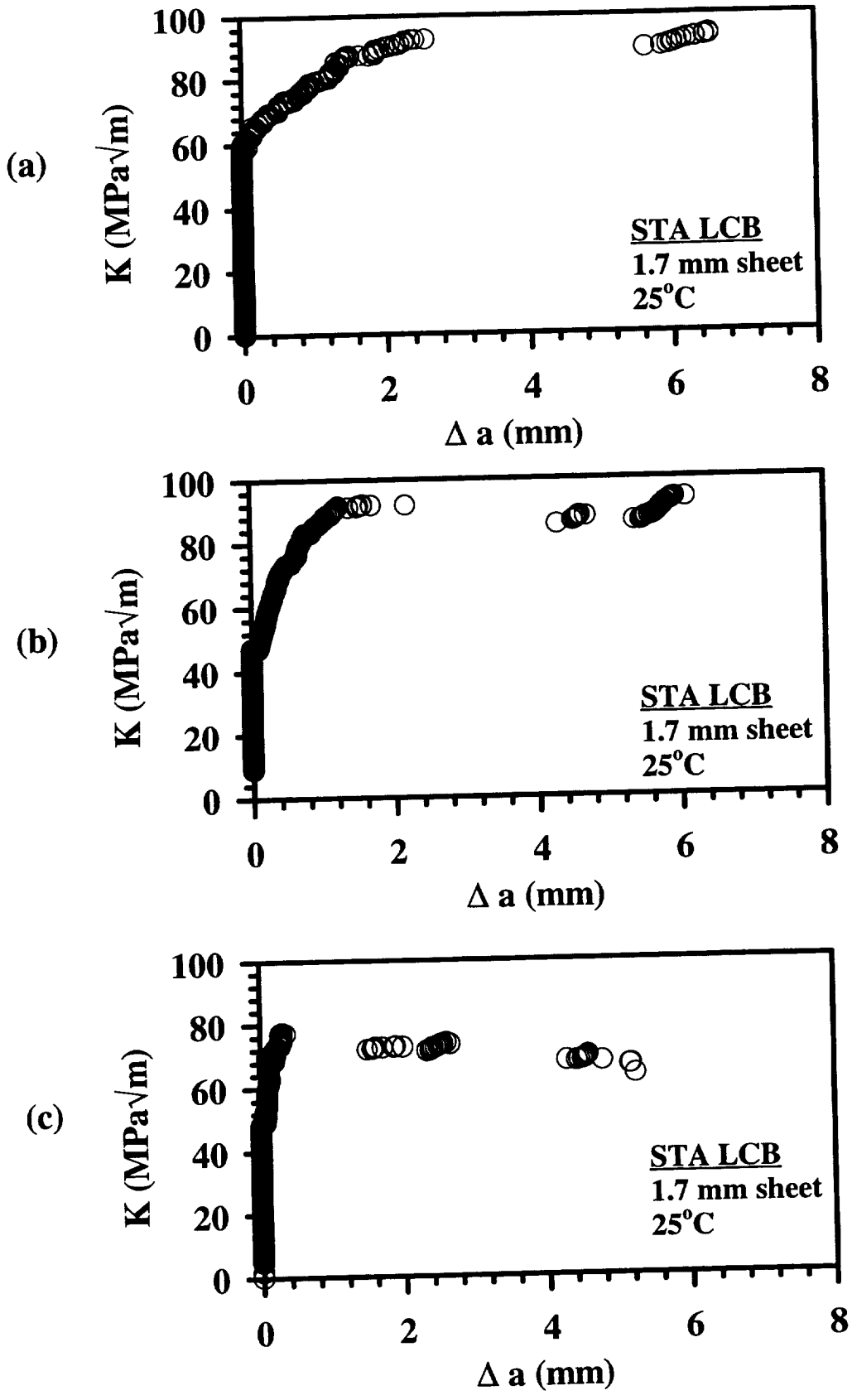

Figure 1 K vs Δ a for TIMET LCB sheet specimens tested at room temperature with $\delta = 5.08$ μm/sec, (a) Sheet 4, (b) Sheet 5, (c) Sheet 6.

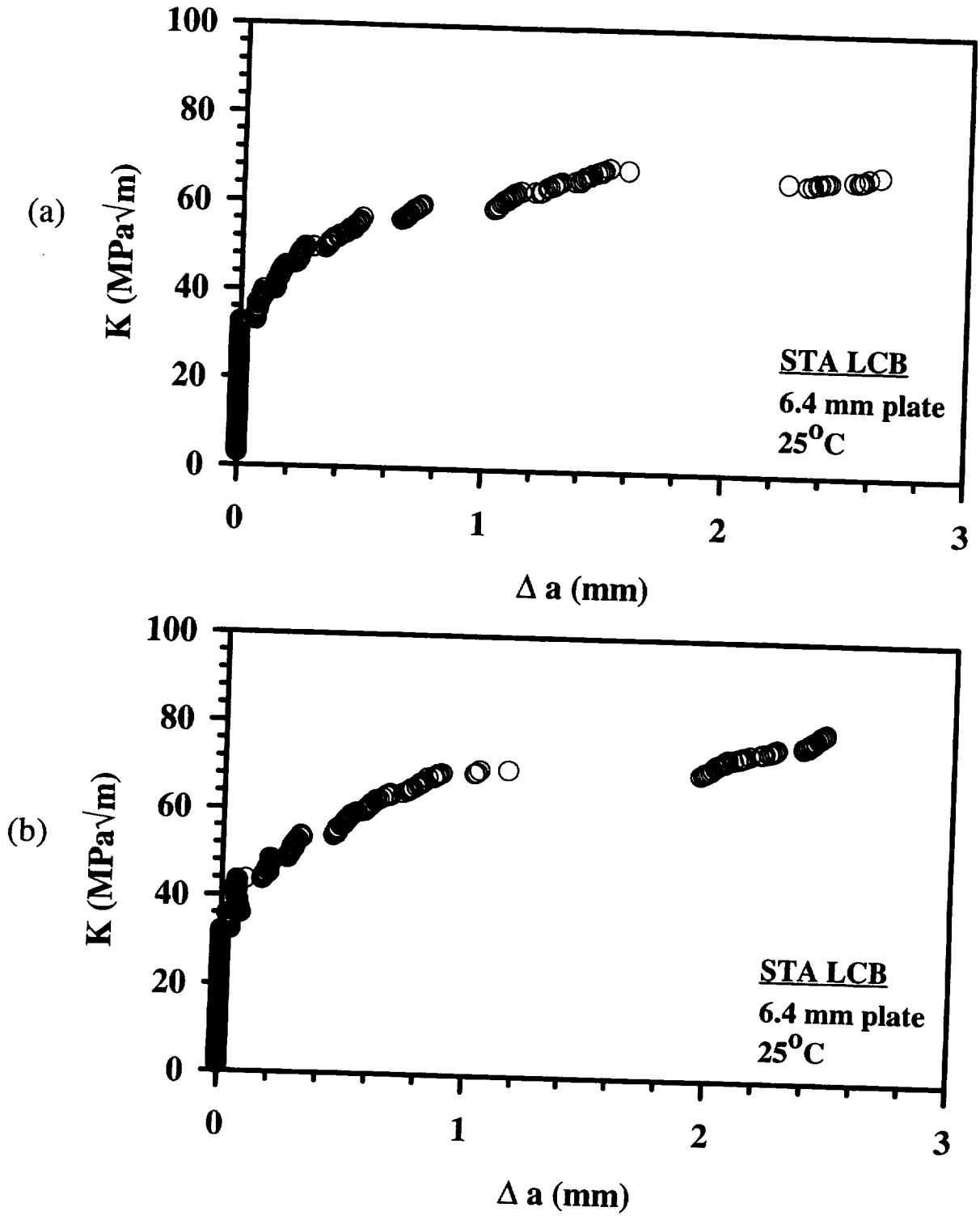

Figure 2 K vs Δ a for TIMET LCB plate specimens tested at room temperature with $\delta = 0.67$ μm/sec, (a) Plate 1, (b) Plate 2.

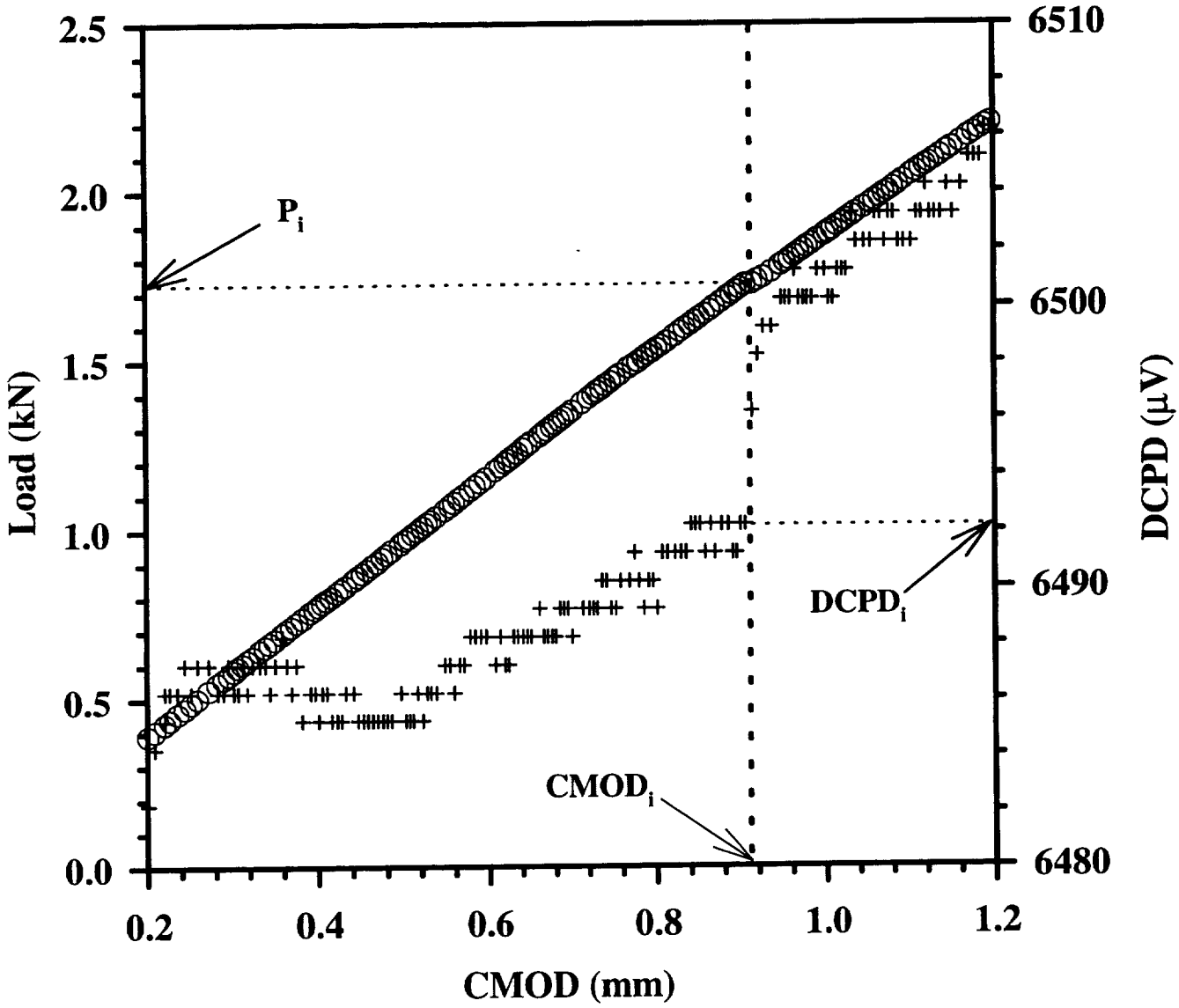

Figure 3 Load and measured electrical potential difference vs CMOD for Sheet 6 LCB. The initiation load, DCPD, and CMOD are labelled.

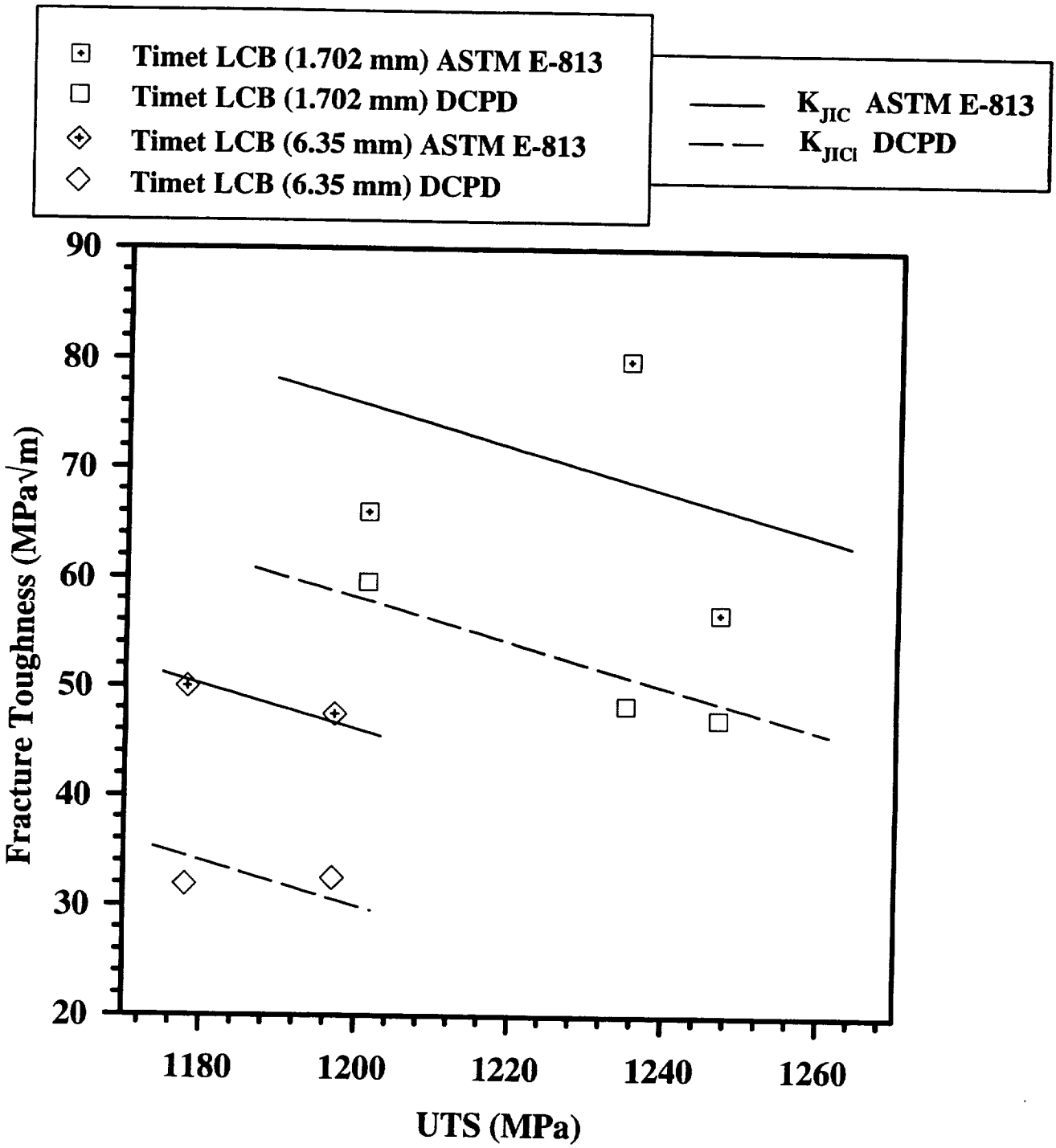

Figure 4 Fracture toughness vs ultimate tensile strength for Timet LCB sheet and plate.

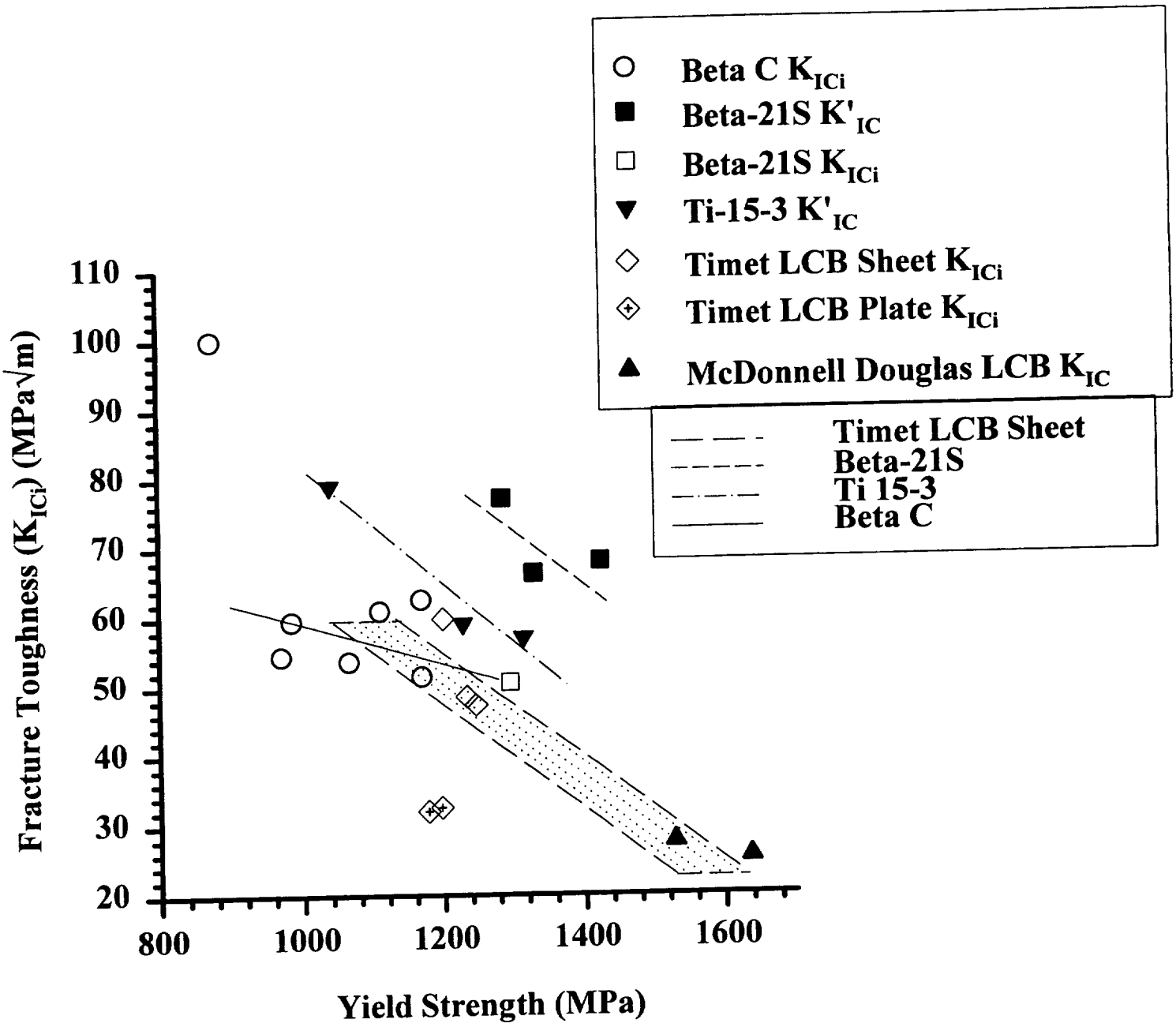

Figure 5 Fracture toughness vs yield strength data and trend lines for various β-titanium alloys.

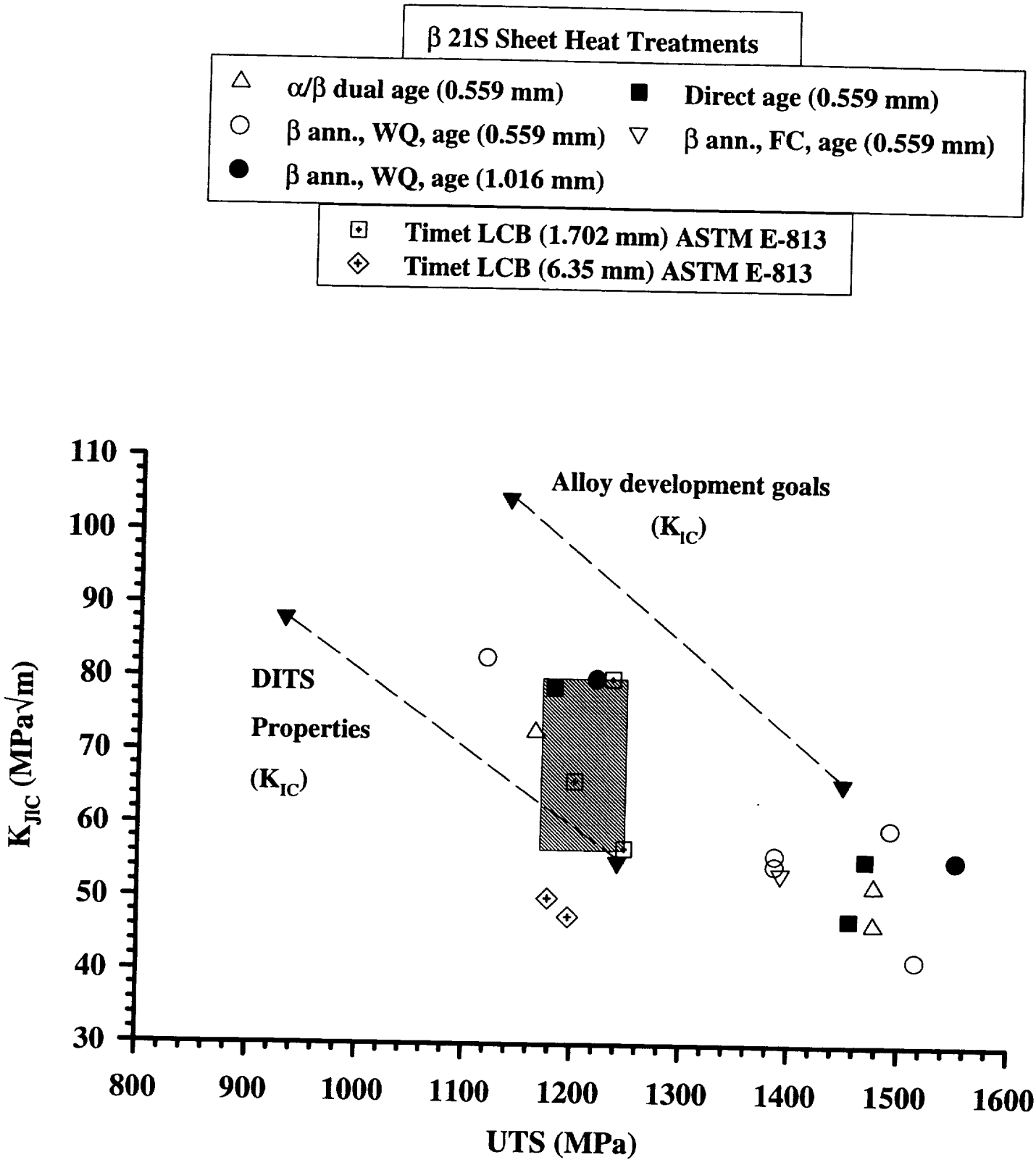

Figure 6 K_{JIC} vs ultimate tensile strength data for various β-titanium alloys.

Project #6b: **MECHANISMS OF DEFORMATION AND FRACTURE IN HIGH STRENGTH TITANIUM ALLOYS: EFFECTS OF TEMPERATURE AND MICROSTRUCTURE**

Faculty Investigator: E.A. Starke, Jr.
Graduate Assistants: S.M. Kazanjian, H. Hargarter

Change in Degree Program

Ms. Kazanjian has committed to the pursuit of a Ph.D. degree and expects completion of this effort in December, 1998.

Dr. Hinrich Hargarter, a post-doctoral fellow visiting from Hamburg, Germany, will contribute his experience in interpretation of titanium microstructures to this research.

Research Objectives

The aim of this project is to identify the mechanisms by which damage occurs in beta-titanium alloys and their dependence on microstructural variations and temperature. The effects of all of the following factors which can influence fracture mechanisms will be investigated for two beta alloys:

1. grain size of the beta phase,
2. alpha volume fraction,
3. grain boundary alpha formation,
4. the presence of metastable phases,
5. alpha morphology,
6. crystallographic texture and
7. temperature at which deformation takes place.

Microstructures and textures will be altered by varying thermomechanical processing sequences so that mechanical properties and deformation modes can be determined for various metallographic conditions.

Background and Approach

The relatively low fracture toughness values initially reported for Timetal LCB (Low Cost Beta: Ti-6.8Mo-4.5Fe-1.5Al)[1] prompted investigation into thermomechanical processing that could produce acceptable fracture toughness in this alloy while maintaining high strength. For comparison, a slightly lower strength, higher fracture toughness beta alloy, Timetal 15-3 (Ti-15V-3Cr-3Sn-3Al) will also be analyzed. The fatigue resistance of Ti-15-3, currently slated for use in the TIGER laminate system, has been recognized as inadequate. Understanding

mechanisms of fracture in these alloys will increase the possibility that processing can be designed to produce microstructures which will optimize the balance of mechanical properties.

Measurements of baseline texture, tensile strength, ductility, fracture toughness[2] and fatigue resistance will be performed on both materials in the form(s) they are received from the manufacturers. Examination of the deformed microstructure compared to the original microstructure will be conducted in a transmission electron microscope (TEM) to identify the nature of deformation taking place. Fracture surfaces will also be evaluated using a scanning electron microscope (SEM).

After examinations of as-received materials are completed, several thermomechanical heat treatments will be performed to produce various microstructures. The applied heat treatments will include at least (a) beta solution heat treatment and quench after rolling, and (b) beta solution heat treatment and direct rolling at various fixed temperatures and percent reductions before quenching and aging. Mechanical tests will again be performed. Deformation modes will be identified using TEM and SEM examination.

This research will be conducted in cooperation with Professor Henry Rack of Clemson University whose students have been developing time-temperature-transformation (TTT) curves for LCB that will aid the selection of processing temperatures for this material[2]. Since alpha phase morphology in these alloys is sensitive to small changes in temperature within the alpha-beta phase field, strict control of the relatively high temperatures required for rolling titanium must be maintained during rolling. For this reason, the rolling will most likely be conducted at a research lab such as G.E. Schenectady, NY.

Progress During the Reporting Period

Initial microstructural, crystallographic and mechanical property evaluation of Timetal LCB sheet and plate received in August has begun. Three sheets (8" x 16" x 0.058") and one plate (7" x 15.75" x 0.370") have been dedicated to this segment of the project. The sheet was processed in the following manner:

1. 7.5" dia. x 10" long ingot
2. Beta forge to 4" x 6" from 2000°F
3. Alpha-Beta forge to 1.75" x 6.5" from 1400°F
4. Beta roll to 0.2" x 6.5" from 1560°F
5. Alpha-Beta roll to 0.12" x 6.5" from 1385°F

---

[2] Fracture toughness will be measured by Sean Hayes and Dr. R. Gangloff, portion "a" of this project.

6. Cold roll to 0.070" (42% reduction)
7. Alpha-Beta solution treat at 1400°F
8. Fan air cool
9. Aged 1100(F for 20 hours

This sequence resulted in the segregated structure shown in Figure 1. Grain size varies significantly both through the thickness of the sheet and across the sheet face. Even more graphic are the layered bands of beta phase separated by thin, continuous layers of alpha. The degree of recrystallization within these beta bands varies, exhibiting maxima at the surface and in one band approximately at the sheet center.

Plate was removed from the above rolling sequence at thickness (0.375", then alpha-beta rolled to final thickness of 0.370", solution treated and aged similarly. Very little alpha-beta rolling is consistent with the microstructure observed, Figure 2. Although drastic segregation is not present in the plate, bands of higher volume fraction of alpha precipitates do exist. Within these bands the precipitates are slightly deformed along the rolling direction. In neighboring bands containing lower alpha volume fractions, the precipitates remain approximately spherical.

Texture measurements made by x-ray diffraction revealed only minimal crystallographic orientation associated with each phase in both sheet and plate. The orientation distribution function (ODF) for the beta phase of LCB sheet is shown in Figure 3. Individual pole figures measured for both sheet and plate are given in Figures 4 and 5. Due to the proximity of their Bragg angles, measurements of $\{0002\}_{alpha}$, $\{10\bar{1}0\}_{alpha}$ and $\{10\bar{1}1\}_{alpha}$ pole figures are dominated by overlapping signal from the $\{110\}_{beta}$ pole, and the $\{10\bar{1}2\}_{alpha}$ pole figure contains the influence of the $\{200\}_{beta}$ pole. Generation of the $\{110\}_{beta}$ pole figure from data measured for $\{200\}_{beta}$ and $\{211\}_{beta}$ accounted for all of the peaks evident on the measured $\{110\}_{beta}$ pole figure. This implies that the alpha peaks do not contribute a significant texture to the measured $\{110\}_{beta}$ pole figure. Because of this relative insignificance, deconvolution of any texture present in the alpha phase is impossible and no pole figures are shown for the alpha phase of either material.

Results of initial mechanical tests of the LCB sheet and plate in the as-received condition measured in three orientations are given in Table I. Tensile tests were performed according to standard ASTM E8 procedure using standard 0.25" gage width sub-size flat specimens for sheet and 0.160" diameter small-size round specimens for plate. Elastic properties of the plate, given in Table II were evaluated ultrasonically by Doug Queheillalt at the University of Virginia.

Table I: Timet LCB Tensile Properties

Specimen	No. of Tests	Yield, 0.2% ksi [MPa]	UTS ksi [MPa]	Fracture Stress Ksi [MPa]	Elongation (%)
Sheet, RD	2	161.8 [1116]	166.6 [1149]	186.4 [1285]	9.9
Sheet, 45°	2	164.0 [1131]	164.4 [1134]	199.0 [1372]	11.4
Sheet, TD	2	171.2 [1180]	172.4 [1189]	189.6 [1307]	5.4
Plate, RD	2	171.0 [1179]	172.7 [1191]	206.6 [1425]	15.8
Plate, 45°	2	166.6 [1149]	166.6 [1149]	220.0 [1517]	17.6
Plate, TD	1	171.8 [1185]	172.3 [1188]	212.8 [1467]	14.9

Table II: Timet LCB Elastic Properties

Specimen	HRC	Ultrasonically Measured Moduli X E06 Psi [GPa]			Poisson's Ratio
		Young's, E	Bulk, K	Shear, G	
Plate	41	18.8 [130]	13.8 [95]	7.4 [51]	.273

Tensile tests revealed little anisotropy of yield and ultimate strength although elongation proved to be orientation dependent. The yield strength of ~162 - 172 ksi is below target of 180 ksi for this alloy when aged at 1100°F. Ultimate tensile strength (UTS) was expected to be 185 ksi rather than the 164 - 173 ksi measured[1]. The lack of work hardening is typical, however. This

material was intentionally processed by Timet to produce a balance of yield strength and fracture toughness.[3] Scanning electron microscopy (SEM) revealed fracture features of the same scale as the alpha-surrounded grains, Figure 6.

Pieces of both sheet and plate were beta solution heat treated in the lab to examine the orientation of the primary and precipitated alpha phase within the beta matrix. These examinations are continuing.

Two sections of 15-3 plate of composition given in Table III were contributed by Dr. John Scully at Univ. of VA for initial evaluation of the material in solution heat treated and quenched condition and peak aged condition. These investigations are getting under way.

Table III: Ti - 15V - 3Cr - 3Sn - 3Al Composition, wt %[5]

	V	Cr	Al	Sn	O
Spec.	14.0-16.0	2.5-3.5	2.5-3.5	2.5-3.5	0.13 max
Actual	14.9	2.99	3.21	3.61	0.123

Remainder Titanium

Conclusions

Non-uniformity of the LCB sheet microstructure developed during rolling contributes to the anisotropy of ductility. This anisotropy is averted when the material is processed to achieve a more uniform microstructure as in the plate.

Since microstructural segregation is severe in the as-received LCB sheet and crystallographic texture is minimal, any property dependence on texture would be overwhelmed by microstructural effects. Study of the effect of texture on deformation modes will be postponed until material with significant texture can be produced.

Identification of deformation modes in the LCB sheet and plate has proven difficult due to their complex microstructures. Testing material in the beta solution heat treated and quenched condition will reduce the complexity and provide information on deformation in the beta phase. Similar tests on Ti-15-3 in the solution treated condition will establish baseline beta deformation information for this alloy as well. After this is determined, deformation in the more complex aged structures will be more easily discernible.

Tasks for the Next Reporting Period

The main thrust of this project during the next few months will be recognition of deformation taking place during testing. TEM samples from LCB sheet specimens strained to failure (5-17%) and to 1% are currently under examination to try to determine the nature of deformation that has taken place. However, examination of beta solution treated material is of higher priority, since the alpha+beta solution treated and aged microstructures are so complicated. The Ti-15-3 currently available will be solution treated and strained to various, relatively low strain levels in order to characterize deformation in the beta phase. After additional material is received from R. Boyer of Boeing, tensile and fatigue properties will be measured and microstructures examined in a variety of aged conditions.

Until the receipt additional Ti-15-3 material, tensile properties as a function of temperature for the as-received LCB sheet will be determined. Center-cracked panel specimens will also be prepared from this material to perform fatigue crack growth rate measurements. The test system will be configured and tests underway by the end of the next reporting period.

References

1. John Fanning, HSCT Program Review, HSR Metallic Materials Task Reviews, Titanium Development Tasks, April 14, 1995, NASA Langley Research Center, Hampton, VA.
2. Sébastien Azimzadeh, "Phase Transformations in Metastable (Titanium Alloys," Master of Science Thesis, Clemson University, December, 1995.
3. John Fanning, TIMET, to R. Gangloff, UVA, communication, Sept. 29, 1995.
4. U.F. Kocks, J.S. Kallend, H.R. Wenk, A.D. Rollet and S.I. Wright, *popLA, Preferred Orientation Package - Los Alamos,* July, 1994, Los Alamos National Laboratory, Los Alamos, NM.
6. George Young, "Hydrogen Effects in Metastable Beta-Titanium Alloys," Master of Science Thesis, Materials Science, Univ. of VA, August, 1993.

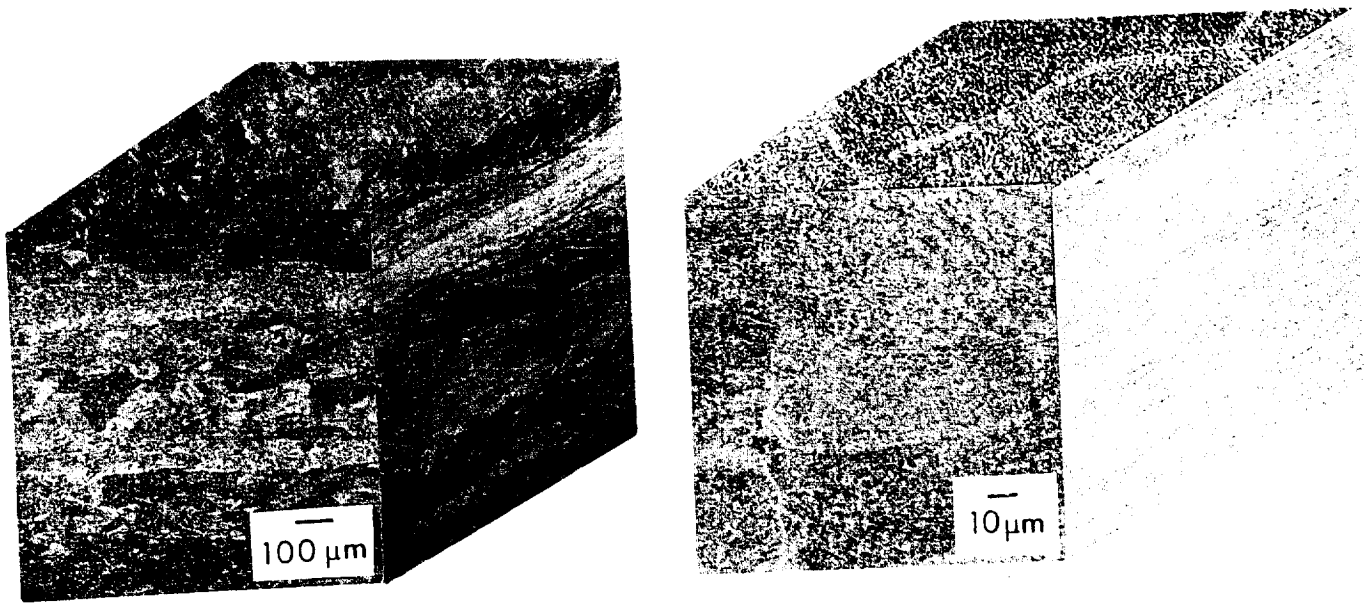

(a) (b)

Figure 1. Bands of beta phase containing unequal amounts of recrystallization are visible in the as-received LCB sheet (a). Continuous alpha phase is present along boundaries of pancake shaped grains oriented in the rolling direction (b).

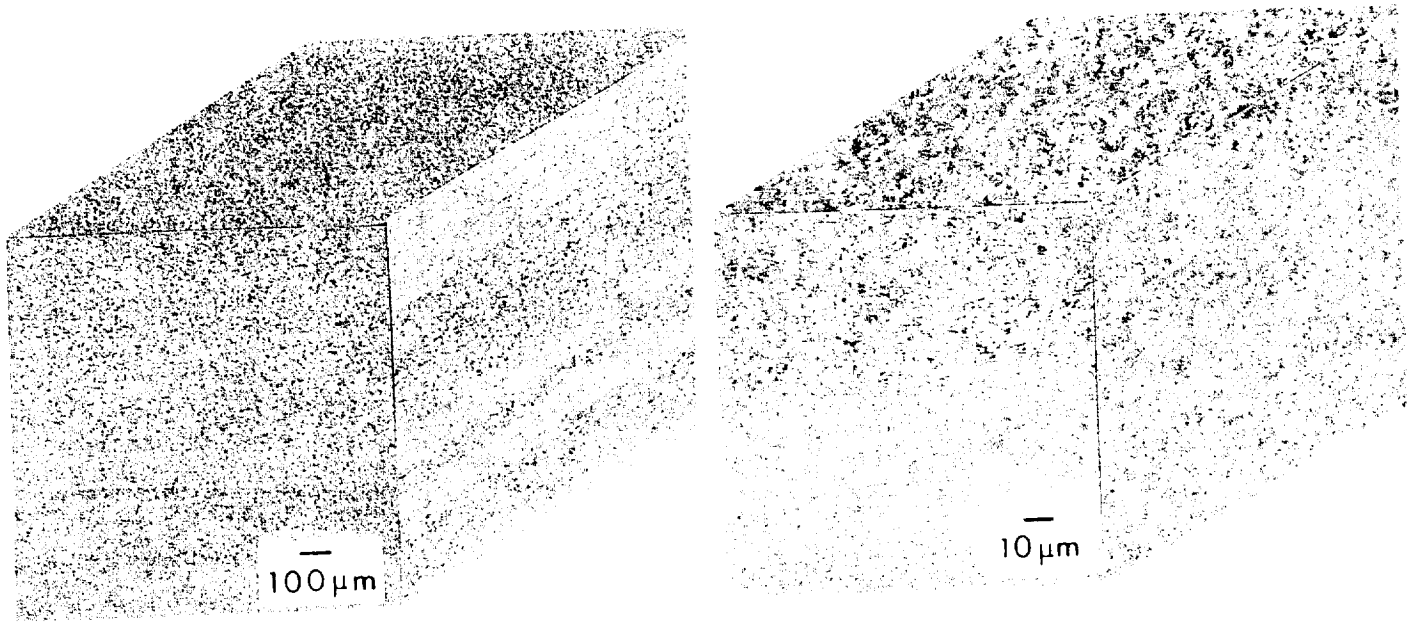

(a) (b)

Figure 2. Distribution of alpha in as-received LCB plate is more uniform than in the sheet (a), however, bands containing higher volume fraction of slightly deformed alpha are evident, as visible in the lower half of (b).

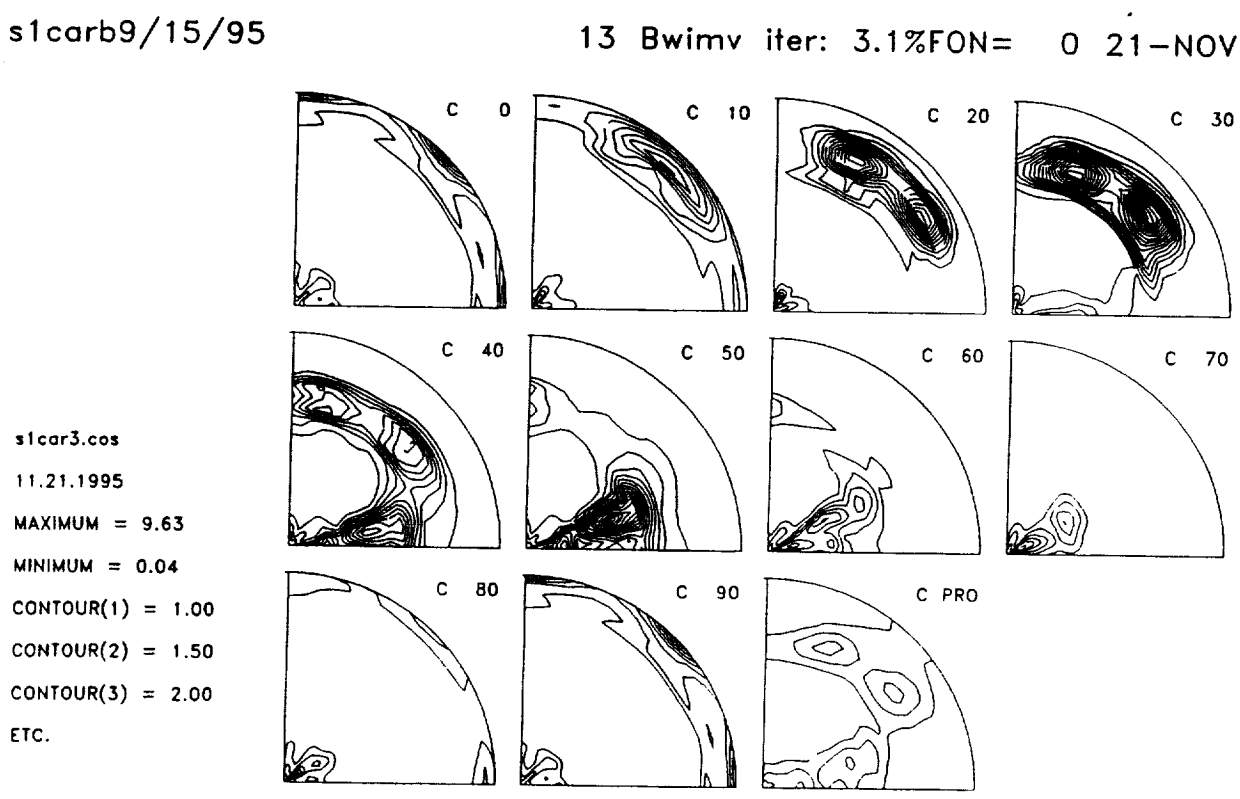

Figure 3. LCB Sheet Orientation Distribution Function (ODF) for the beta phase.

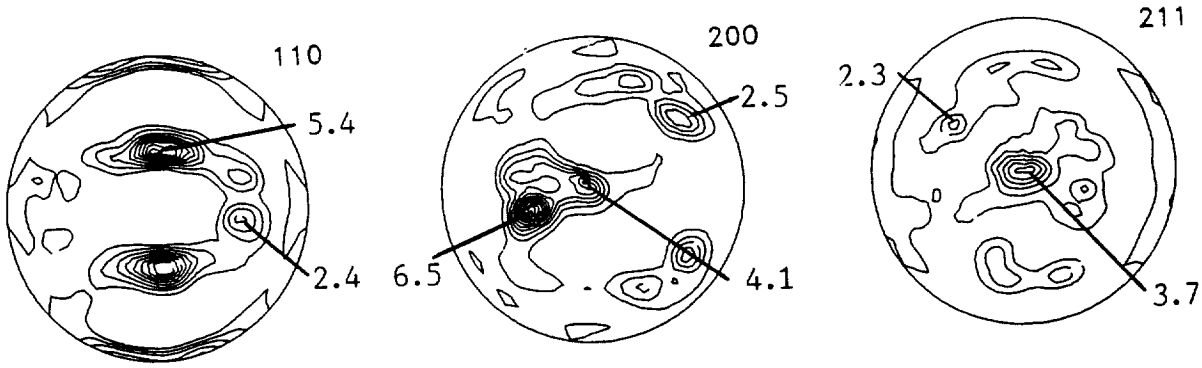

Figure 4. LCB Sheet pole figures for $\{110\}_{beta}$, $\{200\}_{beta}$ and $\{211\}_{beta}$ poles.

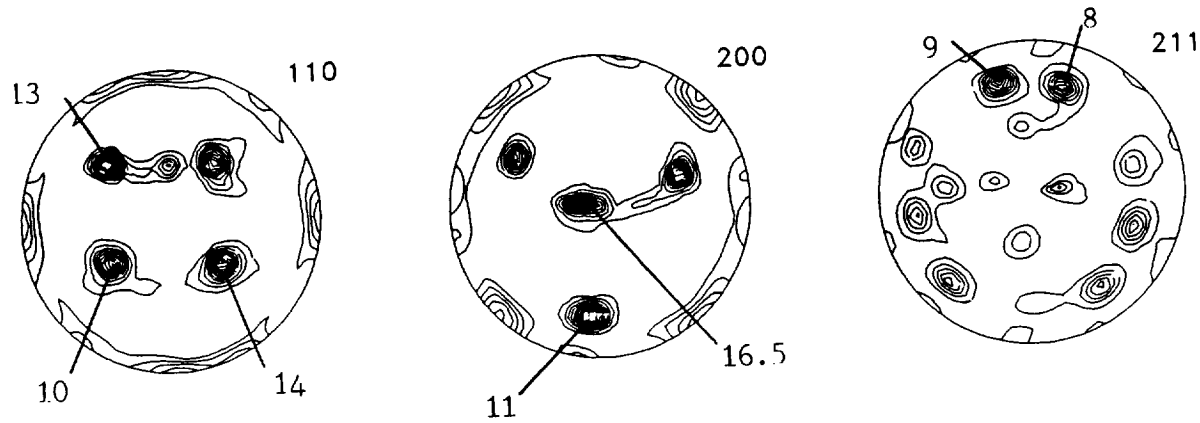

Figure 5. LCB Plate pole figures for $\{110\}_{beta}$, $\{200\}_{beta}$ and $\{211\}_{beta}$ poles.

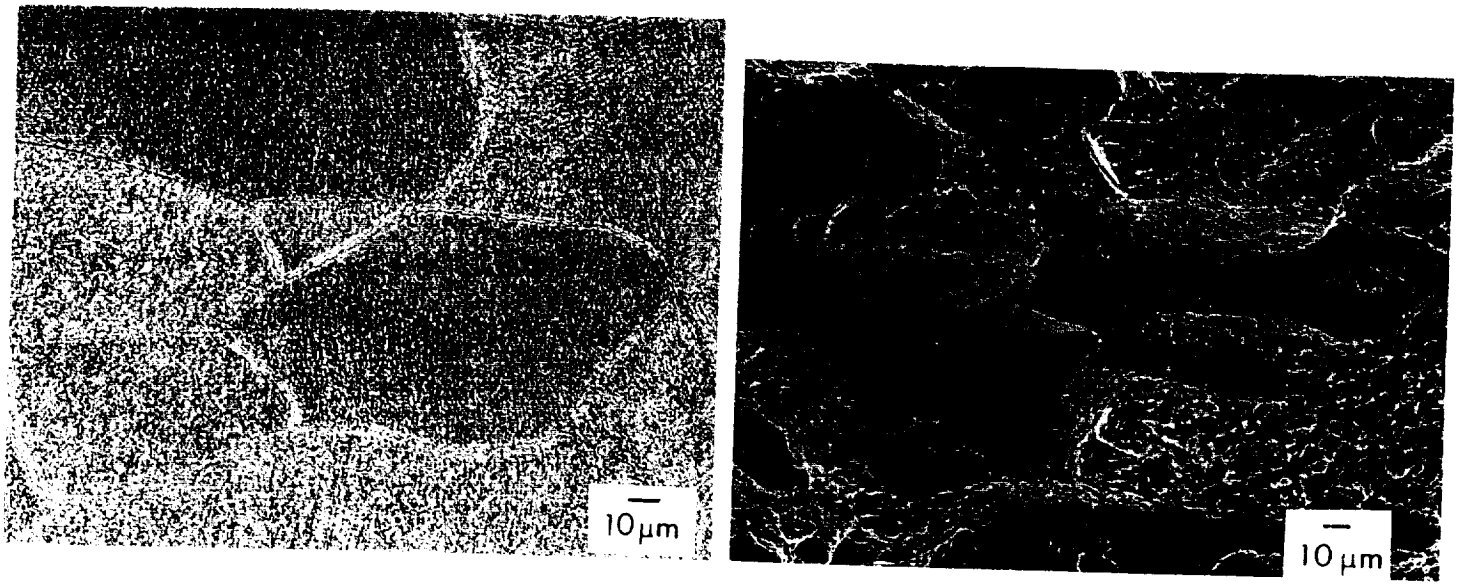

(a) (b)

Figure 6. Correlation between fracture features and grain size for as-received LCB sheet. The alpha phase at grain boundaries plays an important role during fracture.

(a) Optical microscopy

(b) SEM

Project #7: EVALUATION OF WIDE-PANEL ALUMINUM ALLOY EXTRUSIONS

Faculty Investigator: John A. Wert
Graduate Student: Mark T. Lyttle; Ph.D. Candidate

Research Objectives

The overall objective of this project is to experimentally observe and model the effects of microstructure and texture on yield strength in wide panel aluminum alloy extrusions. The modeling results will enable the prediction of locations and tensile axis orientations corresponding to minimum yield strength where localized yielding could occur in service. A generalized form of these models can be applied to any combination of microstructure and texture found in other aluminum alloys.

This progress report describes a series of yield strength observations made with an AA2090 extrusion in which the texture, grain morphology, and precipitate volume fractions vary with location. Comparison of the experimental observations with model predictions provides insight into the influence of precipitates on yield anisotropy, and into the interaction between matrix contributions and multiple precipitate contributions to yield strength.

Background and Approach

The large extrusion presses available in Russia offer the possibility of manufacturing wide panel extrusions with integral stiffeners. The manufacturing process used by the Russians involves extrusion of tubular forms with longitudinal L-shaped stiffeners protruding from the outer surface. The extruded tube is slit longitudinally and flattened in a series of rolling and stretching operations. The final product is a wide, flat panel with integral stiffeners on one side. The integrally stiffened panels may provide an economical alternative to conventional riveted or adhesively bonded aircraft and launch vehicle structures.

The manufacturing operations described above result in complex metal flow patterns in many portions of the panel, creating certain microstructure and crystallographic texture characteristics that are far different from those found in conventional rolled or extruded aluminum products. Because of the shape of the extrusions in the vicinity of the stiffeners, the metal flow pattern during extrusion and flattening operations varies greatly over short distances (on the order of several millimeters). Since mechanical properties depend on microstructure and texture, the mechanical properties are virtually certain to vary with location in the panels, particularly in the vicinity of the stiffeners. In addition, substantial out-of-plane loading is likely to occur in the

vicinity of the stiffeners. Knowledge of the variation of mechanical properties with location in the panels, and with loading direction at these locations, is needed for efficient and safe use of wide-panel aluminum alloy extrusions in aerospace vehicles.

The proposed work will address this problem through a combination of experimental measurements and modeling of the influence of microstructure and texture on tensile properties. Four aspects of the material will be characterized experimentally at selected locations: texture, grain morphology, deformation substructure, and precipitate morphology. These characteristics will be incorporated into previously proposed models that predict yield strength based on separate characteristics. An effort will be made to blend the previous models into an overall model to predict yield strength as a function of stress axis orientation for the selected alloy. The model will be tested and refined by comparison with tensile test results generated by NASA and NASA contractors, and by additional tests at UVa. The model will then be used to predict the extreme values of yield strength, and the associated stress axis orientations, as a function of location in and near the stiffeners. These results can then be used to define limiting load conditions for the panels such that localized yielding is avoided. It is possible that the results could also be used to recommend changes in processing conditions (for example: extrusion temperature, die geometry, or flattening procedure) that would raise the minimum yield strength or change its stress axis orientation, resulting in improved panel performance.

A major goal of this research is the prediction of yield strength as a function of microstructural characteristics. Models based on fundamental principles now exist for understanding the contribution of precipitate particles, solute in solid solution and dislocation substructure to yield strength [1-4]. However, due to the complexity of microstructural features found in real engineering materials, synthesis of these various strengthening mechanisms into a unified model that can accurately predict yield strength directionality has not been previously described.

The three primary microstructural aspects influencing yield strength that will be investigated are slip plane orientation, precipitate location and morphology, and grain morphology. Characterization of the microstructure will be focused on these three areas:

1. Use texture results to perform Taylor/Bishop-Hill yield anisotropy predictions for both in-plane and out-of-plane tensile axis orientations. Using texture results obtained from pole figure data, a set of grains representative of the orientations present in each area of the extrusion can be generated. Combining Taylor/Bishop-Hill analyses and this representative set of grains, the active set of slip systems and corresponding Taylor factor in each grain can be determined.

Averaging over all grains yields the average Taylor factor for the specified uniaxial stress orientation.

2. Microstructural assessment by TEM will reveal the precipitate type, size, habit plane, volume fraction, and morphology as a function of location. Since the dislocation substructure is inhomogeneous, the precipitate characteristics may vary as a function of location within the extrusions. The precipitate characteristics at each location will be incorporated into the appropriate precipitate inclusion model to assess the contribution of precipitate strengthening to yield strength.

3. Grain morphology will be determined by optical metallography. When grains are not equiaxed, some relaxation of the compatibility requirements of the Bishop-Hill model occurs [5]. Modeling the effect of grain morphology and the concurrent relaxed constraint conditions, leads to a reduction in Taylor factor in certain orientations. Incorporation of grain morphology into yield surface predictions seems essential in cases where grain shape is not essentially equiaxed.

Progress During the Reporting Period

The alloy under study is a AA2090 (Al-2.2Li-2.8Cu-0.12Zr, in weight percent) aluminum alloy net shape extrusion. Skin and cap regions of the extrusion were examined as-received and in an overaged condition. The skin region was also subjected to an overaging treatment of 400 h at 160°C, while the cap region was overaged for 24h at 300°C. The overaging treatments were chosen to alter the relative volume fractions of the δ' and T_1 phases while keeping texture and grain shape unchanged.

Microstructure and Texture

The grain structures found in near net shape extrusions of the type being considered here have been described by Hales [6]. The skin region contains pancake-shaped grains, while the cap region contains lath-shaped grains. The difference in morphology can influence the degree of constraint, which manifests itself in a reduced Taylor factor.

The as-received skin and cap regions also have somewhat different precipitate characteristics. The skin microstructure consists primarily of δ' and θ' with small volume fractions of δ'/ θ" and T_1, as shown in Figure 1a. The cap region contains roughly equal volume fractions of T_1 and δ', as shown in Figure 1b. No grain boundary precipitation or inhomogeneous precipitation was observed in either region.

Overaging treatments were chosen to isolate the strengthening increment of individual precipitate phases. This goal was accomplished by overaging the skin region to reduce the volume fraction of T_1, as shown in Figure 1c, and overaging the cap region to increase the volume fraction of T_1, as shown in Figure 1d. The overaged skin region contains coarse δ' precipitates and a smaller volume fraction of θ' precipitates. In addition, a very small volume fraction of T_1 was observed. The overaged cap region appears to have undergone complete δ' reversion. Large T_1 precipitates were observed and there was substantial grain boundary precipitation.

Similar textures, characteristic of a deformation microstructure, were observed in all four regions of the alloy. The ODF for the overaged skin region contains very strong brass and copper components. Other than a weak cube component, there are no other texture components of note. The three other regions of the extrusion contain similar textures. The overaged regions exhibited the same texture as their as-received counterpart indicating that no significant recrystallization or orientation-dependent preferential grain growth had occurred.

The predicted Taylor factor variation for a microstructure consisting primarily of grains with brass and copper texture orientations typically contains a maximum near 0°, a local maximum near 90°, and a minimum near 45°. The magnitude of the Taylor factor anisotropy is dependent on the intensity of the texture types.

Experimental Yield Anisotropy for Skin, Cap, Overaged Skin, and Overaged Cap Regions

Figure 2 shows the experimental variation of yield strength for the four regions/aging treatments examined in the AA2090 alloy. The yield strength of the as-received skin region is virtually isotropic with a slight maximum at 90° to the extrusion direction. The as-received cap region exhibits greater anisotropy. From a minimum near 450 MPa in several orientations of the cap region, a maximum of 600 MPa is observed with the compression axis oriented 90° to the extrusion direction.

The overaged skin region exhibits yield anisotropy characteristic of a typical rolled microstructure. The maximum yield strength of 440 MPa occurs with the compression axis oriented parallel to the extrusion direction, while the minimum yield strength occurs at 45° to the extrusion direction and a lesser maximum occurs at 90° to the extrusion direction. The magnitude of yield strength variation is roughly 50 MPa.

The overaged cap section has the largest yield strength oriented parallel to the extrusion direction, of about 250 MPa, and appears to have a continuously decreasing yield strength as the angle between compression axis and extrusion direction increases. The yield strength reaches a

roughly constant value of 220 MPa for compressive axis orientation between 45° to 90° from the extrusion direction.

These experimental results reveal the strong influence of precipitate morphology on yield anisotropy. Since the overaging treatments did not alter the texture or grain morphology, the significant changes in yield anisotropy associated with overaging can only be attributed to precipitate morphology and volume fraction.

Model Results

For each region, the yield strength measurements from each direction are combined with texture and TEM microstructure information to yield a set of equations of the form

$$\sigma_f = M\,\tau_M\,(1 - f) + f\,\sigma_{PPT}\,N \qquad (1)$$

which are then fitted using the least squares method to determine flow stress parameters for the matrix and precipitate phases [1]. M is the orientation dependent Taylor factor (or a relaxed constraint version of it), τ_M is the CRSS of the matrix phase, f is the volume fraction of precipitates, σ_{PPT} is the yield strength of the precipitate phase, and N is the orientation dependent precipitate strengthening factor.

Figure 3 shows how texture and microstructure measurements are combined in the plastic inclusion model, Equation (1), to predict the yield anisotropy. For the overaged skin region, texture measurements predict a variation in the Taylor factor that is typical of a deformation microstructure, Figure 3a, for pancake-shaped grains. For this texture, the orientation dependence of precipitate strengthening factor, N, is shown for plate-shaped precipitates on {111} planes, T_1, and on {100} planes, θ', in Figures 3b and 3c respectively. For all regions of this alloy, the anisotropy corresponding to Taylor factor and to precipitates on {111} planes is roughly similar. The anisotropy contribution predicted for precipitates on {111} planes is essentially opposite that predicted for precipitates on {100} planes.

Using volume fractions for the precipitates and estimates of precipitate and matrix strengths, i.e. aluminum matrix CRSS is generally between 50 to 70 MPa and the effective flow strengths of θ' and T_1 are much greater than that of δ', the macrostructural strengths of the phases are solved using a least squares method. The yield anisotropy in all orientations can then be predicted as seen in Figure 3d. To measure the effectiveness of the predictions and suitability of

the model construction, the correlation coefficient, r^2, and the standard deviation, SD, are calculated for each region.

Better agreement could be obtained by choosing matrix shear strengths and effective precipitate yield strengths independently for each region. However, setting internally consistent values for these values is more of a true test of the model's viability and as shown in Table 1, these values provide good correlation for all regions tested. For the skin, cap, and overaged skin regions, the predicted results correlate well with the experimental yield strengths ($r^2 > 0.90$), while the skin, overaged skin, and overaged cap regions adequately predict the magnitude of variation as well (standard deviation < 10 MPa).

Comparing the correlation coefficients of Taylor factor alone with those generated from the plastic inclusion model in Table 1 shows that, for all regions tested, the plastic inclusion model provides a better prediction of the yield anisotropy. For example, the fully constrained Taylor factor is a poor predictor of the plastic anisotropy in the as-received skin region, $r^2 = -0.58$, but using the reduced constraint Taylor factor corresponding to pancake-shaped grains and the predominant strengthening effect of θ' precipitates, the correlation is vastly improved, $r^2 = 0.88$.

Taylor factor alone more closely predicts the yield anisotropy in the overaged regions, which is expected since the magnitude of the precipitate strengthening and associated anisotropy is reduced in overaged specimens, thereby emphasizing the Taylor factor contribution. From this, it is apparent that T_1 and θ' play an important role in the strengthening process and in the anisotropy of the yield strength in the peak-aged condition.

In one instance the anisotropic effects of Taylor factor, precipitate information, and grain morphology on yield strength as described by the plastic inclusion model are not enough to accurately predict the magnitude of yield strength variation. In the cap region, the magnitude of yield strength variation is approximately 150 MPa, or a 25% variation depending on compression axis orientation. A corresponding variation in terms of Taylor factor would be 2.6 to 3.3, which is observed only in multicrystals or very highly textured materials. For the present alloy, no single term in the inclusion model exhibits as large a percentage variation as the experimentally observed yield strength variation in the cap region.

Discussion

The present results reveal that the plastic inclusion model is in fair agreement with experimental yield strength measurements for the peak-aged and overaged skin and cap regions. However, some characteristics of the experimental observations are not accurately predicted using

this model. In the discussion section, possible origins for these deviations are considered.

Two possible origins of the inability of the plastic inclusion model to accurately predict the plastic anisotropy and magnitude of anisotropy are considered. The first possibility is that there are additional contributions to anisotropy that are not accounted for in the plastic inclusion model. The second possibility is that the plastic inclusion model, while a good first order approximation to the yield anisotropy, does not completely describe the interdependence of matrix and precipitate strengthening.

To analyze the first possibility, one must consider the role in strengthening that secondary factors play in a typical aluminum alloy. Some of the secondary contributions that have been considered are microstructural factors such as gradients of Li and Cu in solid solution, non-random precipitate distributions, and subgrains, or texture characteristics such as through-thickness texture variation [7]. For the present alloy and other similar aluminum alloys, the strengthening contributions due to solid solution and grain size strengthening are small relative to the strengthening due to the pure matrix and precipitates. For this reason, any anisotropy in the solid solution and grain size terms would appear to have a negligible effect on the overall yield strength anisotropy of the alloy. In this alloy, no non-random precipitate distributions were observed.

For the overaged skin region of the extrusion, yield anisotropy due to through-thickness texture variation is not significant because measurement of quarter-thickness pole figures reveals an ODF that is virtually identical to the ODF generated at the half-thickness location. If this were not the case, accounting for though-thickness texture variation could be accomplished easily be measuring pole figures and creating an ODF from planes other than the half-thickness plane, and attributing an appropriate fractional volume of the alloy to each ODF.

The second possible area of refinement is that the structure of the plastic inclusion model, with matrix and precipitate effects linearly independent, is only a first order approximation that neglects the interdependence of matrix and precipitate strengthening. This possibility is similar to the idea behind the method of superposition used for multiple precipitates.

The inability of the plastic inclusion model to predict the magnitude of the strength variation in the cap region brings into question the assumption that anisotropic precipitate strengthening is correctly described as an independent strengthening term in this, and similar, alloys. In the present form of the plastic inclusion model, yield strength of the precipitate is taken to be a constant. Using an approach outlined by Hosford and Zeisloft [1], if the activated slip systems in the matrix operate likewise on the precipitate, it is just as valid to write:

$$\sigma_{PPT} = M\ \tau_{PPT} \qquad (2)$$

where (τ_{PPT} is taken to be constant.

For a given slip system in a homogeneous alloy, critical resolved shear stress is taken to be a constant, with no strain state or orientation dependence. The consideration above suggests that the precipitate CRSS, rather than yield strength is constant. Incorporating this effect in Equation (1) yields:

$$\sigma_f = M\,\tau_M\,(1-f) + f\,M\,\tau_{PPT}\,N \qquad (3)$$

The effect of multiplying Taylor factor (M) and precipitate strengthening factor (N) in the second term tends to i) accentuate the anisotropy of precipitates on {111} planes which exhibit a similar anisotropy as Taylor factor and ii) minimize the predicted anisotropy associated with precipitates on {100} planes. Multiplying precipitate strengthening factor by Taylor factor increases the magnitude of the plastic anisotropy of precipitates on {111} planes from 12% to 16% and decreases the plastic anisotropy of precipitates on {100} planes from 10% to 6%. This refinement of the model used by Bate [3] substantially improves the agreement between the model results and experimental observations for the case of the 2090 extrusion.

Conclusions

The plastic inclusion model, incorporating grain morphology and precipitate characteristics, accurately predicts the yield anisotropy observed in the four different microstructures tested of the AA2090 alloy.

The plastic inclusion model, $\sigma_y = M\,\tau + \sum f_i\,\sigma_i\,N_i$, predicts the plastic anisotropy of the 2090 alloy better than a model with Taylor factor as the only anisotropic parameter, $\sigma_y = M\,\tau$. The Taylor factor model more accurately predicts the yield strength variation in the two overaged specimens. This indicates that in alloys with a large precipitate strengthening contribution, incorporation of anisotropic precipitate terms into a yield model is essential for accurate prediction of the variation of yield strength.

Increased accuracy in the prediction of yield strength anisotropy will more likely come from refinement of the present anisotropic terms in the plastic inclusion model or from consideration of any interdependence of Taylor factor and precipitate strengthening anisotropies than from construction of additional terms corresponding to secondary anisotropic contributions.

Tasks for the Next Reporting Period

Similar studies to that performed on the 2090 extrusion will be undertaken on the 2195 and the 2096 extrusions. Experimental results from these two alloys should provide a good tool to determine the macrostructural parameters in the inclusion models (effective flow strength of T1, θ'and δ') because of the major difference in phase composition of the two alloys in the as-received condition. Qualitatively, it is known that there is a δ' presence in the 2096 alloy, while there is a complete absence of δ' and a concurrent T1 volume fraction increase in the 2195 alloy. This manifests itself experimentally in a higher strength of 2195, which is apparently due to T1 being a more potent strengthener than δ' [8]. Compression testing of two regions in the 2195 extrusion with distinct textures will allow determination of the effective flow strength of T1. Due to the absence of δ' in the 2195 alloy, the yield anisotropy is primarily dependent on two aspects; texture and T1 orientation. With two independent sets of compression data, the strengthening of each of the two aspects can be explicitly deduced.

Examining the experimental results from three alloys of roughly similar compositions, but containing widely varying microstructures, the basic strength inputs to the inclusion models, i.e. shear stress for single slip of the matrix and the effective flow strength of the precipitates, should be able to be determined. When these macrostructural constants are fixed, the viability of using the plastic and elastic inclusion models for global plastic anisotropy predictions can be evaluated.

References

1. F. Hosford and R. H. Zeisloft, *Metall. Trans.*, **3**, 113 (1972).
2. Y. Chin and W. L. Mammel, *Trans. TMS-AIME*, **245**, 1211 (1969).
3. Bate, W. T. Roberts, and D. V. Wilson, *Acta metall.*, **29**, 1797 (1981).
4. Bate, W. T. Roberts, and D. V. Wilson, *Acta metall.*, **30**, 725 (1982).
5. F. Kocks and H. Chandra, *Acta metall.*, **30**, 695 (1982).
6. J. Hales, microstructure of 2090.
7. K. Vasudévan, W. G. Fricke, Jr., R. C. Malcolm, R. J. Bucci, M. A. Przystupa, and F. Barlat, *Metall. Trans. A*, **19A**, 731 (1988).
8. C. Huang and A. J. Ardell, *Journal de Physique*, **48** (1987) C3-373.

Table 1. Comparison of the correlation coefficients between the plastic inclusion model and experimental results and Taylor factor and experimental results.

Condition	Plastic Inclusion Model ρ^2	Plastic Inclusion Model SD (MPa)	Taylor factor ρ^2
Skin	0.91	3	- 0.58
Cap	0.88	52	0.19
Overaged Skin	0.95	10	0.90
Overaged Cap	0.60	8	0.50

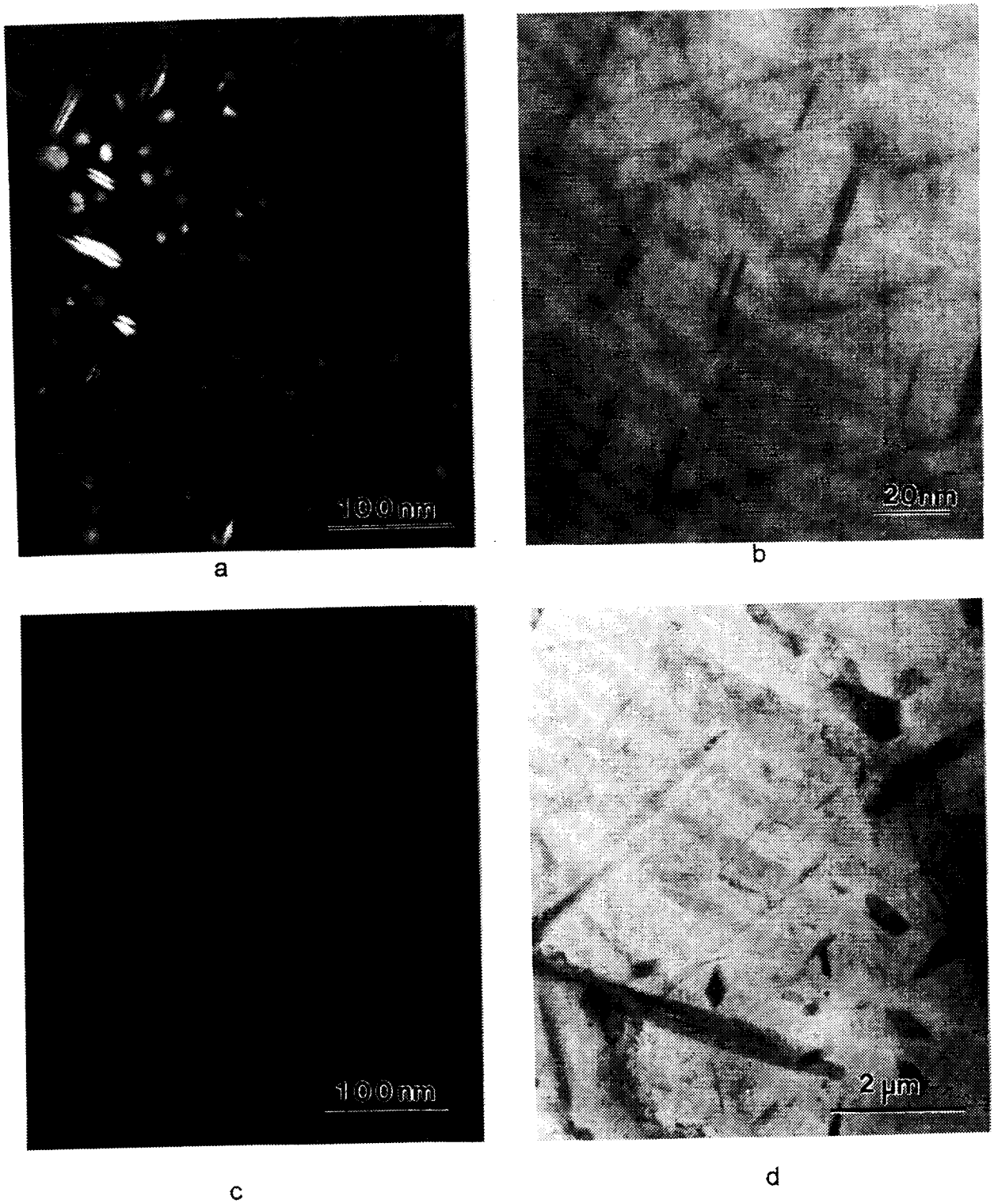

Figure 1. TEM micrographs of the microstructures in (a) the skin region, (b) the cap region, (c) the overaged skin region, and (d) the overaged cap region of the 2090 alloy.

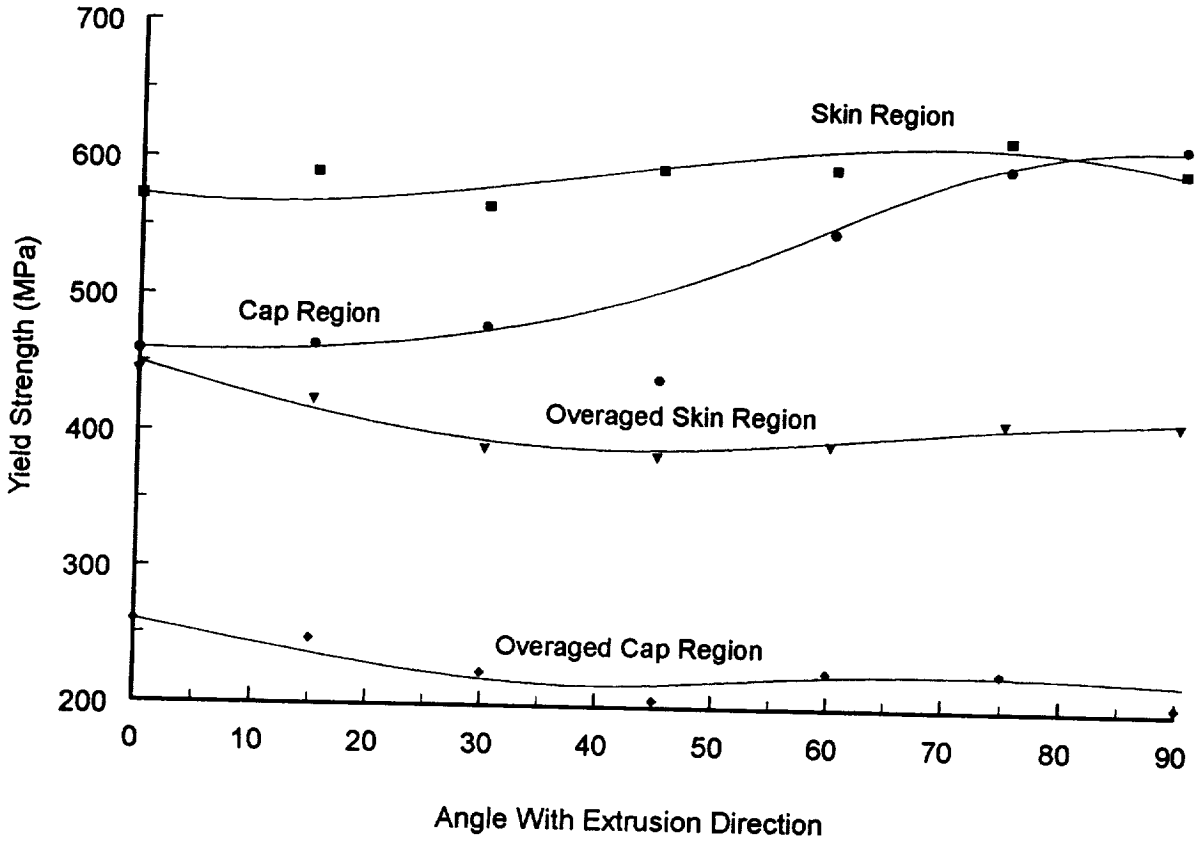

Figure 2. Variation of flow stress for 2090 extrusion in as-received and overaged conditions.

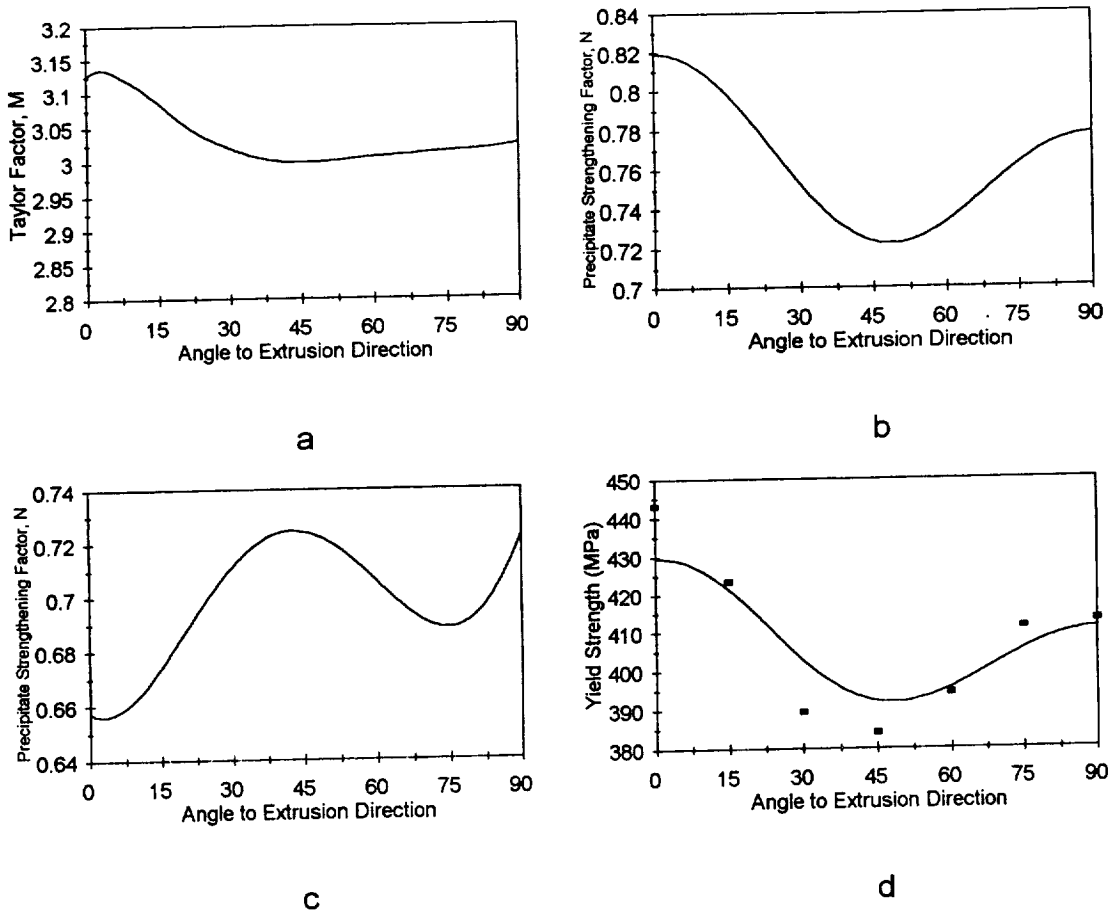

Figure 3. Compressive axis dependence of M, N, and the resulting yield anisotropy curve for the overaged skin region; (a) Taylor factor, (b) precipitate strengthening factor for {111} precipitates, (c) precipitate strengthening factor for {100} precipitates, and (d) the yield anisotropy curve with experimental results superposed.

Project #8: Al-Si-Ge ALLOY DEVELOPMENT

Faculty Investigator: E. A. Starke, Jr.
Graduate Student: H. J. Koenigsmann, Ph.D. Candidate

Research Objective

The objective of this project is to investigate the void nucleation and growth processes in a recently developed Al-0.55Si-2.02Ge (wt.%) alloy. The relationship between precipitate size and critical strain for cavity nucleation during plastic deformation is of primary interest.

Background and Approach

The ductile fracture of Al-Si-Ge alloys occurs by the nucleation, growth, and coalescence of cavities. Since the ductility may be increased if the onset of cavity nucleation is delayed, it is important to study the parameters controlling cavity nucleation [1]. This project investigates cavity nucleation and growth associated with spherical SiGe precipitates that are one to two orders of magnitude smaller than previously studied [1] and analyzes the experimental results using finite element calculations.

Criteria for cavity nucleation are a complex combination of the second-phase particle size, stress and strain levels, and local deformation modes [2]. There has been some debate as to whether or not there exists a critical strain to nucleate cavities [1]. Gurland's studies showed that there was no apparent nucleation strain [3], whereas Goods and Nix found experimental evidence to support the concept of a critical nucleation strain [4]. Goods and Brown pointed out that cavity nucleation is a process involving both stress and strain energy release so that there must be some threshold value below which there is either insufficient stress to break the interface (or fracture the particle itself) or insufficient elastic strain energy available for the creation of the internal surfaces [1].

Brown and Stobbs developed energy and stress criteria that have to be satisfied simultaneously in order to nucleate cavities. The energy criterion is based upon the idea that cavitation by interface separation will not occur unless the elastic energy released by removing the stress from the particle is at least as large as the surface energy created; this criterion predicts that the critical strain for cavity nucleation is independent of the particle size [1, 5]. The stress criterion is based upon a critical stress that reflects the increased difficulty of local flow near a particle due to enhanced dislocation storage, and predicts that the critical strain for cavity nucleation is a linear function of the particle radius if the critical stress is independent of the particle radius [1, 5]. The last prediction correlates directly with experimental observations by Wilson who demonstrated that

in plastically deformed steels, the interfacial stress decreases as the particle size increases [6, 7]. A ternary Al-0.55Si-2.02Ge (wt.%) alloy was provided by Alcoa. This is an ideal alloy to study cavity nucleation and in particular the relationship between the critical strain for cavity nucleation and the precipitate diameter since the alloy was prepared from high purity components and therefore does not contain constituents and since the size of the incoherent SiGe precipitates can simply be changed by varying the aging time. The alloy was homogenized for 30 hours at 500°C, hot rolled, solution heat treated at 490°C, cold water quenched, and aged in an air furnace for up to 16 days at 160°C.

Samples for transmission electron microscopy (TEM) were prepared using standard techniques; all TEM examinations were conducted using a Philips EM-400T operated at 120 kV. Measurements of the average radii were performed by quantitative stereological methods [8] and corrected for truncation and overlap [9]; foil thicknesses were determined under two-beam conditions from oscillations in intensity of convergent beam electron diffraction (CBED) patterns [10].

Scanning electron microscopy (SEM) was employed in order to study fracture surfaces and void sizes using a JXA-840A or JSM-840A operated at 20 kV. Samples studied at high magnifications were sputtered with Au in order to decrease charging effects. Maximum void sizes were determined as a function of strain for different aging times (or precipitate diameters) using gage sections of tensile samples that were longitudinally sectioned and mechanically polished. Since no voids were observed in grip parts of tensile samples that were identically prepared, sample preparation effects could be excluded.

Room temperature tensile tests [11] were performed using an MTS 810 servohydraulic test machine operated in stroke control with an extensometer to monitor strain. The samples were tested in the longitudinal direction at a strain rate of 10^{-3} s^{-1} after aging for different times. The volume fraction of voids was determined through a pycnometer by measuring densities of the deformed gage section and the grip part [12]; all measurements were performed before necking occurred. Both Young's and shear moduli as well as Poisson's ratio of the SiGe precipitates were determined by ultrasonic velocity measurements in the ternary alloy and in pure Al assuming the Voigt linear law of mixtures [13].

Progress during the Reporting Period

Table I shows the results of the room temperature tensile tests performed with the ternary alloy after aging at 160°C for different times [14]. With increasing aging time, i.e. increasing

diameter of the SiGe precipitates, the tensile ductility decreases significantly, whereas the strength decreases only slightly.

Table I. Tensile Properties of Al-0.55Si-2.02Ge (wt.%) after Aging at 160°C.

Aging Time (d)	σ_y* (MPa)	σ_{TS}* (MPa)	ε_f* (%)
1	105	164	17
2	103	162	16
4	100	158	13
8	100	155	9
16	94	153	9

* σ_y - yield strength, σ_{TS} - tensile strength, ε_f - plastic strain after fracture

The low magnification fracture surface of the ternary alloy aged for 16 days at 160°C shown in Figure 1a reveals that fracture occurred as dimpled rupture. SiGe precipitates in the dimples can be seen at high magnification (Figure 1b) [15].

Figure 2 shows the results of the void volume fraction measurements [14] reflecting the combined damage due to void nucleation and growth occurring during straining. Since all measurements were performed before necking occurred, no correction for the effect of hydrostatic tension is necessary [1]. The volume fraction of voids decreases with increasing aging time, i.e. increasing diameter of the SiGe precipitates, at a given true strain value. The critical strain to nucleate cavities (ε_c) determined from the experimental data by linear regression increases from 0.008 for an average precipitate diameter of 5.0 nm to 0.014 for an average precipitate diameter of 14.4 nm.

In order to explain the experimental observation that the tensile ductility decreases with increasing aging time or precipitate diameter (Table I) while the critical strain for cavity nucleation

increases (Figure 2), the maximum void size was determined as a function of strain for different aging times. Figure 3 shows that the void growth rate increases significantly with increasing precipitate diameter [15] resulting in a decrease of the tensile ductility.

The finite element method was employed in order to calculate stress distributions around the SiGe precipitates for different precipitate diameters using both elasticity and plasticity models [16]. Using this analysis, the half angle of the cavity caps was found to be about 35° independent of the precipitate size. This means that the initial void size increases with increasing precipitate size [15]. It has been shown that the void growth rate increases with increasing initial void size [2, 17]. Therefore, an increase of the void growth rate with increasing precipitate size should be expected. This is in agreement with our experimental observation as shown in Figure 3.

The finite element analysis also allows a quantitative comparison between the experimental data and the prediction of a stress criterion for cavity nucleation [16] based on the model developed by Brown and Stobbs as shown in Figure 4. The agreement between the prediction of the stress criterion and the experimental data is excellent considering the experimental errors in the determination of the volume fractions of voids and the appearance of triangular plates at later aging stages in addition to spherical precipitates.

Conclusions

Finite element calculations reveal that the initial void size in a recently developed Al-0.55Si-2.02Ge (wt.%) alloy increases with increasing precipitate size. This leads to an increase of the void growth rate with increasing precipitate size and explains the experimental observation that the tensile ductility decreases with increasing precipitate size while the critical strain for cavity nucleation increases. Furthermore, the finite element analysis allows a quantitative comparison between the experimental data and the prediction of a stress criterion for cavity nucleation developed by Brown and Stobbs and confirms the prediction of their model.

Tasks for the Next Reporting Period

The dislocation generation and structure developed during deformation will be examined as a function of the SiGe precipitate size using a TEM straining stage in order to obtain a better understanding of the void nucleation process. The project is expected to be completed by May, 1996.

References

1. S. H. Goods and L. M. Brown, Acta Metall. 27, (1979), 1.

2. R. H. van Stone et al., Int. Met. Rev. 30, (1985), 157.

3. J. Gurland, Acta Metall. 20, (1972), 735.

4. S. H. Goods and W. D. Nix, Acta Metall. 26, (1978), 739.

5. L. M. Brown and W. M. Stobbs, Phil. Mag. 34, (1976), 351.

6. D. V. Wilson and Y. A. Konnar, Acta Metall. 12, (1964), 617.

7. D. V. Wilson, Acta Metall. 13, (1965), 807.

8. E. E. Underwood and E. A. Starke, Jr., ASTM STP 675, ASTM, Philadelphia, PA (1979), 633.

9. E. E. Underwood, Quantitative Stereology, Addison-Wesley, Reading, MA (1970), 187.

10. P. M. Kelly et al., Phys. Stat. Sol. 31A, (1975), 771.

11. P. C. Fazio et al., eds., Annual Book of ASTM Standards, vol. 03.01, ASTM, Philadelphia, PA (1992), 130.

12. J. A. Walsh, M.S. Thesis, University of Virginia, Charlottesville, VA (1988), 39.

13. M. E. Fine, Scripta Metall. 15, (1981), 523.

14. H. J. Koenigsmann and E. A. Starke, Jr., Proceedings of the 2nd International Conference on Microstructures and Mechanical Properties of Aging Materials, TMS, Warrendale, PA, in press (1996).

15. H. J. Koenigsmann and E. A. Starke, Jr., submitted to Proceedings of the 5th International Conference on Aluminum Alloys - Their Physical and Mechanical Properties (Grenoble, France, July 1-5, 1996).

16. H. J. Koenigsmann, E. A. Starke, Jr., and P. E. Allaire, Acta Metall., in press (1996).

17. T. L. Anderson, Fracture Mechanics: Fundamentals and Applications, CRC Press, Boca Raton, FL (1991), 310.

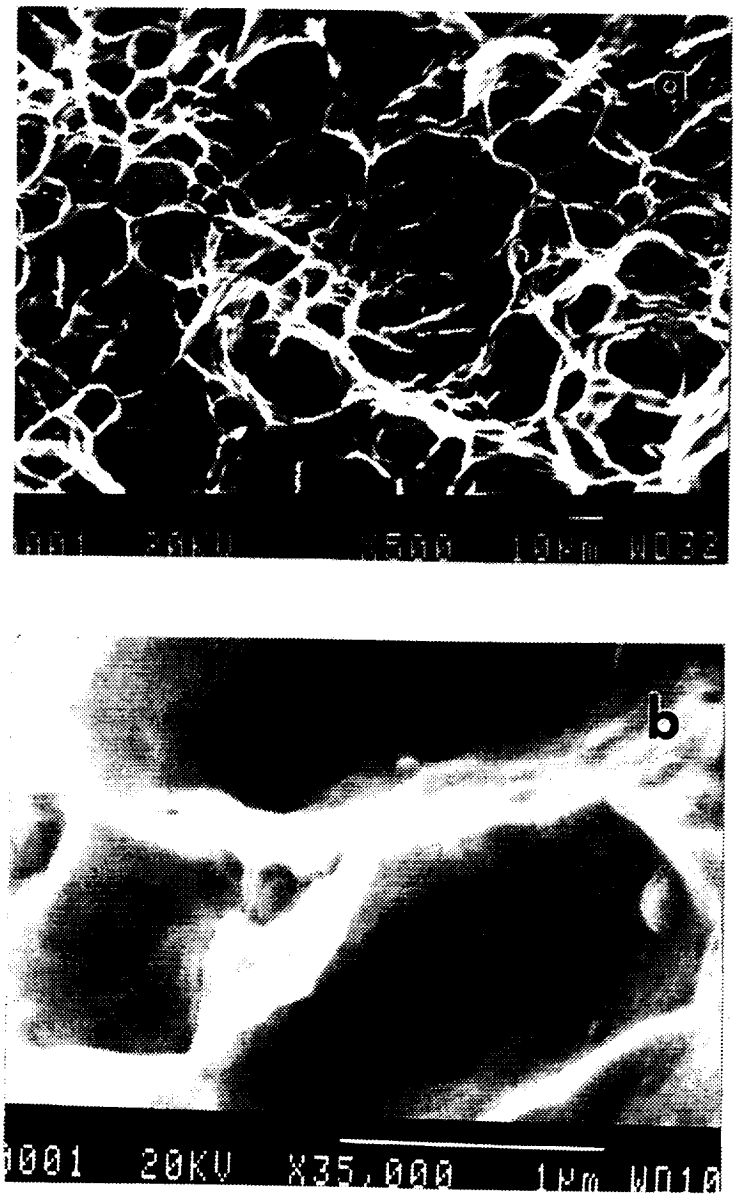

Figure 1. Fracture surface of Al-0.55Si-2.02Ge (wt.%) after aging at 160 °C for 16 days and performing a tensile test in longitudinal direction.

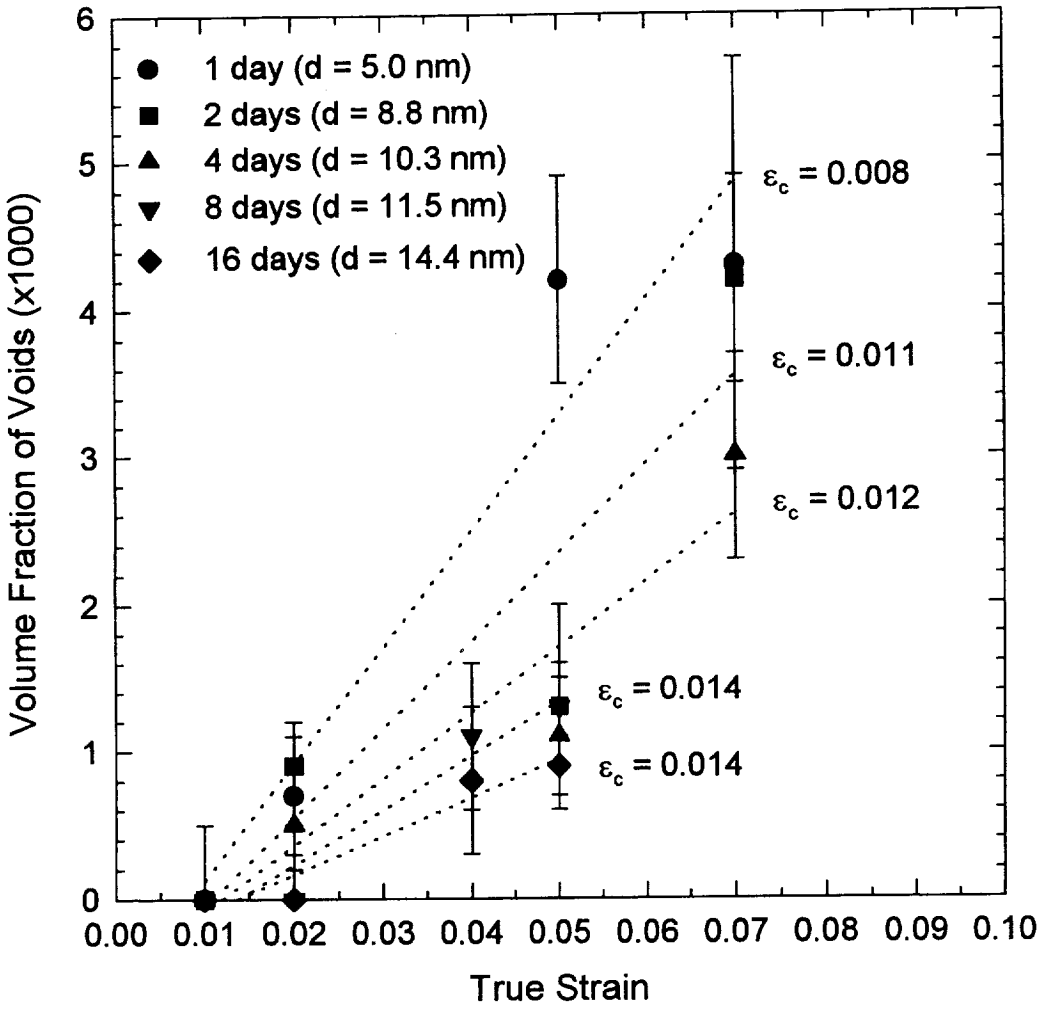

Figure 2. Volume fraction of voids as a function of strain determined in Al-0.55Si-2.02Ge (wt.%) after aging at 160 °C for different times, critical strain for cavity nucleation (ε_c) determined by linear regression.

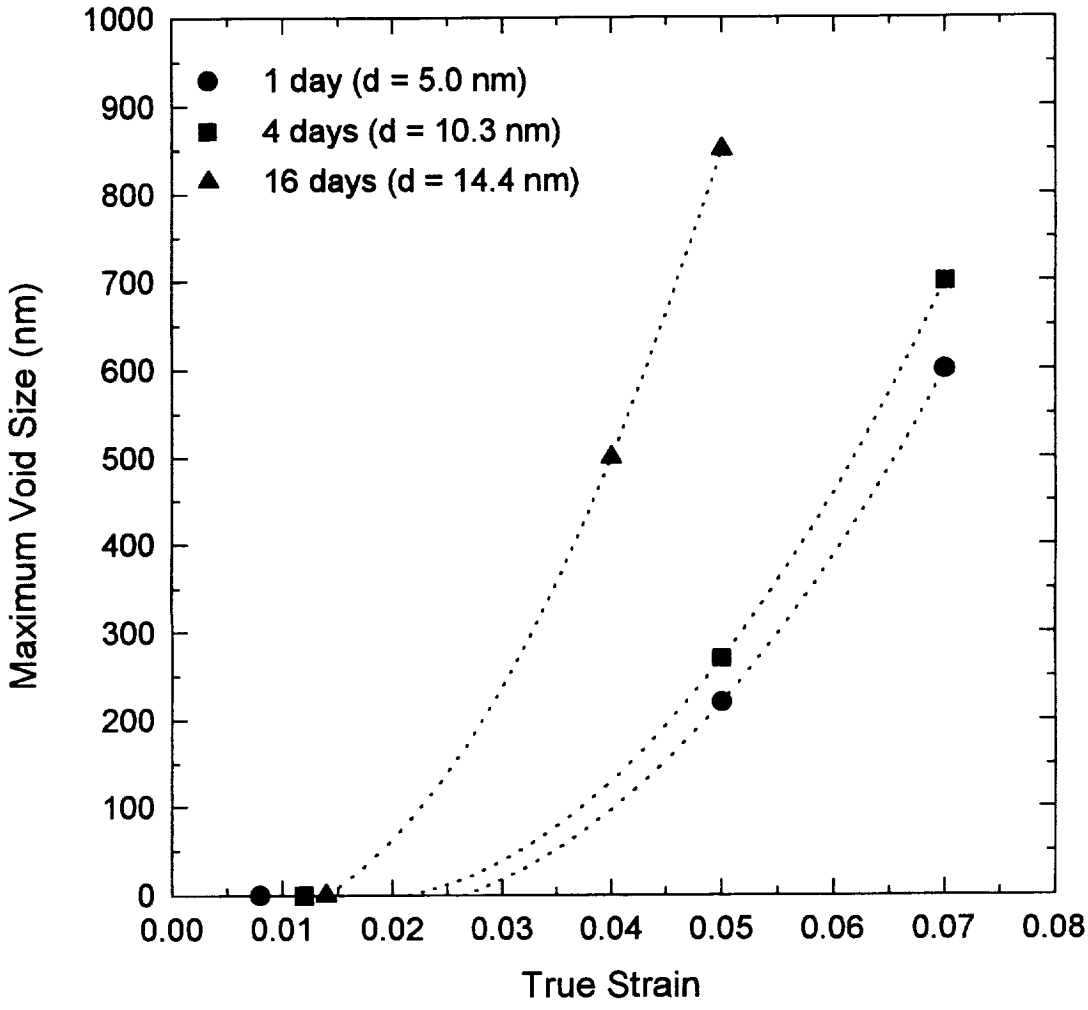

Figure 3. Maximum void size as a function of strain determined in Al-0.55Si-2.02Ge (wt.%) after aging at 160 °C for different times.

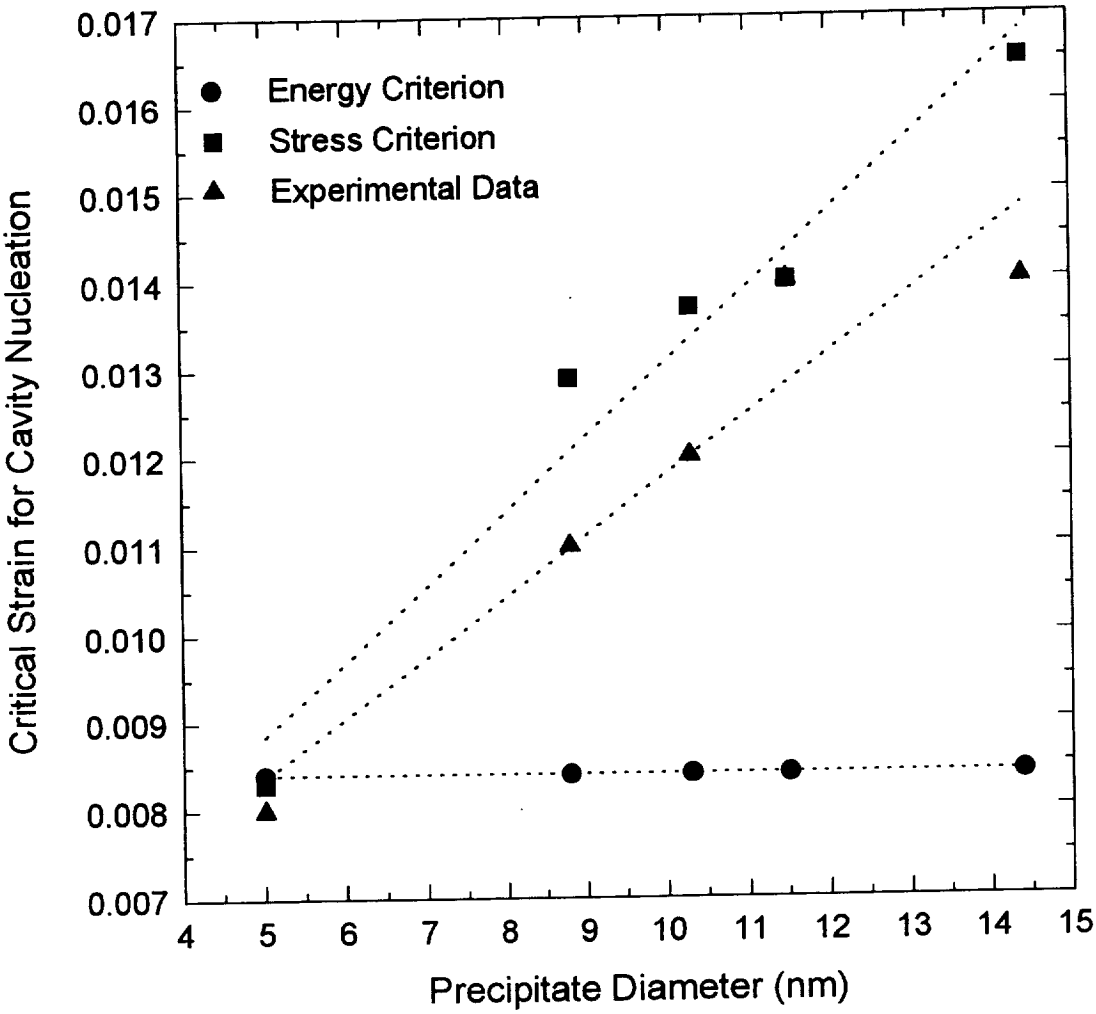

Figure 4. Comparison of cavity nucleation criteria with experimental data.

Project #9: EFFECT OF TEXTURE AND PRECIPITATES ON MECHANICAL PROPERTY ANISOTROPY OF Al-Cu-Mg-X ALLOYS

Faculty Investigators: Gary. J. Shiflet and Edgar A.Starke
Graduate Assistants: Birgit Skrotzki, Hinrich Hargarter

Dr. B. Skrotzki accepted a position at the Institut fuer Werkstoffe, Ruhr Universitaet Bochum, Germany and left the University of Virginia at the end of August 1995. Her work as a Post Doctoral Research Associate at UVA has been taken over by Dr. H. Hargarter.

Research Objectives

It is the objective of this project to determine the effect of texture on the precipitation of the Ω phase and the θ' phase in modified Al 2519 with T6 and T8 heat treatment conditions and to evaluate the effect of applied elastic and plastic stresses on nucleation and growth of the strengthening precipitate phases. The associated relationship with anisotropy of the mechanical properties will also be examined.

During the reporting period the investigations focused on the influence of creep exposures on the precipitate microstructure of two recrystallized Al-Cu-Mg-Ag alloys in a T8 heat treatment condition. The aim was to obtain quantitative data for the coarsening and possible preferential growth of matrix precipitates as well as for the stability of grain boundary phases during creep.

Background and Approach

The Al-Cu-Mg-Ag alloys C415 and C416 had earlier been identified to have attractive combinations of room temperature properties as well as good creep resistance, which makes them promising candidates for HSCT applications. The hexagonal shaped Ω plates on the $\{111\}$ matrix planes, whose precipitation is stimulated by the Ag addition, are known to have a high thermal stability [1]. Still, a degradation of the fracture toughness has been observed in the alloys after long term high temperature exposure [2]. Therefore the stability of the precipitate structure under typical creep exposures needed to be investigated in detail. The study was also used to investigate whether preferential orienting of precipitates in the Al-Cu-Mg-Ag alloys in the T8 occurs when creep loads are applied, since earlier work on solution heat treated and T6 material indicated that external stresses might only cause such orienting during precipitate nucleation.

The two alloys used in this study were provided by Alcoa as sheet material of 2.3 mm thickness in the T8 heat treatment condition, with 2% stretch before aging. The chemical

composition is given in Table 1. details of the heat treatment and the mechanical properties have already been reported [2]. Only material with grain structure "A" was used.

Table 1. Actual chemical composition (wt-%)

Alloy	Cu	Mg	Mn	Ag	Zr	Fe	Si	Al
C415	5.09	0.82	0.66	0.51	0.13	0.07	0.06	Balance
C416	5.38	0.53	0.31	0.52	0.13	0.07	0.05	Balance

Alcoa also provided creep specimens which had been tested with the load parallel to the rolling direction under conditions of either 1000 hr./ 30 ksi/ 275°F or approximately 500 hr./ 40 ksi/ 225°F. The creep specimens were prepared form the same sheet material with grain structure "A" , but besides the 2% stretch before aging, also specimens with 0.5% and 8% stretch were provided.

TEM samples were prepared form the center of the sheet in the rolling plane and the rolling direction was marked to allow the measurement of the angle between the precipitate habit plane and the load direction during creep. The volume fraction, number density, diameter and thickness of the precipitates were quantitatively evaluated, using the approach of Underwood for projected images [3]. The fracture surfaces of tensile specimens, which were prepared from the crept specimens and from the T8 sheet, were quantitatively investigated in a SEM.

Progress During the Reporting Period

Optical microscopy revealed that the sheet and the creep specimens of C415 used for the study contained grains which were elongated parallel to the rolling direction whereas the grains in C416 were mostly equiaxed.

The precipitate microstructure within the grains was investigated in the TEM for the initial T8 heat treatment condition and for all different creep conditions. In both alloys only very few S' precipitates were found. Therefore S' did not have to be taken into account for the quantitative Stereology measurements, which were carried out for the Ω precipitates and the θ' precipitates to determine the influence of the creep exposure on volume fraction, number density and dimensions of the precipitates. It was found, that the precipitate microstructure is very stable.

For C415 the results are presented in Fig. 1. Compared to the T8 condition with 2% stretch before aging, the volume fractions of Ω and θ' in the investigated creep specimens with the same amount of cold work did not change much. Only a very moderate increase in the average diameter of Ω and θ' was observed as a result of the creep test. The growth of the precipitate thickness seems to be somewhat more pronounced, especially in the θ' phase. The Ω phase shows a higher resistance against coarsening than θ'. The measurements of volume fraction and number density do not show clear trends. However, the results do not indicate a relevant shift in volume fraction from one phase to the other or significant precipitate growth on the expense of already precipitated particles.

The results for C416, presented in Fig. 2, show for both phases increased precipitated volume fractions after the creep tests. Like in C415 some precipitate growth was observed in the thickness as well as the diameter. The moderate coarsening did not occur on the expense of already precipitated particles, because the number density of precipitates did not drop. For Ω even an increase in the number of precipitates per volume was found.

Comparing the two alloys it was found that C416 had a higher volume fraction of θ' than C415, probably due to the higher Cu content in C416. The number density of Ω in the latter alloy is significantly lower than in C415. This indicates that θ' is formed at the expense of Ω. Higher strength levels of C415 than of C416, reported in [2], can be related to this fact since the overall dimensions, volume fraction and number density of precipitates are comparable in both alloys. It seems that different stretch level before aging do not significantly affect the growth behavior of the precipitates under the investigated creep conditions. At least no perceptible trend was observed. As an earlier result of this project it was found in a comparable alloy that under creep conditions preferential nucleation and/or precipitate growth occurred depending on the orientation of the habit planes relative to the load axis [4]. Therefore the volume fractions of Ω and θ' were determined separately for every precipitate habit plane and the angle between the precipitate and the direction of the applied load was measured. No preferential orientation of either Ω or θ' was found in the crept specimens. Since in the initial T8 condition the precipitates were randomly oriented the results show that no preferential growth/coarsening occurred during the creep tests.

The result is in contradiction to observations for other alloys where it has been found that stress orienting occurs primarily by selective coarsening and that the nucleation effect is rather

small [5]. This might be due to the fact that the precipitates in the other alloy systems have a different morphology and different amounts of positive or negative misfit with respect to the matrix. As a certain threshold stress has to be exceeded before preferential nucleation occurs it might as well be that for preferential coarsening a threshold stress exist [4]. This would mean, that the applied stresses in the creep tests were not high enough to result in oriented precipitate growth. It has also been suggested, that there is critical temperature [6]. However, it appears very likely that in the investigated Al-Cu-Mg-Ag alloys precipitate orienting is purely a nucleation effect because of the high misfit between the nucleus and the matrix. During growth, the elastic accommodation strain should be minimized by the requisite height of the growth ledge.

The influence of creep on the grain boundary precipitates was investigated by studying the grain boundary areas in the initial T8 material and in samples that had been creep tested for 1000 hr./30 ksi/275°F in the TEM. The material with 2% stretch before aging was chosen. The grain boundaries were found to be almost continuously covered with very fine particles. EDX analysis as well as electron diffraction patterns indicated these precipitates to be most likely of the Ω phase.

Larger but more irregularly spaced particles of the Ω or S phases with a wide spread of sizes were also found on all grain boundaries. Less often, the large constituent phases with dimensions in the micrometer range were located at the boundaries. An evaluation of the grain boundary precipitates in a quantitative way as had been done for the matrix precipitates proved to be very difficult. The large scatter in spacing and size and the many involved factors like orientation of the grain boundary with regard to the load axis and the influence of the misalignment between adjacent grains resulted in statistically insufficient data. However, some qualitative conclusions can be drawn from the TEM observations. No obvious differences in the appearance of grain boundary precipitates could be found between the crept samples and the initial sheet material. Also precipitate free zones along the grain boundaries with a width of about 50 nm were found before as well as after the creep tests. No significant differences could be detected between C416 and C415.

In order to obtain quantitative data for the grain boundary precipitates to proof the high microstructural stability of both alloys under the investigated creep conditions, tensile specimens were prepared from the remainders of the creep specimens and from the sheet and pulled to fracture. Quantitative analysis of the area fractions with grain boundary fracture and transgranular fracture was conducted using a SEM. Fig. 4 shows typical SEM micrographs of the fracture surfaces for both alloys. Fracture occurred in the T8 heat treatment condition in C415 and in C416 by a mixed mode, consisting of transgranular dimple fracture as well as fracture along grain

boundaries. The fracture surfaces from crept specimens were of similar appearance. Micrographs with higher magnification demonstrate the dimples on the fractured grain boundaries, which were induced by the grain boundary particles (Fig. 5). The results of analyzing the area fraction with grain boundary fracture, representing about 300 grains for each condition, are presented in Fig. 6. The change in the percentage with grain boundary fracture as a result of the creep tests is well below the experimental error, indicating that no significant change in grain boundary precipitates or growth of particle free zones occurred.

Conclusions

For the Al-Cu-Mg-Ag alloys C415 and C416 it has been found, that the precipitate microstructure in the T8 heat treatment condition is very stable for investigated creep conditions of 1000 hr./ 30 ksi at 275°F and 500 hr./ 40 ksi at 225°F. Slow coarsening of the predominant strengthening phases Ω and θ' under these conditions has directly been shown by performing quantitative analysis of the matrix precipitates. Also, no evidence of selective growth or a preferential alignment in the direction of the load axis during creep exposure was found for both precipitate phases. In these alloys precipitate orienting might therefore be a pure nucleation effect. As for the stability of the grain boundary precipitates only qualitative results could been obtained in the TEM observations. No obvious coarsening of the grain boundary precipitates or growth of the precipitate free zones was found for both alloys. Indirectly the stability of the grain boundary precipitate structure has been proofed by a performing a quantitative analysis of the fracture surface of room temperature tensile tests. No change in the area fraction with grain boundary fracture occurred due to the creep exposure. Their high microstructural stability makes the Al-Cu-Mg-Ag alloys very promising candidates for HSCT applications.

Tasks for the Next Reporting Period

At an earlier stage of this project it has been shown, that in the Al-Cu-Mg-Ag alloys a preferential alignment of the different precipitate phases can be achieved by aging under stress. The influence of such orienting on the directionality of the mechanical properties needs to be investigated. Aging under stress also offers the opportunity to investigate, whether the platelike precipitates on {111}-planes differently influence the mechanical properties than precipitates on the {100}-planes.

Therefore work has already begun to study effect of preferential precipitate orientation on the tensile properties. By performing the aging under stress at different stress levels, either only θ'

(on {100}) or Ω plus θ' will be preferentially oriented. The tensile properties of the aged material will then be determined parallel, perpendicular and under 45 degrees. to the stress axis during aging. To separate the effect of the preferential orientation of the precipitates from texture effects, the experiments will be performed using an early lot of modified 2519 material (#689248B: Al-5.75Cu- 0.52Mg- 0.3Mn- 0.49Ag- 0.16Zr). This material was found to have an almost random texture. Quantitative Stereology will be used to establish the degree of orienting. Based on the tensile data, the mechanical behavior will be modeled.

References

1. I.J. Polmear, J.J. Couper, Metall. Trans. **19A** (1988), 1027
2. Aluminium-Based Materials for High Speed Aircraft - Subcontract No. 5-28406, Biannual Report No. 6
3. E.E. Underwood, Quantiative Stereology, Addison-Wesley Publishing Company (1970), Reading, MA, 178
4. Effect of Texture and Precipitates on Mechanical Property Anisotropy of Al-Cu-Mg-X Alloys, B. Skrotzki, G.J. Shiflet and E.A. Starke, NASA-UVA Light Aerospace Alloy and Structues Technology Program, Report No. UVA/528266/MS95/18, (1995), 79
5. G. Sauthouff, Z. Metallkunde, **68** (1977), 500
6. T. Eto, A. Sato, T. Mori, Acta Metall. **26** (1978), 499

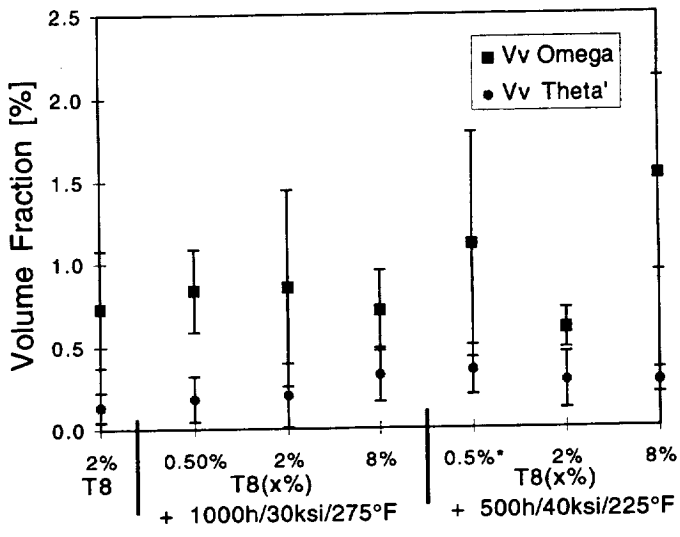

(a) Volume Fraction

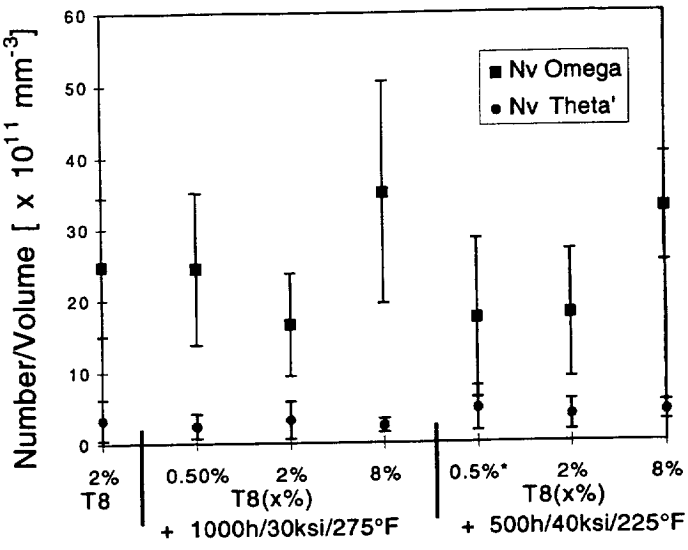

(b) Number Density

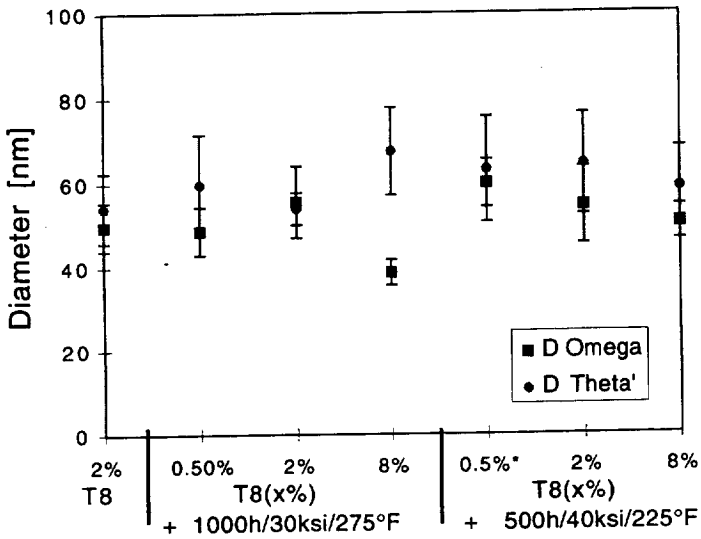

(c) Average Precipitate Diameter

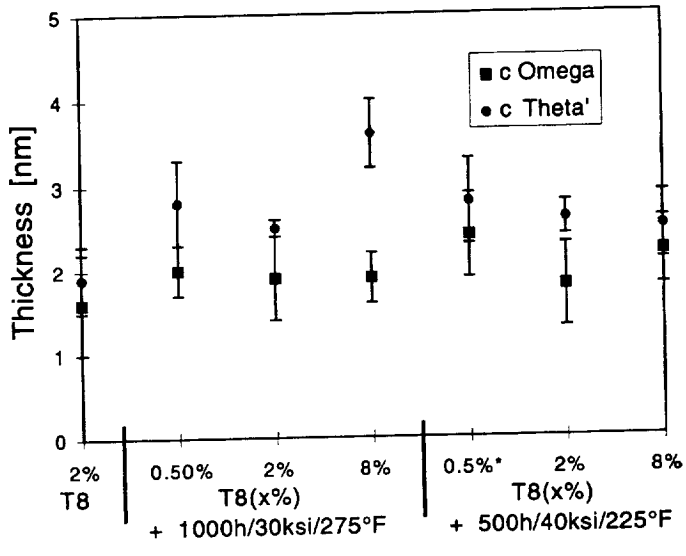

(d) Average Precipitate Thickness

Fig.1 Alloy C415: Quantitative stereology data for Ω and θ`precipitates in T8 (2% stretch) and T8 + creep samples.

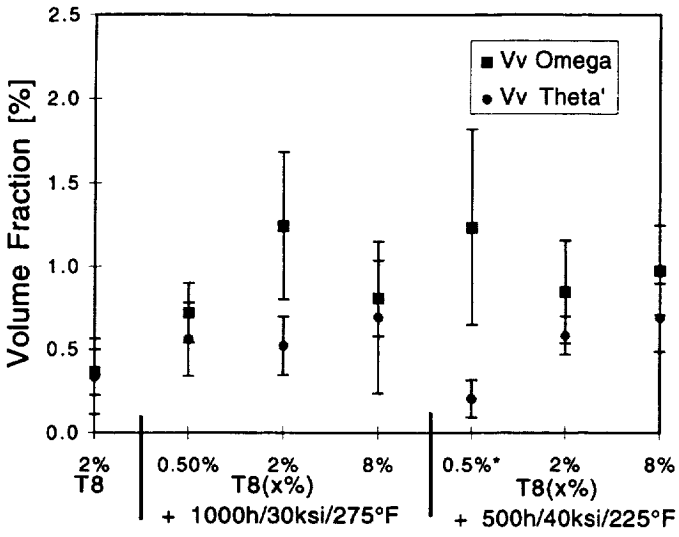

(a) Volume Fraction

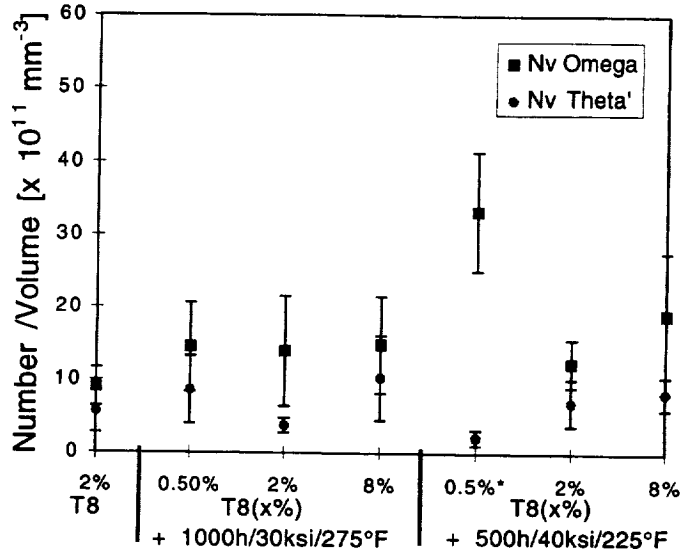

(b) Number Density

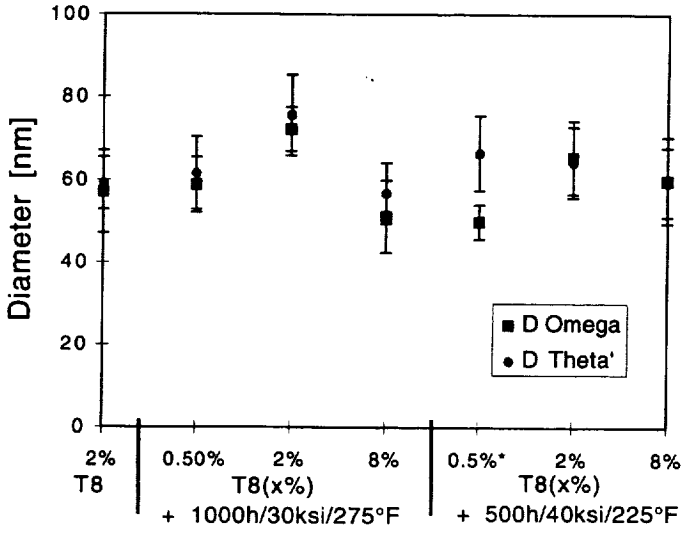

(c) Average Precipitate Diameter

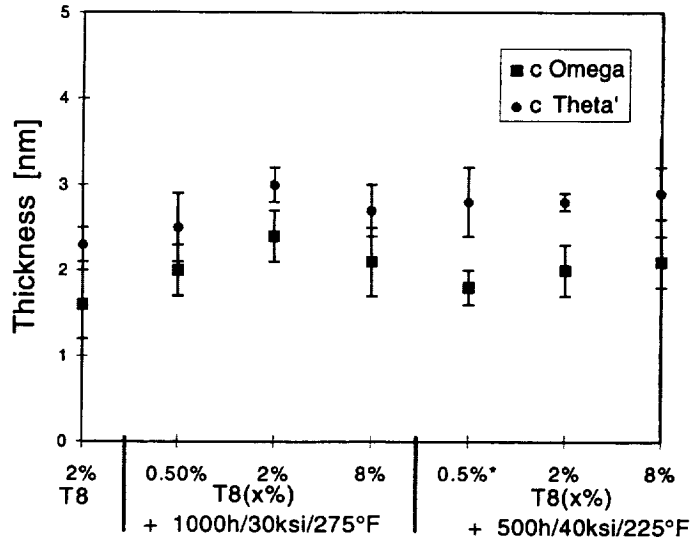

(d) Average Precipitate Thickness

Fig.2 Alloy C416: Quantitative stereology data for Ω and θ`precipitates in T8 (2% stretch) and T8 + creep samples.

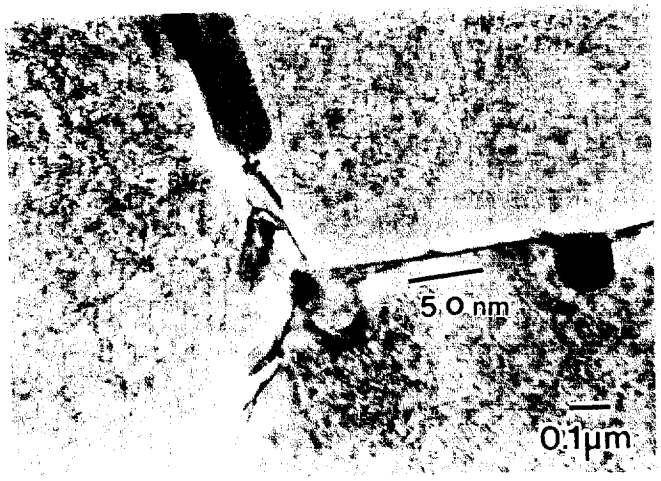

(a) C415-T8

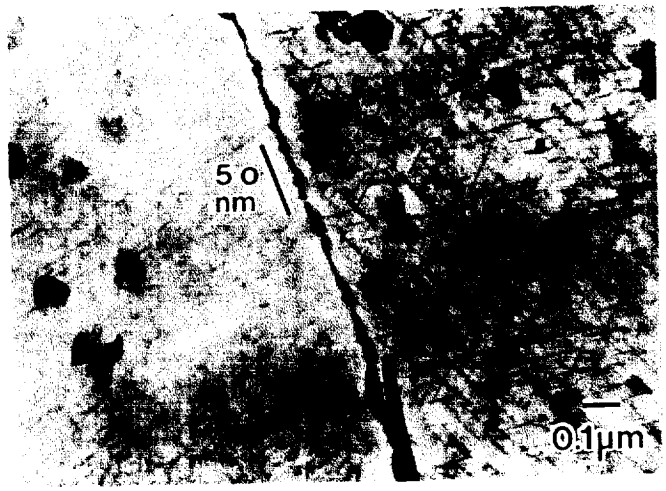

(b) C415-T8 + 1000hr./ 30 ksi / 275°F

(c) C416-T8

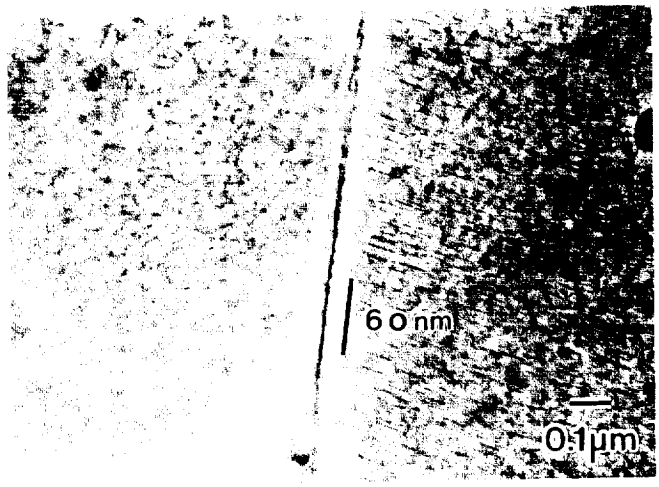

(d) C416-T8 + 1000hr./ 30 ksi / 275°F

Fig.3 Grain boundaries (TEM). No change in width of adjacent precipitate free zones during creep tests.

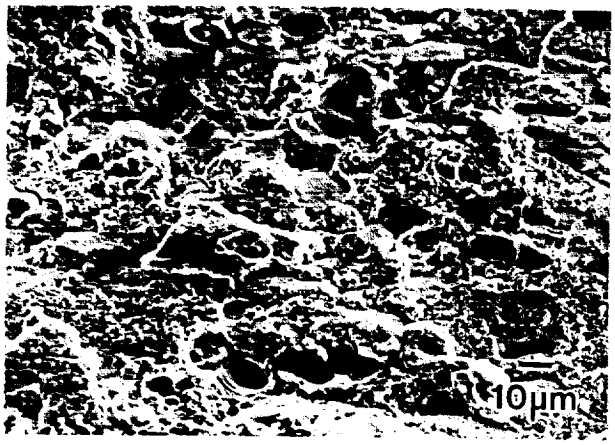

(a) C415-T8

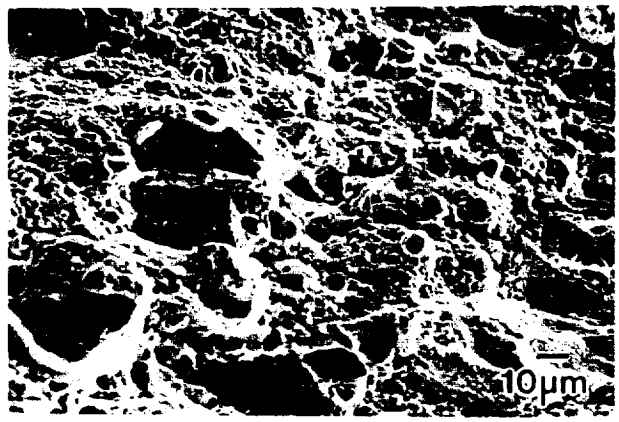

(b) C415-T8 + 1000hr./ 30 ksi / 275°F

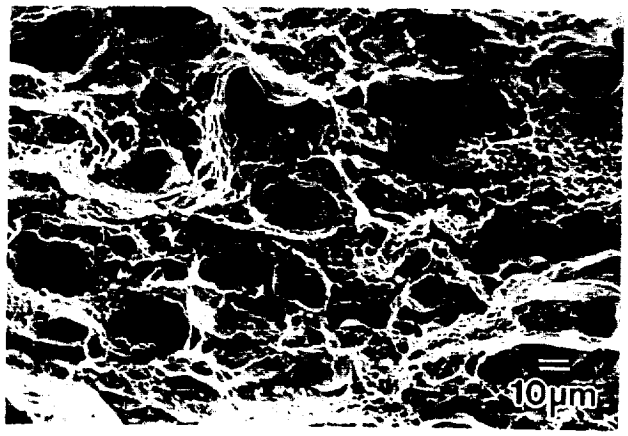

(c) C416-T8

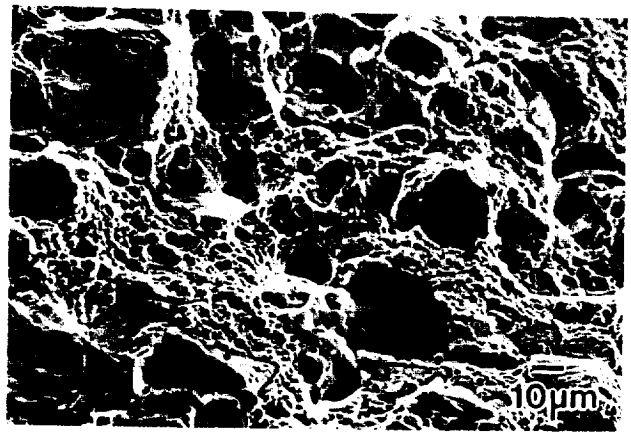

(d) C416-T8 + 1000hr./ 30 ksi / 275°F

Fig.4 Tensile fracture surface (SEM). Mixed fracture mode before and after creep.

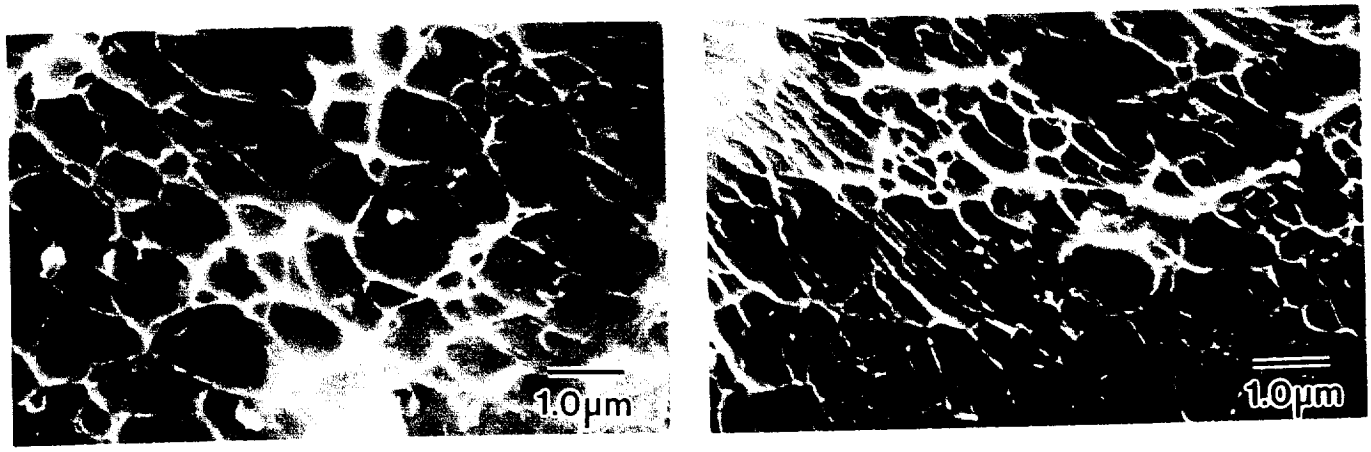

(a) C415-T8 (b) C416-T8

Fig.5 Detail from Fig. 4. Dimpled type of grain boundary fracture, due to grain boundary precipitates.

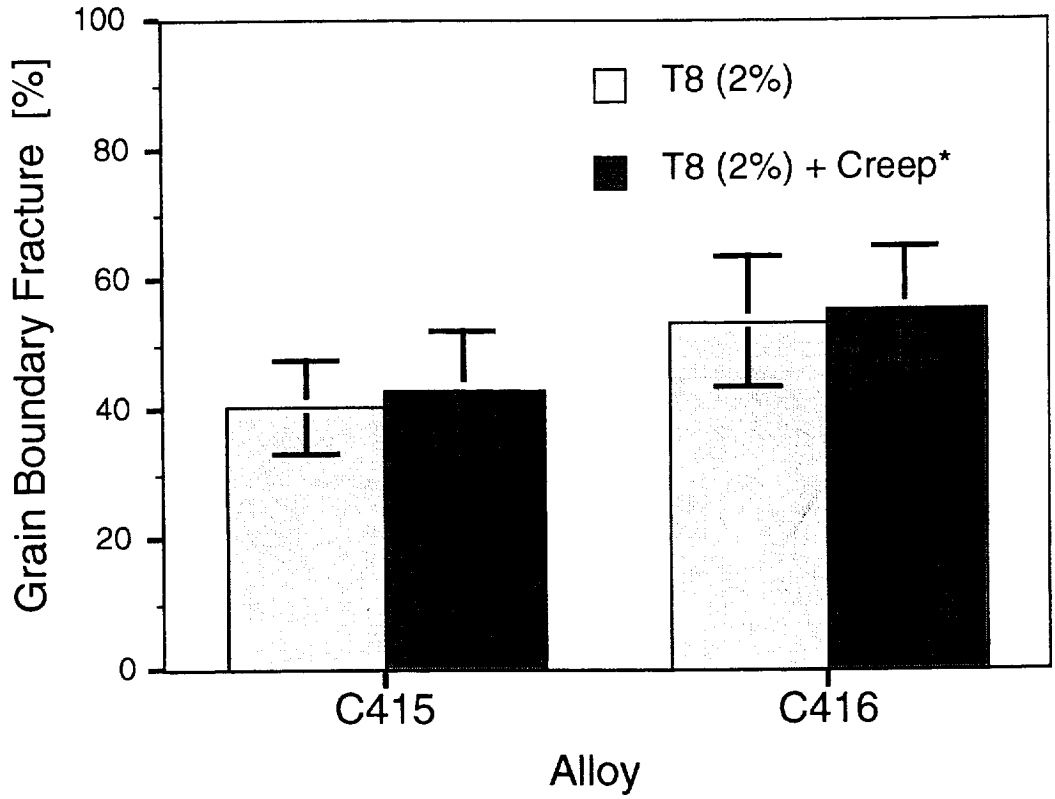

Fig.6 Area fraction with grain boundary fracture on tensile specimens before and after creep. * : 1000hr./ 30 ksi / 275°F

Project # 10a: FREQUENCY-DEPENDENT FATIGUE CRACK PROPAGATION IN 7000 SERIES ALUMINUM ALLOYS IN AN AGGRESSIVE ENVIRONMENT

Faculty Investigator: R.P. Gangloff
Graduate Assistant: Zuhair M. Gasem

Research Objectives

The current goal of this Ph.D. research is to gain a better understanding of loading frequency effects on the corrosion fatigue crack propagation behavior of precipitation hardened 7000 series aluminum alloys in aqueous chloride. The underlying premise of this research has been to determine inputs for micro-mechanical/chemical modeling of fatigue crack propagation in aggressive environments. We ultimately seek to understand mechanisms of crack tip process zone damage. Specific objectives are to :

- characterize intrinsic and extrinsic environmental effects on da/dN-ΔK behavior for high strength aluminum alloys, of different tempers, as a function of loading frequency for exposure to an aqueous chloride solution.
- understand environment-induced fatigue crack closure and its contribution to environment-assisted fatigue growth.
- characterize the microscopic path of environmental fatigue.
  understand alloy composition and microstructure factors that govern the time-dependence of da/dN.

Background and Significance

The understanding of environmental effects on fatigue crack propagation in high-strength aluminum alloys used in structural components of aerospace systems is essential for incorporation into software such as NASA/FLAGRO. This code is used to analytically predict the growth and stability of preexisting cracks. Fatigue crack propagation rates in metallic alloys strongly depend on the environment [1]. The extent of the deleterious interaction between the environment and the alloy is time-dependent, and thus cyclic loading frequency effects are of great importance for realistic life predictions. Effort has been expended on determining the suitability of a superposition model for aluminum and titanium alloy systems [2,3]. It was concluded that time-based crack growth rates from quasi-static load experiments are an order of magnitude too small for acceptable linear superposition prediction of fatigue crack growth rates for loading frequency above 0.001 Hz in aqueous chloride. A more fundamental approach must be identified for accurate life prediction.

Technical Approach

Various variables affect fatigue crack propagation of 7000 series aluminum alloys in aqueous chloride [4]. Crack growth kinetics, crack path, and fracture surface topography are influenced by aggressive environments [5-7]. Loading frequency, stress intensity factor range, stress ratio, crack orientation, microstructure, electrode potential, loading wave-form, and environment- induced crack closure must be considered in order to fully characterize the corrosion fatigue process. The current effort was concerned initially with the effects of frequency and stress intensity level.

Materials

The widely used commercial aluminum alloy 7075, in peak-aged (T651) and over-aged (T7351) conditions, has been investigated in 3.5% NaCl solution. The composition and mechanical properties of the 7075 aluminum alloy are given in Table 1.

Table 1: Chemical Composition and Mechanical Properties of 7075 Aluminum Alloy

Chemical Composition (wt. %)

Zn	Mg	Cu	Cr	Mn	Ti	Fe	Si	Al
5.1-6.1	2.1-2.9	1.2-2.0	0.2-0.4	0.3*	0.2*	0.7*	0.5*	bal

* maximum wt. %

Mechanical Properties(T651)

Yield Strength (MPa)*	Tensile Strength (MPa)*	Elongation* %	K_{Ic}** (MPa$\sqrt{m}$)
472	540	4.0	22.2

* loading axis parallel to L.
** S-L orientation

Fatigue Crack Growth Experiments

Fatigue crack propagation experiments were conducted on WOL specimens, 7.62 mm in thickness, machined in the sensitive S-L orientation. Crack growth rates were measured in constant stress intensity control at different frequencies using a sinusoidal loading wave-form. All tests were performed at the open circuit electrode potential in aerated 3.5% solution of NaCl in

deionized water (-770 mV vs. Ag/AgCl electrode). The solution was circulated in a plexiglass cell designed to fully immerse the machined notch and the crack path region.

A constant stress ratio of 0.1 was employed throughout each test. The crack length and crack closure levels were monitored using the elastic compliance method with a clip gage mounted across the mouth of the machined notch . A constant crack length increment was used to store a crack length measurement versus number of cycles and $K_{closure}$. A total crack length interval of 2.5 mm was employed for each test. Fatigue crack growth rates were obtained using linear regression analysis. The closure level was evaluated in the unloading direction at an offset of 2% from the linear slope behavior of the load-displacement curve. The closure level varied over the crack length interval at constant applied ΔK and only the average value has been reported.

All tests were conducted in a computer automated MTS servohydraulic machine and performed in general accordance with the ASTM Standard Test Method for Measurement of Fatigue Crack Growth Rates, E647-91.

Progress During the Reporting Period

Environmental fatigue crack growth rate data were obtained for a wide range of DK (6 to 15 MPa$\sqrt{m}$) and frequency (0.01 to 50 Hz) for both alloy variants. Data obtained correspond to the Paris regime of the fatigue crack growth curve. The variation of fatigue crack growth rate with frequency at ΔK of 9 and 15 MPa$\sqrt{m}$ is shown for the T6 (Figure 1 a) and T7 (Figure 1 b) conditions of AA 7075. For the uninhibited chloride solution, the behavior is reasonably described by three distinct frequency-dependent FCP rate regimes. At high frequency regime ($f > 1$ Hz, Region 1), FCP rate increases as the frequency decreases until a maximum rate is reached at about 1 Hz. This maximum FCP rate is hypothesized to be associated with a saturation of environmental damage. This regime can be rationalized; more time is available for environmental interaction, as the loading frequency decreases, and crack tip damage increases until saturation is reached.

Region 3 ($f < 0.1$) is believed to be extrinsic in nature where a high closure level has occurred, as can be inferred from Figure 2. The closure level increases, from environment-independent plasticity-induced closure at high frequencies to enhanced closure at lower frequencies due to an accumulation of corrosion debris on the fracture surface. The closure level (defined as $K_{closure}/K_{max}$) at 50 Hz approached a plasticity-induced closure value (0.34) estimated from Newman's closure model [8]. This behavior was evident for both variants of 7075, as shown in Figure 2. The relatively high scatter in closure data is attributed to the variation of closure along the crack interval, while only the average value is reported. A more appropriate

method of reporting should be used in the future.

Region 2 describes mildly frequency-dependent FCP rates governed by a competitive process between extrinsic retardation from the high closure level and the operating (saturated) environment-assisted fatigue process. Data for 7075-T651 at K of 15 MPa$\sqrt{m}$ were obtained in inhibited solution which might alter the trend found for the uninhibited condition due to a different corrosion product production rate and consequently different closure levels. Figure 1 also indicates that Region 2 is sustained over a narrower frequency range for the T7351 variant compared to T651. The higher closure level associated with the former temper is apparently responsible for this behavior.

Figure 3 presents limited data on 7075 in 3.5 %NaCl solution for the high frequency regime at additional constant ΔK levels (6 and 12 MPa$\sqrt{m}$) . The similar frequency-dependent FCP rates at different ΔK suggests that the environment-assisted fatigue process in this frequency regime not only depends on time, but also depends on the mechanical driving. In other words, it is a cycle-time-dependent process. Further tests are required in this region to better understand the frequency-dependent FCP rates.

The extent of the environmental effect on FCP rates, defined as $[da/dN]_{NaCl} / [da/dN]_{air}$, depends on stress intensity range as evidenced in Figure 4 for both tempers. Data for FCP in air were based on testing at constant ΔK at a single frequency of 1 Hz. This finding emphasizes the time nature of environmental fatigue, since at lower ΔK (slower da/dN) more time is available for damage to evolve and hence a larger environment contribution to FCP rate is observed. For example, considering 7075-T651 at 0.5 Hz , the ratio of $[da/dN]_{NaCl} / [da/dN]_{air}$ is about 15 at ΔK of 6 MPa$\sqrt{m}$ while the ratio is 8 at ΔK of 12 MPa$\sqrt{m}$.

Overaging is often used to improve the stress corrosion cracking resistance of alloy 7075 [9]. The T7351 temper has exhibited better resistance to SCC in both laboratory evaluations and outdoor exposure over the peak strength temper, T651. For ΔK of 9 MPA$\sqrt{m}$, Figure 5 indicates that the corrosion fatigue crack propagation resistance of the overaged variant of 7075 is only slightly higher than that of the peak strength at high and intermediate frequencies (Regions 1 and 2). However, the difference between the performance of these variants is more pronounced in Region 3 where retardation from closure is predominant. Reasons for higher closure levels associated with the overaged temper are under investigation.

Tasks for the Next Reporting Period

Work is in progress to better understand frequency effects on FCP rates for 7075 in aqueous chloride. Further tests are required which examine the sensitivity of closure to variables

such as test frequency-sequence and exposure time. At present no effort has been directed to investigate the underlying environment-assisted fatigue mechanisms involved in this system. The following are possible future routes for study:

- generate FCP data at a single low ΔK level (2 to 3 MPa$\sqrt{m}$) at a high frequency and a high load ratio to determine if the environmental fatigue mechanism and microstructural sensitivities change.
- find a method to clean the fracture surface without altering surface features for high resolution fractographic studies and/or find a suitable inhibitor which does not obscure the environmental effect but preserves the fracture surface.
- study load frequency-sequence effects and exposure effects, if any, on FCP rates and closure.
- minimize the high variation in $K_{closure}$ levels by reducing the crack growth interval or/and by using a better method of analysis.
- study the load ratio effect on the closure level in both the high and low frequency regimes. Higher load ratio would reduce the closure effect and thus present more intrinsic behavior.
- determine the microstructural features which influence environmental-assisted FCP. In addition to 7075, 7050 will be studied. A parallel study sponsored by Alcoa is examining the effect of heat treatment and Cu content on the quasi-static load SCC resistance of 7050. These results, and associated TEM work at Lehigh University, will provide a basis to analyze microstructral effects on time-cycle dependent environmental fatigue in 7000 series alloys.

References

1. R.P. Gangloff, "Corrosion Fatigue Crack Propagation in Metals", in Environmental-Induced Cracking of Metals, R.P. Gangloff and M.B. Ives, eds., NACE, Houston, TX, pp.55-109, 1990.

2. M.E. Mason, "Time-Dependent Corrosion Fatigue Crack Propagation in 7000 Series Aluminum Alloys", M.S. Thesis, University of Virginia, 1995.

3. E. Richey,III, "Empirical Modeling of Environment-Enhanced Fatigue Crack Propagation in Structural Alloys for Component Life Prediction", M.S. Thesis, University of Virginia, 1995.

4. N.J.H. Holroyd and D. Hardie, "Factors Controlling Crack Velocity in 7000 Series Aluminum Alloys During Fatigue in an Aggressive Environment", Corrosion Science, Vol. 23, pp. 527-546, 1983.

5. M. Gao, P.S. Pao, and R.P. Wei, "Chemical and Metallurgical Aspects of Environmentally Assisted Fatigue Crack Growth in 7075-T651 Aluminum Alloy", Metallurgical Transactions A, Vol. 19A, pp.1739-1750, 1988.

6. M.O. Speidel, "Stress Corrosion and Corrosion Fatigue Crack Growth in Aluminum Alloys", in Stress Corrosion Research, H. Arup and R.N. Parkins, eds., Sijthoff&Noordhoff, Alphen aan den Rijn, The Netherlands, pp.117-176, 1979.

7. N.J.H. Holroyd and D. Hardie, "Corrosion Fatigue of 7000 Series Aluminum Alloys", in Environment Sensitive Fracture: Evaluation and Comparison of Test Methods ASTM STP 821, S.W. Dean, E.N. Pugh, and G.M. Ugiansky, eds., American Society for Testing and Materials, Philadelphia, PA, pp. 534-547, 1984.

8. J.C. Newman, Jr., " A Crack Opening Stress Equation for Fatigue Crack Growth", International Journal of Fracture, Vol. 24, R 131-135,1984.

9. N.J.H. Holroyd, "Environment-Induced Cracking of High-Strength Aluminum Alloys", in Environmental-Induced Cracking of Metals, R.P. Gangloff and M.B. Ives, eds., NACE, Houston, TX, pp.311-345, 1990.

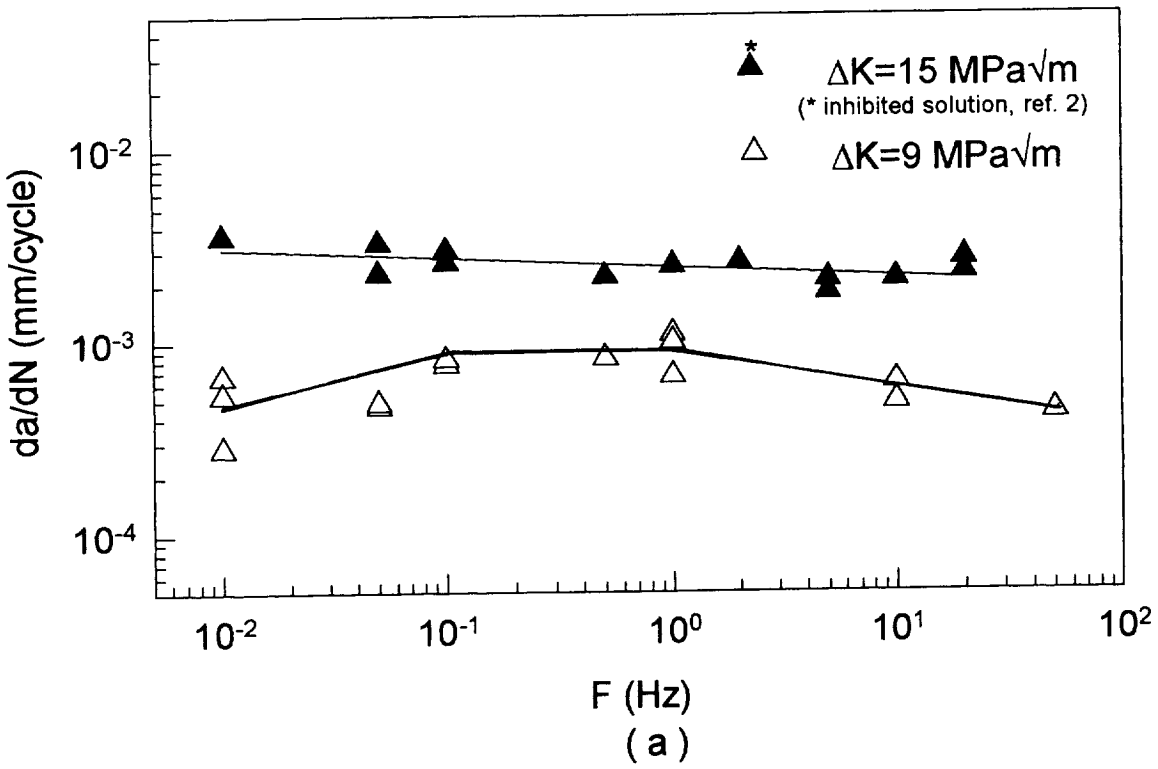

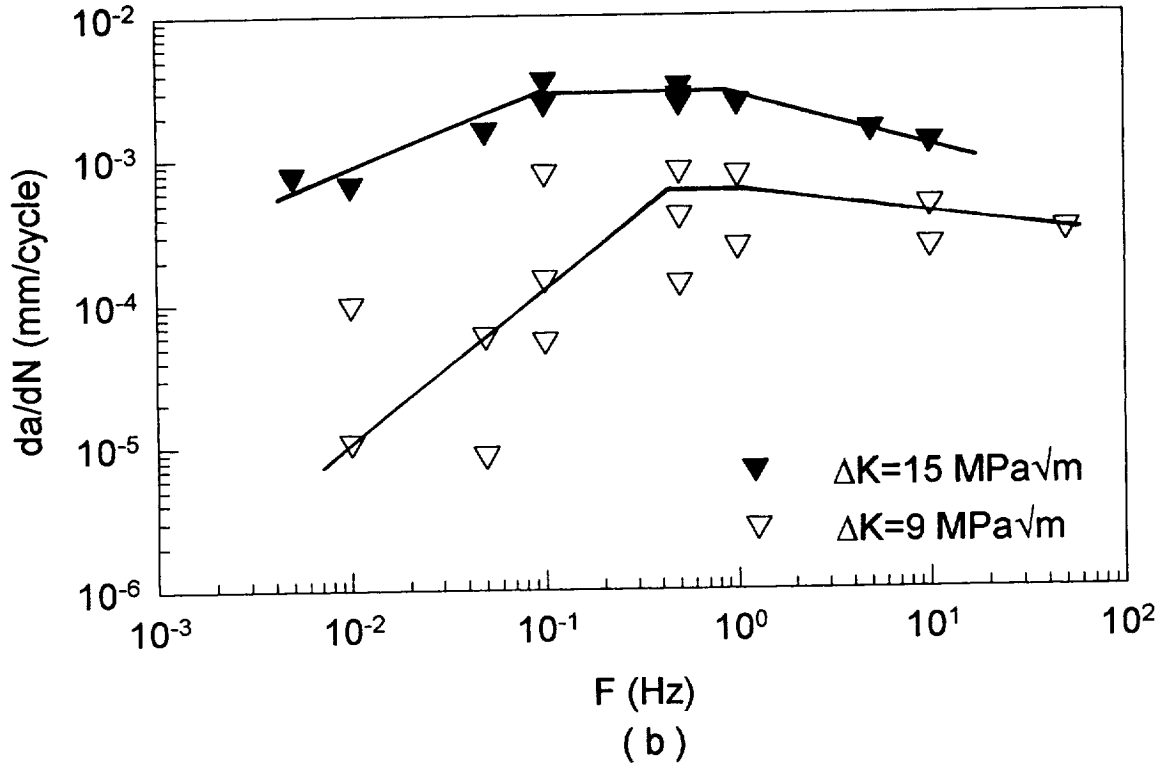

Figure 1 Fatigue crack propagation rate as a function of frequency for 7075 in S-L orientation in 3.5% NaCl solution at R=0.1 (a) T651 (b) T7351.

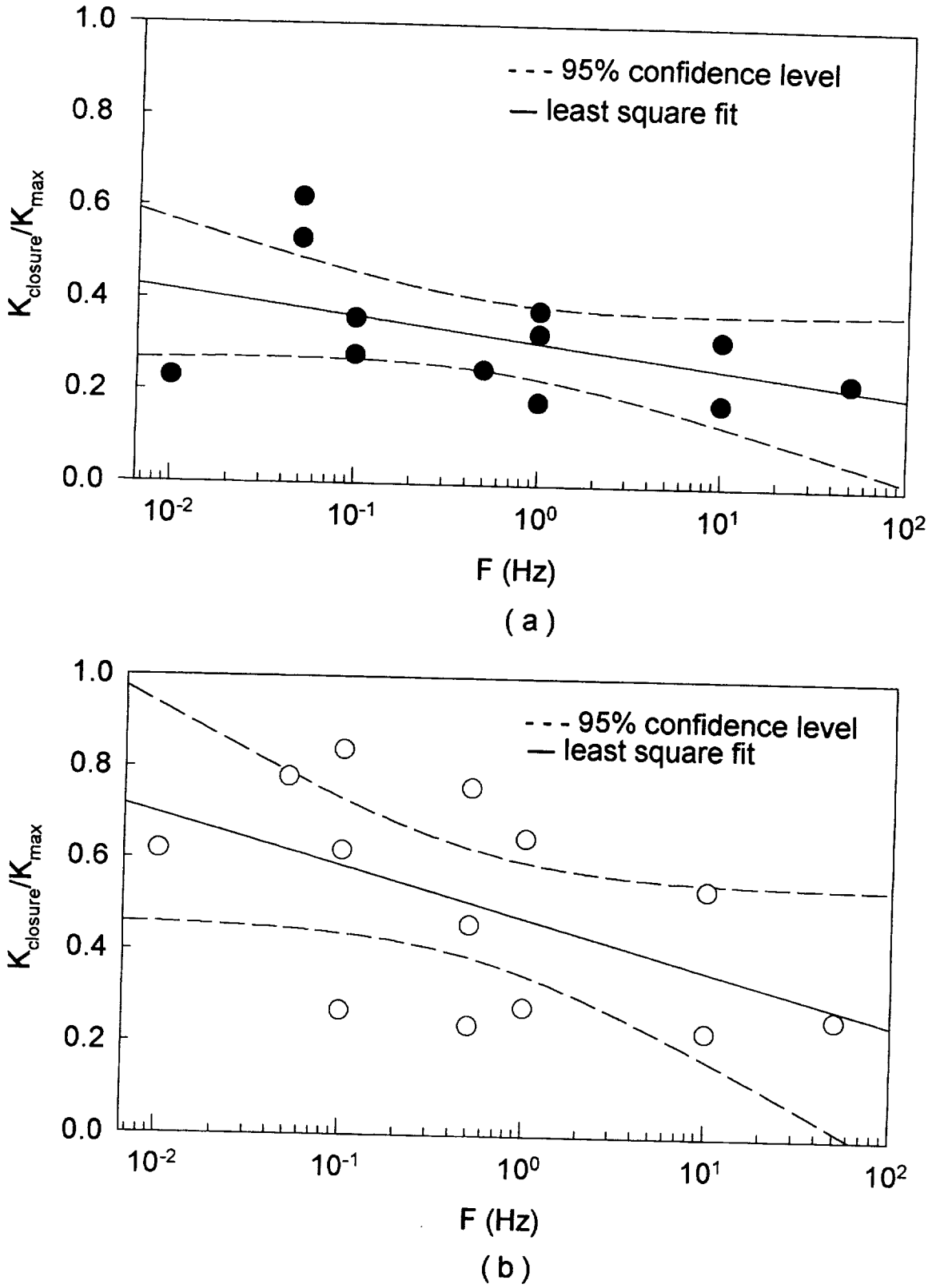

Figure 2 Crack closure level as a function of frequency for 7075 in S-L orientation in 3.5% NaCl solution at R=0.1 and ΔK=9 MPa$\sqrt{m}$ (a) T651 (b) and T7351.

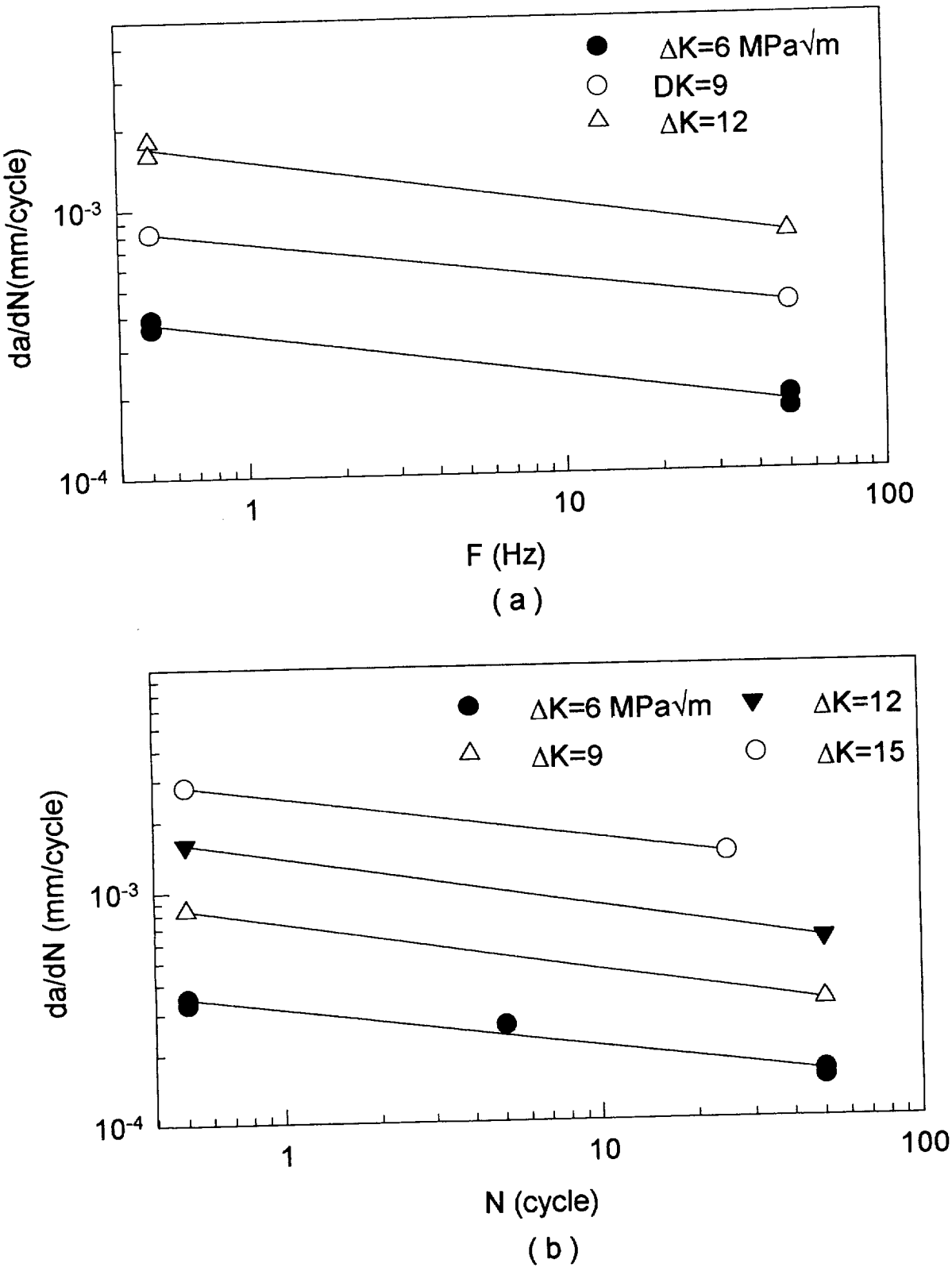

Figure 3 Fatigue crack propagation rate as a function of frequency and ΔK for 7075 in S-L orientation in 3.5% NaCl solution at R=0.1 (a) T651 (b) T7351.

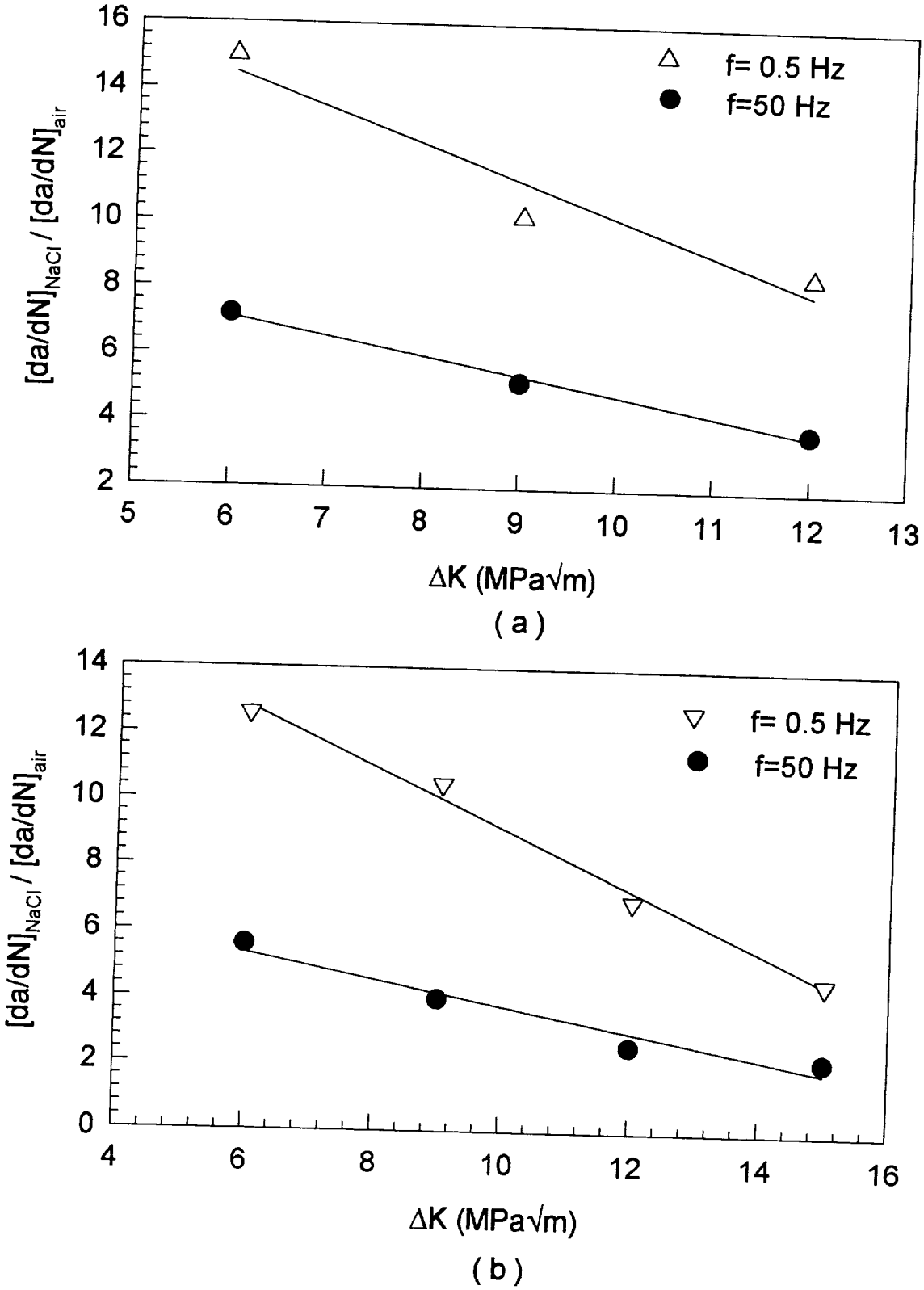

Figure 4 Effect of environment on fatigue crack propagation rate, as influenced by ΔK and frequency for 7075 in 3.5% NaCl solution at R=0.1 (a) T651 (b) T7351.

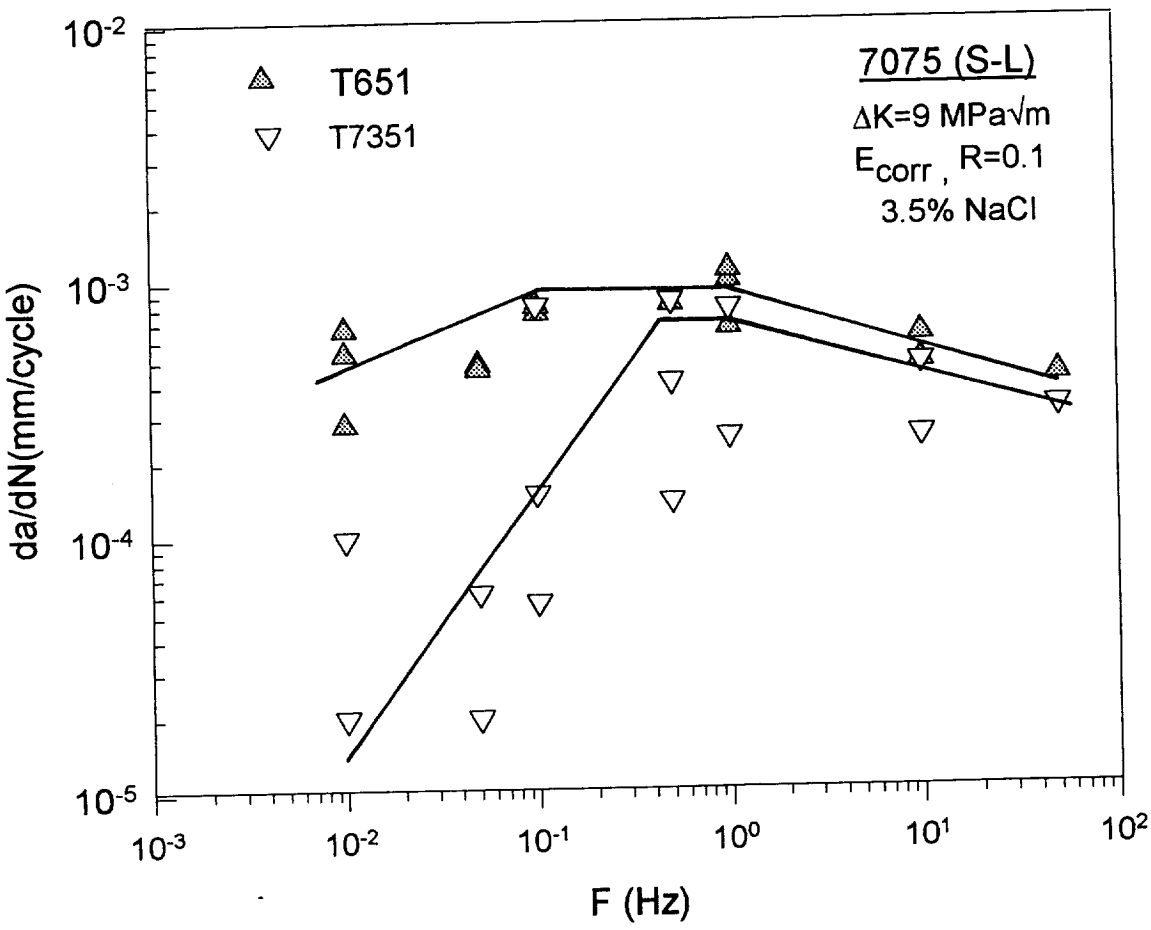

Figure 5 Comparison of crack growth rates for the two variants of 7075 in 3.5% NaCl solution at R=0.1

Project #10b: MODELING ENVIRONMENTAL EFFECTS IN FATIGUE CRACK PROPAGATION

Faculty Investigator: R.P. Gangloff
Graduate Assistant: E. Richey III

Objective

The general objective of this research was to develop a method for incorporating environmental effects on fatigue crack propagation (FCP) rates in metals into damage tolerant life prediction codes such as NASA FLAGRO. Specific goals of the research were to:

- Develop a computer program which models the effect of corrosive environments on FCP behavior, including:
  - implementation of the Wei and Landes linear superposition model.
  - an interpolative model which extends the empirical approach used in NASA FLAGRO.
  - the capability for the user to fit multiple power law segments to da/dN versus K data.
- Establish a data base of environmental crack growth rate data for Ti-6Al-4V in aqueous chloride to provide a basis for testing the computer models. Specifically:
  - Determine the effect of loading rate on the stress corrosion cracking (SCC) susceptibility of Ti-6Al-4V (MA, ELI) in a 3.5% NaCl solution through constant crack mouth opening displacement rate tests.
  - Determine the effect of frequency and stress ratio on FCP in Ti-6Al-4V (MA, ELI) in moist air and a 3.5% NaCl solution.

Progress During the Reporting Period

Computer Modeling Methods

Recent research on this project included successfully defending a Master's Of Science dissertation[1] in May 1995. The thesis is being published as a NASA contractor report, and details the research conducted in developing the computer models as well as the experimental results for Ti-6Al-4V (MA, ELI).

A computer program was developed which implemented the Wei and Landes linear superposition model, the interpolative model, and allowed users to fit multiple power law segments to fatigue data. The program, UVAFAS.EXE, was sent with the source code to NASA Langley Research Center and NASA Johnson Space Center for possible implementation into FLAGRO. The program was written in FORTRAN 77, and compiled using a professional multi-platform FORTRAN compiler from WATCOM, Inc. The linear superposition and interpolative models are discussed in detail in the NASA contractor report "Computer Modeling the Fatigue Behavior of Metals in Corrosive Environments."[2]

The interpolative model was tested for Ti-6Al-4V in 3.5% NaCl, 1.0% NaCl, and moist air environments. The model was used to interpolate the effects of frequency (f) and stress ratio on FCP. The model accurately interpolated trends in fatigue behavior when the interpolated load characteristics were inside the range of data used to determine the constants in the crack growth rate equations. Interpolative models do, however, show substantial deviation between predicted and experimental results when the target load characteristics are outside the range of data used to establish the constants in the crack growth rate equations.[3]

The linear superposition model was tested for the same material-environment systems employed by Wei and Landes[4], Speidel[5], and Harmon *et. al.*[6] in an attempt to duplicate their results. The current linear superposition model yielded improved results due to the improved accuracy of the numerical algorithm used to calculate the stress corrosion component of corrosion fatigue. The model was also tested for standard and ELI grade Ti-6Al-4V in 3.5% NaCl. The linear superposition model accurately predicted FCP rates in standard grade Ti-6Al-4V for K values where K_{max} exceeded the SCC threshold, K_{ISCC}. The model was not applicable to ELI grade Ti-6Al-4V due to the increased SCC resistance of the alloy.

Environment Assisted Cracking (EAC) of Ti-6Al-4V

Mill annealed Ti-6Al-4V in the extra low interstitial (ELI) condition (heated for eight hours at 760°C, vacuum furnace cooled) was obtained from President Titanium. Compact tension (CT) specimens were machined in the L-T orientation with a width of 63.5 mm and a thickness of 6.4 mm. The chemical composition and selected mechanical properties of the alloy are shown in Table 1.

Recent research regarding the corrosion fatigue behavior of Ti-6Al-4V (MA, ELI) focused on determining the effect of frequency on da/dN at constant ΔK values, as well as determining the effect of loading rate on the SCC susceptibility of Ti-6Al-4V. Figure 1 presents results which demonstrate the effect of frequencies between 0.03 and 40 Hz on the da/dN versus ΔK behavior of

Ti-6Al-4V (MA, ELI) in 3.5% NaCl solution (-500 mV_{SCE}) for fixed ΔK values of 12.5 and 25 $MPa\sqrt{m}$. As seen in Figure 1, da/dN increases with increasing frequency, with da/dN ($f^{0.1 \text{ to } 0.2}$. ELI Ti-6Al-4V does not exhibit the "frequency crossover" seen in standard grade Ti-6Al-4V by Dawson and Pelloux.[7]

Table 1: Chemical Composition and Mechanical Properties of Ti-6Al-4V

Chemical Composition (wt. %)

Al	V	C	N	Fe	O	H	Y	Ti
6.17	4.33	0.025	0.011	0.19	0.12	0.0055	0.0005	balance

Mechanical Properties

Yield Strength MPa (ksi)	Tensile Strength MPa (ksi)	Elongation Percent, %	Reduction Area, %
940 (136)	982 (142)	13	30.2

The SCC susceptibility of ELI Ti-6Al-4V was studied as a function of loading rate. Figure 2 is a plot of the stress intensity for crack initiation (K_{TH}) for Ti-6Al-4V (MA,ELI) in 3.5% NaCl (-500 mV_{SCE}) for all experiments conducted to date. These experiments were conducted under constant crack mouth opening displacement (CMOD) rate, with dK/dt determined prior to crack initiation. The experiments conducted during this reporting period were for CMOD rates of 4.0×10^{-3} mm/sec (dK/dt = 0.32 $MPa\sqrt{m}$/sec) and 6.0×10^{-4} mm/sec (dK/dt = 5.3×10^{-2} $MPa\sqrt{m}$/sec). Table 2 summarizes the K_{TH} values determined for these loading rates, as well as the results of previous experiments. The alloy exhibits a minimum value of K_{TH} at a dK/dt between 4×10^{-3} and 5×10^{-2} $MPa\sqrt{m}$/sec. The alloy does exhibit greater resistance to SCC than standard grade Ti-6Al-4V. Standard grade Ti-6Al-4V exhibits a K_{ISCC} of 23 $MPa\sqrt{m}$ [7], while ELI grade Ti-6Al-4V exhibits K_{TH} values greater than 44 $MPa\sqrt{m}$. Moskovitz and Pelloux[8] reported a similar dependence of K_{TH} on loading rate for another α+ ß titanium alloy, Ti-6Al-6V-2Sn in 3.5% NaCl.

Table 2: K_{TH} as a Function of Loading Rate for Ti-6Al-4V (MA,ELI)

CMOD Rate (mm/sec)	dK/dt (MPa√m/sec)	K_{TH} (MPa√m)
2.9×10^{-5}	1.6×10^{-3}	58.7
4.5×10^{-5}	3.7×10^{-3}	54.7
1.3×10^{-4}	1.1×10^{-2}	> 44.0[3*]
6.0×10^{-4}	5.3×10^{-2}	59.4
4.0×10^{-3}	3.2×10^{-1}	71.0

Conclusions

Computer Modeling Methods

1. The computer program developed during this research, UVAFAS.EXE, provides a reasonable method for modeling time dependent environmental FCP rates as a function of stress ratio, frequency, and hold time.
2. Linear superposition is effective for limited material/environment systems where the alloy is extremely sensitive to SCC, and the contribution of SCC to crack growth is significantly greater than that of inert environment mechanical fatigue.
3. Linear superposition is effective for standard grade Ti-6Al-4V (MA) in aqueous chloride when K_{max} exceeds K_{ISCC}. Linear superposition is not applicable to ELI grade Ti-6Al-4V due to the increased stress corrosion resistance of the alloy.
4. The interpolative model can be used to describe environmental FCP when the loading variables where data are interpolated lie within the range of the establishing data base.

[3*] For this CMOD rate, the load was increased monotonically in 65 minutes to a level corresponding to a stress intensity of 44 MPa√m. Since cracking was not observed, the load was held constant for 137 hours at this level. The crack did not grow during this time.

Environment Assisted Cracking (EAC) of Ti-6Al-4V

1. ELI Ti-6Al-4V exhibits a greater resistance to SCC than standard grade Ti-6Al-4V, possibly due to the lower oxygen content of the ELI grade or a texture difference. Standard grade Ti-6Al-4V exhibits a K_{ISCC} value of 23 MPa$\sqrt{m}$ in 3.5% NaCl, while ELI grade Ti-6Al-4V exhibits K_{TH} value greater than 44 MPa$\sqrt{m}$. Ti-6Al-4V exhibits a slower da/dt than standard grade Ti-6Al-4V.
2. ELI Ti-6Al-4V does not exhibit the "frequency crossover" effect seen in standard grade Ti-6Al-4V. ELI Ti-6Al-4V exhibits a mild frequency dependence for ΔK levels of 12.5 and 25 MPa$\sqrt{m}$ in a 3.5% NaCl solution for R = 0.1. For both K levels, da/dN is proportional to $f^{0.1 \text{ to } 0.2}$.

Future Work

This project was completed in 1995. Mr. Richey obtained his Master's of Science degree in Mechanical Engineering and has been accepted into the PhD program in the Materials Science and Engineering Department at the University of Virginia. Research in 1996 will emphasize corrosion fatigue in 7xxx aluminum alloys, as outlined in the 1996 renewal proposal for this LA^{2}ST grant. Mr. Zuhair Gasem is the graduate student who will conduct this work.

References

1. E. Richey, "Empirical Modeling of Environment-Enhanced Fatigue Crack Propagation in Structural Alloys for Component Life Prediction," M.S. Thesis, University of Virginia, Charlottesville, VA, 1995.
2. E. Richey, III, A. W. Wilson, J. M. Pope, and R. P. Gangloff. "Computer Modeling the Fatigue Behavior of Metals in Corrosive Environments," NASA Contractor Report 194982, NASA Langley Research Center, Hampton, VA, 1994.
3. G. Haritos, T. Nicholas, and G. O. Painter. "Evaluation of Crack Growth Models for Elevated Temperature Fatigue," Fracture Mechanics: Eighteenth Symposium, D. T. Reed and R. P. Read, Eds., American Society for Testing and Materials, Philadelphia, PA, 1988, pp. 206-220.
4. R. P. Wei and J. D. Landes. "Correlation Between Sustained Load and Fatigue Crack Growth in High-Strength Steels," Materials Research and Standards, MTRSA, Vol. 9, No.7, 1969, pp. 25-27,44-46.
5. M.O. Speidel. "Stress Corrosion and Corrosion Fatigue Crack Growth in Aluminum Alloys," Stress Corrosion Research, Hans Arup and R. N. Parkins, Eds., Sijthoff & Noordhoff International Publishers, The Netherlands, 1979, pp. 117-176.

6. D. M. Harmon, C. R. Saff, and J. G. Burns. "Development of An Elevated Temperature Crack Growth Routine," AIAA Paper 88-2387, American Institute of Aeronautics and Astronautics, 1988.

7. D. B. Dawson and R. M. Pelloux. "Corrosion Fatigue Crack Growth of Titanium Alloys in Aqueous Environments," *Metallurgical Transactions*, Vol. 5, 1974, pp. 723-731.

8. J. A. Moskovitz and R. M. Pelloux. "Dependence of K_{ISCC} On Loading Rate and Crack Orientation in Ti-6Al-6V-2Sn," *Corrosion*, Vol. 35, 1979, pp. 509-514.

APPENDIX I: GRANT PUBLICATIONS (July 1 to December 31, 1995)

1. J.A. Wert and M.T. Lyttle, "Microstructure Evolution During High-Temperature Deformation of Aluminum Alloys", 16th Riso International Symposium on Microstructural and Crystallographic Aspects of Recrystallization, N. Hansen, D. Juul Jensen, Y.L. Liu and B. Ralph (eds), Riso National Laboratory, Roskilde, Denmark, 1995, pp.589-594.

2. B. Skrotzki, G.J. Shiflet, and E.A. Starke, Jr. On the Effect of Stress on Nucleation and Growth of Precipitates in an Al-Cu-Mg-Ag Alloy. Submitted to Metallurgical Transactions A.

3. B. Skrotzki, H. Hargarter and E.A. Starke, Jr. Microstructural Stability Under Creep Conditions of Two Al-Cu-Mg-Ag Alloys. Submitted to The 5th International Conference on Aluminum Alloys, ICAA-5, Grenoble, France.

4. B. Skrotzki, E.A. Starke, and G.J. Shiflet, "Alterung einer Al-Cu-Mg-Ag-Legierung unter äußerer Spannung," Hauptversammlung 1995 der Deutschen Gesellschaft für Materialkunde e.V., Bochum, Germany, June 6-9, 1995.

5. H. J. Koenigsmann and E. A. Starke, Jr., "Cavity Nucleation and Fracture in an Al-Si-Ge Alloy", submitted to Proceedings of the 5th International Conference on Aluminum Alloys - Their Physical and Mechanical Properties (Grenoble, France, July 1-5, 1996).

6. H. J. Koenigsmann, E. A. Starke, Jr., and P. E. Allaire, "Finite Element / Experimental Analysis of Cavity Nucleation in an Al-Si-Ge Alloy", Acta Metallurgica et Materialia, in press (1996).

7. J.R. Scully, Co-editor *"Electrochemical Noise-Application to Analysis and Interpretation of Corrosion Data,"* American Society for Testing of Materials Special Technical Publication, Philadelphia, PA, in press, 1995.

8. J.R. Scully, S.T. Pride, H.S. Scully, J.L.Hudson, "Some Correlations Between Metastable Pitting and Pit Stabilization in Metals" Electrochemical Society Localized Corrosion II Symposia Proceedings, P. Natishan, R. Newman, G. Frankel, R. Kelly, eds. Electrochemical Soc., in press, 1995. (invited)

9. S.T. Pride, S.T. Pride, J.L.Hudson, "Analysis of Electrochemical Noise from Metastable Pitting in Al, Aged Al-2%Cu and AA 2024-T3," in *"Electrochemical Noise - Application to Analysis and Interpretation of Corrosion Data,"* American Society for Testing of Materials Special Technical Publication, Philadelphia, PA, in press, 1995.

10. Michael J. Haynes and Richard P. Gangloff, "High Resolution R-Curve Characterization of the Fracture Toughness of Thin Sheet Aluminum Alloys", Journal of Testing and Evaluation, in review (1996).

11. Michael J. Haynes, Brian P. Somerday, Cynthia L. Lach and Richard P. Gangloff, "Micromechanical Modeling of Temperature-Dependent Initiation Fracture Toughness in Advanced Aluminum Alloys", in 27th National Symposium on Fatigue and Fracture Mechanics, ASTM STP, R.S. Piascik, R.P. Gangloff, N.E. Dowling and JC. Newman, eds., ASTM, Philadelphia, PA, in press (1996).

APPENDIX II: GRANT PRESENTATIONS (July 1 to December 31, 1995)

1. J.A. Wert and M.T. Lyttle, "Microstructure evolution during high-temperature deformation of aluminum alloys", 16th Riso International Symposium on Microstructural and Crystallographic Aspects of Recrystallization, N. Hansen, D. Juul Jensen, Y.L. Liu and B. Ralph (eds), Riso National Laboratory, Roskilde, Denmark, 1995, pp.589-594.

2. J.R. Scully, S.T. Pride, H.S. Scully, J.L. Hudson, "Some correlations between metastable pitting and pit stabilization in metals," ECS Localized Corrision II Symposia, P. Natishan, R. Newman, G. Frankel, R. Kelly, eds. Electrochemical So., Chicago, IL, October, 1995. (Invited)

3. J.R. Scully, S.W. Smith, M.A. Gaudett, D. Enos, "Use of thermal desorption spectroscopy to study hydrogen interactions in metals," TMS Fall Meeting Symposia on New Techniques for Characterizing Corrision and Stress Corrosion, Cleveland, OH, 1995. (Invited)

APPENDIX III: GRANT PROGRESS REPORTS (January, 1988 to December, 1995)

1. R.P. Gangloff, G.E. Stoner and R.E. Swanson, "Environment Assisted Degradation Mechanisms in Al-Li Alloys", University of Virginia, Report No. UVA/528266/MS88/101, January, 1988.

2. R.P. Gangloff, G.E. Stoner and R.E. Swanson, "Environment Assisted Degradation Mechanisms in Advanced Light Metals", University of Virginia, Report No. UVA/528266/MS88/102, June, 1988.

3. R.P. Gangloff, G.E. Stoner and R.E. Swanson, "Environment Assisted Degradation Mechanisms in Advanced Light Metals", University of Virginia, Report No. UVA/528266/MS89/103, January, 1989.

4. T.H. Courtney, R.P. Gangloff, G.E. Stoner and H.G.F. Wilsdorf, "The NASA-UVa Light Alloy Technology Program", University of Virginia, Proposal No. MS NASA/LaRC-3937-88, March, 1988.

5. R.P. Gangloff, "NASA-UVa Light Aerospace Alloy and Structures Technology Program", University of Virginia, Proposal No. MS NASA/LaRC-4278-89, January, 1989.

6. R.P. Gangloff, "NASA-UVa Light Aerospace Alloy and Structures Technology Program", University of Virginia, Report No. UVA/528266/MS90/104, August, 1989.

7. R.P. Gangloff, "NASA-UVa Light Aerospace Alloy and Structures Technology Program", University of Virginia, Report No. UVA/528266/MS90/105, December, 1989.

8. R.P. Gangloff, "NASA-UVa Light Aerospace Alloy and Structures Technology Program", UVa Report No. UVA/528266/MS90/106, June, 1990.

9. R.P. Gangloff, "NASA-UVa Light Aerospace Alloy and Structures Technology Program", UVa Report No. UVA/528266/MS91/107, January, 1991.

10. R.P. Gangloff, "NASA-UVa Light Aerospace Alloy and Structures Technology Program", UVa Report No. UVA/528266/MS91/108, July, 1991.

11. R.P. Gangloff, "NASA-UVa Light Aerospace Alloy and Structures Technology Program", UVa Report No. UVA/528266/MS92/109, January, 1992.

12. R.P. Gangloff, "NASA-UVa Light Aerospace Alloy and Structures Technology Program", UVa Report No. UVA/528266/MS93/111, July, 1992.

13. R.P. Gangloff, "NASA-UVa Light Aerospace Alloy and Structures Technology Program", UVa Report No. UVA/528266/MSE93/112, March, 1993.

14. R.P. Gangloff, "NASA-UVa Light Aerospace Alloy and Structures Technology Program", UVa Report No. UVA/528266/MSE93/113, July, 1993.

15. R.P. Gangloff, "NASA-UVa Light Aerospace Alloy and Structures Technology Program", UVa Report No. UVA/528266/MSE93/114, March, 1994.

16. R. P. Gangloff, "NASA-UVa Light Aerospace Alloy and Structures Technology Program," UVA Report No. UVA/528266/MSE94/116, July, 1994.

17. E.A. Starke, Jr. and R.P. Gangloff, "NASA-UVa Light Aerospace Alloy and Structures Technology Program", UVa Report No. UVA/528266/MSE94/117, March, 1995.

18. R.P. Gangloff, and E.A. Starke, Jr., "NASA-UVa Light Aerospace Alloy and Structures Technology Program", UVa Report No. UVA/528266/MS95/118, July, 1995.

DISTRIBUTION LIST

1-4	Mr. D.L. Dicus Contract Monitor Metallic Materials Branch, MS 188A NASA Langley Research Center Hampton, VA 23681-0001
5-6*	NASA Scientific and Technical Information Facility P.O. Box 8757 Baltimore/Washington International Airport Baltimore, MD 21240
7	Mr. Joseph S. Murray Grants Officer, M/S 126 NASA Langley Research Center Hampton, VA 23681-0001
8	Dr. Darrel R. Tenney Materials Division NASA Langley Research Center Hampton, VA 23681-0001
9	Dr. Charles E. Harris Mechanics of Materials Branch NASA Langley Research Center Hampton, VA 23681-0001
10	Mr. W. Barry Lisagor Metallic Materials Branch NASA Langley Research Center Hampton, VA 23681-0001
11	Mr. T.W. Crooker Code RM NASA Headquarters Washington, DC 20546
12	Dr. Robert S. Piascik Mechanics of Materials Branch NASA Langley Research Center Hampton, VA 23681-0001
13	Mr. W. Brewer Metallic Materials Branch, MS 188A NASA Langley Research Center Hampton, VA 23681-0001

14 Mr. Thomas T. Bales
Metallic Materials Branch, MS 188A
NASA Langley Research Center
Hampton, VA 23681-0001

15 Mr. John Wagner/Ms. Cynthia Lach
Metallic Materials Branch, MS 188A
NASA Langley Research Center
Hampton, VA 23681-0001

16 Dr. William F. Bates
Lockheed Aeronautical Systems Co.
86 South Cobb Drive
Marietta, GA 30063-0648

17 Dr. Alex Cho
Reynolds Metals Co.
4th and Canal Street
Richmond, VA 23261

18 Mr. E.A. Colvin
Alcoa Technical Center
Route 780, 7th Street Road
Alcoa Center, PA 15069

19 Dr. L.M. Karabin
Alcoa Technical Center
Route 780, 7th Street Road
Alcoa Center, PA 15069

20 Dr. Ravi Kahandal
McDonnell Douglas Aerospace
Mail Stop 36-90
3855 Lakewood Boulevard
Long Beach, CA 90846

21 Mr. Fred Casey
Space Transportation Systems Division
Rockwell International
Dept. 289, MC/AC 56
12214 Lakewood Boulevard
Downey,CA 90241

22-23 E.A. Starke, Jr.; MS&E

24-25 R.P. Gangloff; MS&E

26 G.J. Shiflet; MS&E

27 G.E. Stoner; MS&E

28 J.A. Wert; MS&E

29 J.R. Scully; MS&E

30 C.T. Herakovich; CE and AM

31-32 S.S. Kerbel; Clark Hall

33 SEAS Preaward Administration Files

34 Mr. Gwyn Faile
Code ED 24
Marshall Space Flight Center
Huntsville, AL 35812

35 Mr. Brian McPherson
Code ED 24
Marshall Space Flight Center
Huntsville, AL 35812

36 Dr. William E. Quist
Boeing Aerospace and Electronics
Aerospace Group
Mail Stop GH-CJ
P.O. Box 3707
Seattle, WA 98124

37 Dr. Howard G. Nelson
NASA-Ames Research Center
EEM: 213-3

38 Dr. R.G. Forman
Mail Code ES-5
NASA-L.B. Johnson Space Flight Center
Houston, TX 77058

39 Professor A.K. Noor
Center for Computational Structures Technology
NASA Langley Research Center
Hampton, VA 23681-0001

40 Professor A.K. Ghosh
Department of Materials Science & Engineering
University of Michigan
2102 Dow Building
Ann Arbor, MI 48109-2136

41 Dr. D. Ferton
Pechiney Centre de Recherches
De Voreppe
B.P. 27 -- 38340 Voreppe
FRANCE

42 Dr. John Papazian
Grumman Aerospace & Electronics
Mail Stop A02-026
Bethpage, NY 11714-3582

43 Dr. Richard Lederick
McDonnel Douglas Aircraft Company
Mail Stop 111-1041
P.O. Box 516
St. Louis, MO 36166

44 Dr. Alan Hopkins
Senior Research Metallurgist
The University of Dayton, Research Institute
300 College Park
Dayton, H 45469-0172

45 Dr. Frances Hurwitz
Ceramic Composites
NASA Lewis Research Cneter
21000 Brookpark Road
Cleveland, OH 44135

46 Dr. Malcolm Ozelton
Manager, Metallic & Ceramic Materials
Northrop Corporation, B-2 Division
8900 E. Washington Boulevard
T241/GK
Pico Rivera, CA 90660-3737

47 Dr. S. Sampath
Technical Center
Federal Aviation Administration
Atlantic City International Airport, NJ 08405

48 Dr. James Staley
Alcoa Laboratories
Alcoa Center, PA 15069

49 Dr. Jeffrey Waldman
Code 6063
Naval Air Development Center
Warminster, PA 18974

DISTRIBUTION LIST

50 - 51	M. Rodeffer, Clark Hall
**	SEAS Postaward Research Administration
52	SEAS Preaward Research Administration

*One reproducible copy
**Cover letter

Updated: January 1996

JO#6886:ph